Title
Polycaprolactone Thin Films for Retinal Tissue Engineering and Drug Delivery

Author
Steedman, Mark Rory

Publication Date
2010

Peer reviewed|Thesis/dissertation

POLYCAPROLACTONE THIN FILMS FOR RETINAL TISSUE ENGINEERING AND DRUG DELIVERY

by

MARK RORY STEEDMAN

DISSERTATION

Submitted in partial satisfaction of the requirements for the degree of

DOCTOR OF PHILOSOPHY

in

BIOENGINEERING

in the

GRADUATE DIVISION

of the

UNIVERSITY OF CALIFORNIA, SAN FRANCISCO

AND

Acknowledgements

This dissertation is the culmination of the past 10 years of academic research at the University of Washington, University of California Berkeley and the University of California San Francisco. During this time I have met too many people to count who have helped me along this journey, so I will only attempt to thank a few of them.

I would first like to thank my research advisor Professor Tejal Desai. I admire her leadership, ability to balance family life with her duties as a professor and advisor, and for all the help throughout the past 5 years. You are truly an inspiration to me.

I would like to thank Janice DeCosmo and the Washington NASA Space Grant Consortium for giving me the opportunity to work in a research lab at the University of Washington the summer before my freshman year of college. With zero experience under my belt, Professors Martin Gouterman, Gamal Khalil, and James Callis took a chance on an 18-year old kid with lots of potential and gave me the training, tools, and mentoring needed to succeed in academic research.

I would like to thank Professor Paul Yager whom I worked with for there years at the University of Washington. Under his tutelage I presented at a conference and co-authored my first journal article. I also met three graduate students who were amazing role models and advice givers throughout my three years in the Yager Lab. Matthew Munson, Hugh Chang, and Kenneth Hawkins were great friends and coworkers who were invaluable in my development as a researcher.

After moving down to the Bay Area for graduate school I met several people from the Bioengineering Departments at UCSF and UCB who have been instrumental in helping me complete a PhD. The program administrators, Rebecca Pauling and

SarahJane Taylor, have always been helpful and ready to answer any and all questions I have had. My qualifying exam committee, Professors Jeffrey Lotz, Robert Bhisitkul, Dorian Liepmann, Daniel Fletcher, and David Sretavan, were all very helpful and supportive during what is typically a very stressful period for graduate students. Sharmila Majumdar has been an excellent academic advisor the past three years, and I appreciate her always willing to meet with me and offer advice.

I would also like to thank other professors that I have worked with through the Bioengineering Association of Students. Steven Conolly and Sarah Nelson have always put the best interests of the students at the forefront, and I also appreciate their willingness to write recommendation letters whenever asked.

Graduate school has also been an amazing social experience. Fellow students such as David Breslauer, Maral Gharib, Robin Held, Anuj Patel, An-Chi Tsou, Eric Jabart, Karl Saldanha, Jennifer Luu, Chat Hull, Mimi Zhang, Zac Lee and many others have been great friends, soccer teammates, cheesecake eaters, BBQ hosts, and partners in crime during nights out in San Francisco and Berkeley.

To the current and former Desai Lab post-docs, Sarah Tao, Rahul Thakar, Kristy Ainslie, Dan Bernards, Rachel Lowe, and Kelly Chavez, I thank you for always being helpful and available. You have made my life much easier than it would have been if I had to figure out everything myself. To Adam Mendelsohn, Kayte Fischer, and Lily Peng, thanks for living the dream with me, we made it! I would also like to thank all the other Desai lab members over the past 5 years who have made it a fun place to work.

I have been extremely lucky to have incredible roommates the past 5 years. Derek Greenfield, Phillip Elms, and Boryana Manz were three great people to live with

for 2 years in Berkeley. Ovijit Chaudhuri and Dave Schumaker are two of the coolest guys I know and I feel privileged to call them friends and former roommates. The past year Jennifer Gilmore has been an awesome addition to the Carillon family and I am sad to leave her and miss out on more good times in San Francisco.

I would like to thank my good friend and climbing partner, Debbie Cheng, for always being ready and willing to motivate me to go to the gym. Without your determination and encouragement I would never have improved so much, and the stressful parts of graduate school would have been even worse.

I would like to thank Alana Lerner, one of my best friends and confidants over the past few years. I will miss our soccer games together, tissue culture confessions, and trips to Seattle, Tahoe, and campgrounds around the Bay Area. You have always been there to teach me biology, participate in Desai lab events as an honorary member, and enjoy my cheesecake more than anyone else.

I would like to thank my two best friends and comrades in arms, Henry Lee and Rob Tucker. We all met as undergrads and have followed the same path to graduate school and beyond. We've been together through thick and thin, European World Cup games, and everything in between. Here's to many more soccer games and experiences together.

Finally, I would like to thank my family for their everlasting love and support.

Polycaprolactone Thin Films for Retinal Tissue Engineering and Drug Delivery

Mark Rory Steedman

Abstract

This dissertation focuses on the development of polycaprolactone thin films for retinal tissue engineering and drug delivery. We combined these thin films with techniques such as micro and nanofabrication to develop treatments for age-related macular degeneration (AMD), a disease that leads to the death of rod and cone photoreceptors. Current treatments are only able to slow or limit the progression of the disease, and photoreceptors cannot be regenerated or replaced by the body once lost.

The first experiments presented focus on a potential treatment for AMD after photoreceptor death has occurred. We developed a polymer thin film scaffold technology to deliver retinal progenitor cells (RPCs) to the affected area of the eye. Earlier research showed that RPCs destined to become photoreceptors are capable of incorporating into a degenerated retina. In our experiments, we showed that RPC attachment to a micro-welled polycaprolactone (PCL) thin film surface enhanced the differentiation of these cells toward a photoreceptor fate.

We then used our PCL thin films to develop a drug delivery device capable of sustained therapeutic release over a multi-month period that would maintain an effective concentration of the drug in the eye and eliminate the need for repeated intraocular

injections. We first investigated the biocompatibility of PCL in the rabbit eye. We injected PCL thin films into the anterior chamber or vitreous cavity of rabbit eyes and monitored the animals for up to 6 months. We found that PCL thin films were well tolerated in the rabbit eye, showing no signs of chronic inflammation due to the implant. We then developed a multilayered thin film device containing a microporous membrane. We loaded these devices with lyophilized proteins and quantified drug elution for 10 weeks, finding that both bovine serum albumin and immunoglobulin G elute from these devices with zero order release kinetics.

These experiments demonstrate that PCL is an extremely useful biomaterial that may be used to treat AMD in multiple ways. Through both tissue engineering and drug delivery techniques we have established that PCL thin films have the potential to revolutionize the treatment of AMD.

Table of Contents

List of Figures

List of Tables

Chapter 1 – Introduction

The phenomenon of sight is truly miraculous. It is said a picture is worth a thousand words, and yet our eyes are constantly alert, taking in a continuous stream of pictures of our surroundings. This occurs faster than we could ever possibly produce enough words to describe everything we see. Yet as we age the senses are not what they always were, and for some, can be lost forever. The loss of sight is a particularly terrifying prospect but is all too common for many of the earth's population, particularly the elderly. The work presented in this dissertation was motivated by the potential to reverse or prevent the incidence of blindness from occurring.

1.1 Components and Functions of the Eye

The human eye converts light into electrochemical signals, enabling vision. Light enters the eye through the cornea, the transparent covering of the iris, pupil and anterior chamber (Figure 1.1). In conjunction with the lens, the cornea refracts the entering light and focuses it onto the retina. This begins an intricate process by which light is converted to electrochemical signals that converge on the brain. Each structure in the eye has a specific purpose that enables this process to occur every day. The iris, for example, does much more than simply give the eye its color. This circular structure controls the diameter of the pupil, regulating the amount of light that enters the eye[1].

In between the cornea and the iris is the anterior chamber, a space filled with aqueous humor, which regulates intraocular pressure, provides nutrients to nearby structures, and removes waste products. The aqueous humor is under constant flow, such

that small variations in either production or removal of aqueous humor from the anterior chamber can lead to unwanted changes in intraocular pressure.

Inside the eye between the retina and lens is the vitreous humor, or simply the vitreous, a clear gelatinous avascular mass that remains stagnant in the eye. It is composed almost entirely of water, although approximately 1% of it is either collagen or hyaluronic acid[1]. Despite the small quantities of these components, their ability to bind large quantities of water gives the vitreous its gel-like viscosity.

The choroid is a vascular layer of connective tissue that provides oxygen and other nutrients to the outer layers of the retina. The choroid is located in between the retina and the sclera, the white protective outer layer of the eye.

1.2 The Retina

The central nervous system consists of the brain, spinal cord, and retina and is responsible for receiving environmental information and coordinating appropriate responses. The retina lines the back of the eye and is comprised of a thin, layered, semitransparent sheet of tissue[1]. It contains a variety of cells (Figure 1.2) that work together to convert light into electrochemical signals that are sent first to the optic nerve and then to the brain.

The most celebrated cells of the retina are two types of photoreceptors, rods and cones, named after the shape of their outer segments[2]. Rod cells are concentrated at the outer edges of the retina and are responsible for night vision and peripheral vision. Conversely, cone cells are mainly found in the central part of the retina and are only very sparsely found in the outer regions of the retina. Like their rod counterparts, cone cells

have a complex structure involving an axon terminal connected to bipolar and horizontal cells, a cell body, an inner segment, and an outer segment responsible for absorbing light. These outer segments contain discs filled with different photon-absorbing opsins, depending on the specific cell type. Only one type of rod cell exists in humans, whereas cone cells come in three varieties. This leads to trichromatic vision, which allows for the perception of color. Together, the human eye's 4.6 million cones and 92 million rods convert energy from absorbed photons into electrochemical signals that are eventually processed by the brain through a complex process called signal transduction[3].

Horizontal cells, named for their orthogonal orientation, regulate and integrate information from multiple photoreceptors. Although numerically small compared to other cell types in the retina, horizontal cells play an important role in vision. The complex process of signal transduction begins with photoreceptor hyperpolarization in response to light, which leads to a reduction in the release of glutamate. Horizontal cells respond to this glutamate reduction by reducing the release of γ-Aminobutyric acid (GABA), an inhibitory neurotransmitter that leads to a depolarization of the photoreceptors. This negative feedback loop allows the eye to function correctly under both bright and dim conditions[4].

The retinal bipolar cells are found in between the photoreceptors and retinal ganglion cells and are named for their synaptic connections to both retinal layers. These cells are separated into rod bipolar cells and cone bipolar cells, according to which photoreceptor cell type they receive synaptic connections from, although they may also accept connections with horizontal cells. The function of bipolar cells is to transmit

information from the photoreceptors or horizontal cells to the ganglion cells via graded potentials[4].

Amacrine cells act similarly to horizontal cells, acting mainly as a regulatory cell, although they also have unique differences from their counterparts. There are at least 29 different types of amacrine cells, each with a specific function[4]. Additionally, amacrine cells can actually outnumber retinal ganglion cells by a ratio of 15:1 and are responsible for up to 70% of the information collected by the ganglion cells[4].

Retinal ganglion cells are the last of the retinal cells involved in signal transduction and contain long axons that travel all the way to the brain. Together, these axons make up the optic nerve. A small percentage of retinal ganglion cells have little or no involvement in signal transduction and express an opsin called melanopsin similar to the photoreceptors[5]. These photosensitive ganglion cells are involved in synchronizing circadian rhythms and resizing the pupil in response to changing light levels[6].

Through a complex cascade the retina transforms information in the form of light into electrochemical signals that reach the brain. From the photosensitive rod and cone cells to the retinal ganglion cells that extend axons through the optic nerve and everything in between, the interconnected layers of cells that make up the retina work together to make sight possible. The system is not infallible however, and specific diseases target the retina in different ways.

1.3 Retinal Degeneration

Degenerative diseases of the retina, including retinitis pigmentosa and age-related macular degeneration, are characterized by photoreceptor loss and eventually lead to

irreversible visual disability[7-10]. Progress of retinal degeneration is typically slow, and many current clinical treatments focus primarily on delaying disease progression[11-13]. In the advanced stages of the diseases, photoreceptors are irreversibly lost due to the minimal innate ability of the eye to regenerate damaged tissue. To overcome this problem, a promising technique has emerged whereby an exogenous source of photoreceptors is introduced into the subretinal space[14].

During retinal degeneration, retinal circuitry initially remains intact, and implanted cells only need to make short synaptic connections to host tissue. Implanted multipotent retinal progenitor cells (RPCs) have been shown to migrate through a degenerating retina, extend processes as far as the optic nerve, and express markers of mature retinal neurons and glial cells[14-19]. Additionally, RPCs committed to a photoreceptor cell fate integrate, differentiate, form synaptic connections, and improve visual function upon implantation[20]. Despite these successes, bolus injections of cells to the subretinal space lead to a high degree of cell death[21]. Minimizing cell death during implantation and increasing the number of viable cells implanted are subsequently areas for significant improvement of retinal tissue engineering.

1.4 Retinitis Pigmentosa

The term retinitis pigmentosa describes a set of hereditary diseases that lead to death of rod and cone photoreceptors. To date, over 45 genes have been implicated in retinitis pigmentosa, although these genes only account for 60% of all retinitis pigmentosa cases, with the remaining 40% of cases resulting from unidentified genes[7]. Typically, retinitis pigmentosa first affects the rod photoreceptors in the eye, leading to

loss of night vision during adolescence, while the central vision is affected due to the loss of cone photoreceptors later in life[8] (Figure 1.3B). Approximately 1 in 4000 individuals are affected by retinitis pigmentosa, resulting in over 1 million affected individuals in the world today[7].

1.5 Age-related Macular Degeneration

Age-related Macular Degeneration (AMD) is the most common form of retinal degeneration and is also the leading cause of blindness in the United States in individuals over the age of 60[10] (Figure 1.3C). AMD mainly affects the elderly and is clinically divided into two subgroups: atrophic (dry or non-neovascular AMD) and exudative (wet or neovascular AMD)[22]. The dry form typically progresses slowly and is characterized by degeneration of the photoreceptors and retinal pigment epithelium (Figure 1.4A-C). Conversely, wet AMD can progress very quickly due to its vastly different pathology. Dry AMD is a pre-cursor to the wet form, in which the progression of dry to wet AMD is characterized by the formation of new blood vessels on the choroid known as choroidal neovascularization (CNV). These vessels often are not fully formed and can easily bleed, leading to scarring on the macula (Figure 1.4D). Other complications associated with CNV are retinal pigment epithelium detachment, subretinal hemorrhages, and fibrovascular disciform scarring, all of which can cause vision to rapidly deteriorate[10].

1.6 Diabetic Retinopathy

Both type 1 and type 2 diabetes mellitus can manifest in the eye and lead to diabetic retinopathy, characterized by damage and occlusion of small blood vessels in the

retina[1]. Complications of diabetic retinopathy can include dark spots in the field of vision, blurred vision, and blindness if left untreated[23] (Figure 1.3D). Typically, diabetic retinopathy is divided into two categories: nonproliferative and proliferative. The nonproliferative form of diabetic retinopathy results in thickening of the capillary endothelial basement membrane and a loss of pericytes, a support cell for small blood vessels[1]. The most drastic complication and cause of vision loss due to nonproliferative diabetic retinopathy is macular edema, although it is prevalent in only 10% of those with diabetes[1]. Proliferative diabetic retinopathy is characterized by neovascularization similar to wet AMD and results in the most severe ocular complications of diabetes mellitus[23]. It occurs in up to 50% of patients with type 1 diabetes[24] and 10% of patients who have had type 2 diabetes for 15 years[25].

1.7 Current Treatments for Retinal Degeneration

Treatment options for retinitis pigmentosa are limited and have been largely unsuccessful. Clinical trials have been performed to test whether high doses of vitamin A, vitamin E, and docosahexanoic acid, but results were mostly inconclusive[7]. In some cases the progression of the disease seemed to decrease with treatment, leading some clinicians to recommend adding daily supplements of vitamin A to those patients in the early stages of retinitis pigmentosa[7].

For dry AMD, the Age-Related Eye Disease Study (AREDS), a recent clinical trial by the National Eye Institute, found that increased intake of antioxidants and zinc slows the progression of dry AMD to the advanced stage[26]. Although treatments such as

this may for a time preserve vision in patients with early and intermediate AMD there is presently no cure for the disease.

There are currently three types of treatments for wet AMD that have shown to delay the progression the disease: laser photocoagulation, photodynamic therapy, and anti-Vascular Endothelial Growth Factor (anti-VEGF) therapy. Laser photocoagulation is used to destroy the new vessels formed through CNV but has several disadvantages. Laser treatment may damage other healthy areas of the eye near the leaky blood vessels and treatment often must be repeated, as the risk of re-growth of vessels after treatment is high. Additionally, laser photocoagulation is only appropriate for approximately 15% of patients with CNV, due to the restrictive nature of how it can be used[27].

Photodynamic therapy using the drug verteporfin has also been used as a treatment for wet AMD. This drug selectively binds to the leaky blood vessels caused by CNV and is then activated with a laser, resulting in clotting in the vessels. Photodynamic therapy results were initially encouraging, but later results showed that it induced an inflammatory response and contributed to the recurrence of CNV and is therefore no longer a preferred treatment for wet AMD[28], although its use in conjunction with other therapies is currently being investigated[29].

Anti-VEGF therapy was first used through the drug Macugen, an anti-VEGF pegylated aptamer delivered via intravitreal injection that was approved by the FDA in 2004[30]. More recently, Lucentis (Ranibizumab), a recombinant antibody fragment, has been approved and used extensively. Alternatively, Avastin (Bevacizumab), the full antibody that Lucentis is derived from, has been used off-label to treat wet AMD[31]. Anti-VEGF therapy requires monthly injections for treatment to be successful, and can even

improve visual acuity in patients with wet AMD[32]. Although the most effective treatment to stop the progression of wet AMD, anti-VEFG therapy will not cure the disease.

1.8 Retinal Tissue Engineering

Once retinal degeneration has reached the advanced stages and photoreceptors have been lost they cannot be regenerated. Many studies have investigated replacing degenerated photoreceptors with new cells such as RPCs via needle injection[20]. Although some implanted cells have been shown to incorporate into the host retina and express mature retinal cell markers, the vast majority of cells soon die after implantation. To preserve the fate of the implanted cells, polymer scaffolds have been generated to act as delivery vehicles for the implanted cells. The first such polymer scaffolds were fabricated from poly(L-lactic acid)/poly(lactic-*co*-glycolic acid) (PLLA/PLGA) and resulted in a ten-fold increase in cell delivery[21] (Figure 1.5). However, significant complications resulted from implantation including: inflammation, fibrosis, a significant foreign body response, and some cases led to retinal detachment due to scaffold thickness (~250 μm)[21, 33, 34].

To improve host response to implanted scaffolds, new materials were investigated. Ideally, a material would not induce an inflammatory response in the host, and would eventually degrade and be completely replaced by normal tissue. The next generation of implanted scaffolds, however, were fabricated from poly (methyl methacrylate) (PMMA), a non-degradable polymer[35]. The goal of this work was to determine if a thin film polymer could deliver progenitor cells to the retina as effectively as the thicker previous PLLA/PLGA version without damaging the host or causing

trauma. The advantage of using PMMA was that it could be spin-cast into a thin film fewer than 10 μm thick. In the design of the thin film one other variable was introduced. Pores approximately 11 μm in diameter were micromachined into the PMMA thin films to allow for nutrient diffusion from one side of the thin film to the other once implanted into the host retina. Figure 1.6 shows progenitor cell migration into the host retina after implantation of a PMMA thin film. After four weeks, the porous PMMA scaffolds successfully delivered 150% more progenitor cells to the animal hosts than the non-porous scaffolds, and the trauma associated with the previous thicker scaffolds was avoided[35].

Due to the success of the thinner polymer scaffold, significant interest was placed in finding a biodegradable polymer that could be spin-cast or otherwise fabricated into a thin film similar to the PMMA. Since then, two polymers have been used: poly (glycerol-sebacate) (PGS) and polycaprolactone (PCL). Similar to the porous PMMA scaffolds, microfabricated topographical cues were micromachined into the PGS scaffolds[36]. These 50 μm diameter wells provided secluded areas for the progenitor cells to attach to the polymer scaffolds (Figure 1.7). The PGS scaffolds were of an intermediate thickness (45 μm) compared to the PLLA/PLGA and PMMA scaffolds, but have not yet been implanted into host animals. PGS scaffolds have been used with mouse retinal explants, however, to model implantation and determine if progenitor cells grown on PGS will migrate into the host retina and differentiate into appropriate retinal neurons. Figure 1.8 shows the delivery of progenitor cells grown on PGS scaffolds and placed on top of retinal explants. Experiments were performed with wild type mouse explants (C57bl/6) and explants from a retinal degeneration model mouse (rho-/-).

Implanted progenitor cells survived on the retinal explants for an extended period and expressed markers for mature retinal cells[36].

PCL scaffolds did not contain the same sort of microfabricated topographical features as found in the PGS scaffolds but instead were nanostructured using an aluminum oxide template[37]. Progenitor cells were grown on PCL scaffolds containing short nanowires (SNW) (2.5 μm long), long nanowires (LNW) (27.5 μm long), and smooth PCL scaffolds. Similar to the PGS scaffolds, PCL scaffolds were grown on retinal explants to determine if implanted cells could survive extended periods of time and integrate into a host retina. Figure 1.9 shows progenitor cells grown on the different PCL scaffolds for 3 and 7 days. Interestingly, cells grown on different types of PCL demonstrated vastly different morphologies depending on the nanotopography of the surface. Cells grown on the SNW extended lamelapodia-like structures toward other cells, while cells grown on LNW retained a more spheroidal shape. Cells grown on smooth PCL attached randomly and also did not exhibit a vastly different morphology[37]. Cells grown on SNW and LNW and placed on retinal explants showed high levels of RPC integration into host retina and also expressed markers of mature retinal cells such as recoverin. Figure 1.10 shows progenitor cells delivered to a C57bl/6 (wild type) retinal explant via SNW or LNW scaffolds[37].

Retinal tissue engineering using polymer scaffolds is a promising technique that could eventually be used to treat or cure diseases such as age-related macular degeneration and retinitis pigmentosa. In the future, large animal studies using polymer scaffolds will need to be investigated to determine if retinal tissue engineering could be a viable treatment strategy for late stage retinal degeneration.

1.9 Intraocular Drug Delivery

The retina has long been a difficult target for drug delivery methods and devices. Topical eye drops, an effective and noninvasive method for treating multiple eye diseases, are ineffective at treating retinal diseases as the drugs do not efficiently reach the back of the eye. The blood-retinal barrier (BRB), similar to the blood-brain barrier, obstructs objects and large molecules circulating in the vasculature from gaining admittance to the retina[2]. The BRB is composed of the retinal vascular endothelium and the retinal pigment epithelium, two separate layers of cells that each contains tight junctions[38]. While this structural anatomy protects the retina from harmful exploits such as bacterial infections, it also effectively blocks most therapeutics such as antibodies from reaching disease-affected areas.

Anti-VEGF formulations such as Lucentis and Avastin have revolutionized the treatment of wet AMD but are unable to penetrate the blood-retinal barrier and must be repeatedly injected directly into the vitreous in order to reach the retina. Although an effective method, intravitreal injections are invasive and inconvenient for patients (Figure 1.11). Complications from intravitreal injections can include endophthalmitis, intraocular pressure elevation, cataracts, and retinal detachment[39]. Consequently, recent attention has been focused on the development of drug delivery devices that circumvent the blood-retinal barrier and limit the number of intraocular injections required for effective treatment.

Several sustained-release drug delivery devices have been developed for ocular diseases in the past several years. The most successful have mainly involved the use of

corticosteroids. One example, dexamethasone, has been used as an anti-inflammatory for many years, but its short half-life in the vitreous is problematic[40]. The Dexamethasone Posterior Segment Drug Delivery System (DEX-PS DDS), also known by its brand name Ozurdex, is made by Allergan Inc and is a biodegradable implantable device that can deliver therapeutic concentrations of dexamethasone for up to six months[39]. Recently, phase 2 clinical trials have shown that the surgically implanted DEX-PS DDS results in significant improvement in visual acuity and fluorescein leakage in patients suffering from persistent macular edema[41] and macular edema resulting from uveitis or Irvine-gass syndrome[42].

Fluocinolone acetonide (FA) is another corticosteroid currently under investigation or already used in multiple sustained-release devices. Retisert, manufactured by Bausch and Lomb, was FDA-approved in 2005 to treat uveitis[43] and is currently under investigation for the treatment of retinal vein occlusion and diabetic macular edema[39]. It designed to last up to three years and is a nonbiodegradable implant surgically implanted into the vitreous (Figure 1.12). Although a successful treatment for uveitis, it has also resulted in elevated intraocular pressure in a number of patients[44]. Recent studies have investigated re-implanting Retisert for chronic noninfectious posterior uveitis[45] and managing elevated intraocular pressure after receiving a Retisert implant[46].

Iluvien is another nonbiodegradable FA sustained-delivery device manufactured by Alimera Sciences that delivers a low dose of FA (0.2 or 0.5 μg/day) for up to three years[39]. This device is inserted into the vitreous using a proprietary injector system that targets the inferior vitreous and attempts to limit the elevation of intraocular pressure

(Figure 1.13). A recent phase 2 clinical trial using Iluvien reported sustained intraocular delivery of FA for over a year that resulted in improvement in visual acuity and mild increases in intraocular pressure[47].

Another Bausch and Lomb product, Vitrasert, was FDA-approved in 1996 to treat AIDS-related cytomegalovirus retinitis. This device provides the sustained-delivery of ganciclovir, an antiviral, into the vitreous for 5 to 8 months at a higher dose than possible intravenously[48].

Although effective in treating several eye diseases, these sustained-release drug delivery devices are ineffective at treating macular degeneration. Corticosteroids and antivirals are considerably more stable and therefore much simpler to deliver than antibodies or other proteins over a long period of time. However, anti-VEGF treatments have shown over the past several years to be the most effective treatment for any disease consisting of neovascularization, in particular wet AMD. A device able to deliver an antibody over a sustained period would therefore be highly advantageous for treating wet AMD and other eye diseases featuring neovascularization.

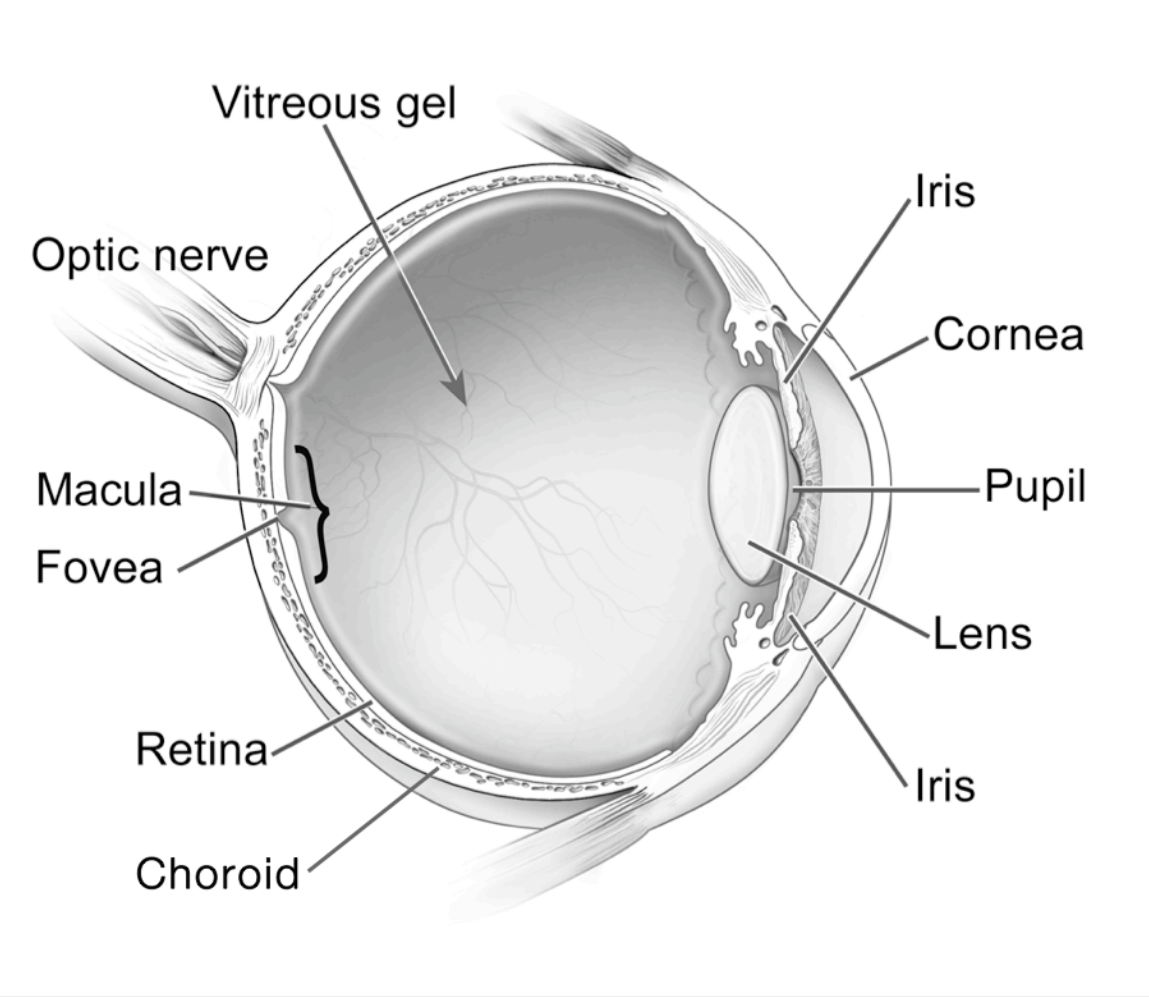

Figure 1-1: The human eye.

Light passes through the cornea and pupil and is refracted onto the retina by the lens. The iris controls the diameter of the pupil and also gives the eye its color. Inside the eye is the vitreous, a clear gelatinous avascular mass that remains stagnant in the eye. The choroid is a vascular layer of connective tissue that provides oxygen to the outer layers of the retina. Finally, the macula is a spot near the center of the retina that contains the fovea, the area of the eye with the highest concentration of cone photoreceptor cells. Image modified from the National Eye Institute (http://www.nei.nih.gov/).

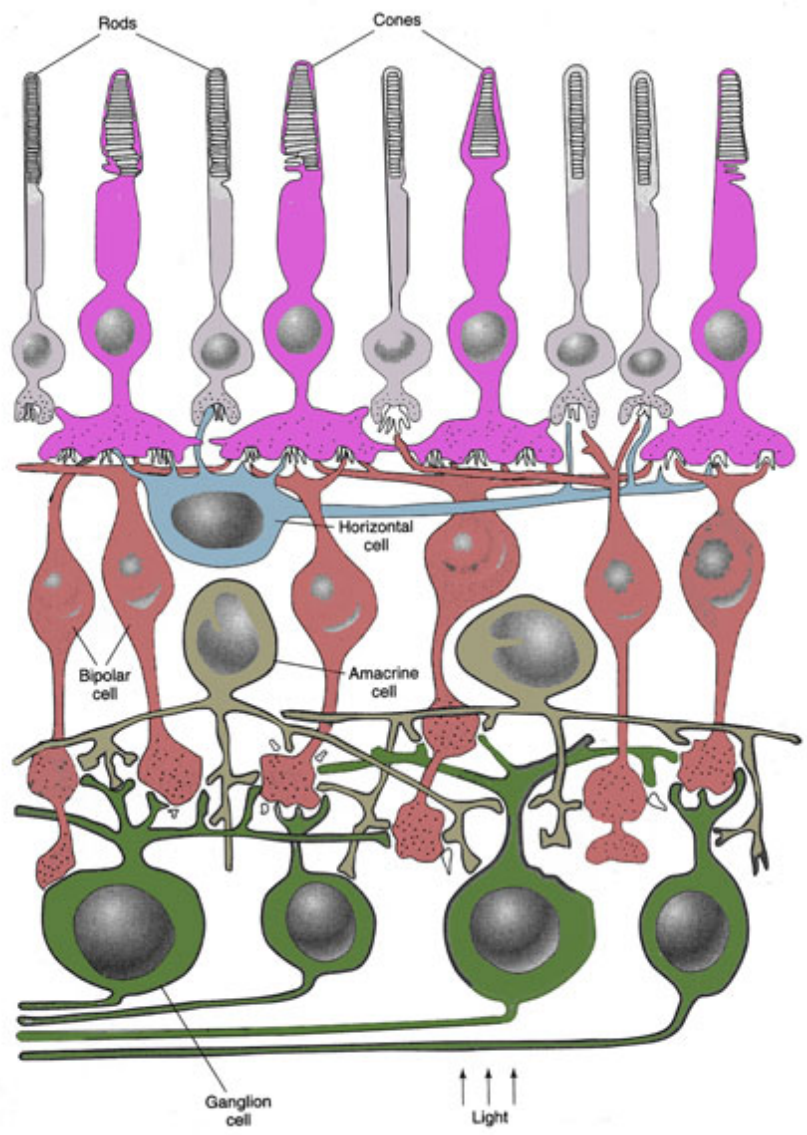

Figure 1.2: The Retina.

Light enters the eye and passes through several layers of cells before reaching the photosensitive rods and cones. Relatively sparse horizontal cells integrate information from several photoreceptors at once. Bipolar cells transmit information from the photoreceptors and horizontal cells to the ganglion cells, while amacrine cells regulate these transmissions. Image courtesy of Hugh J. Foley (www.skidmore.edu/~hfoley/images/Retina.jpg).

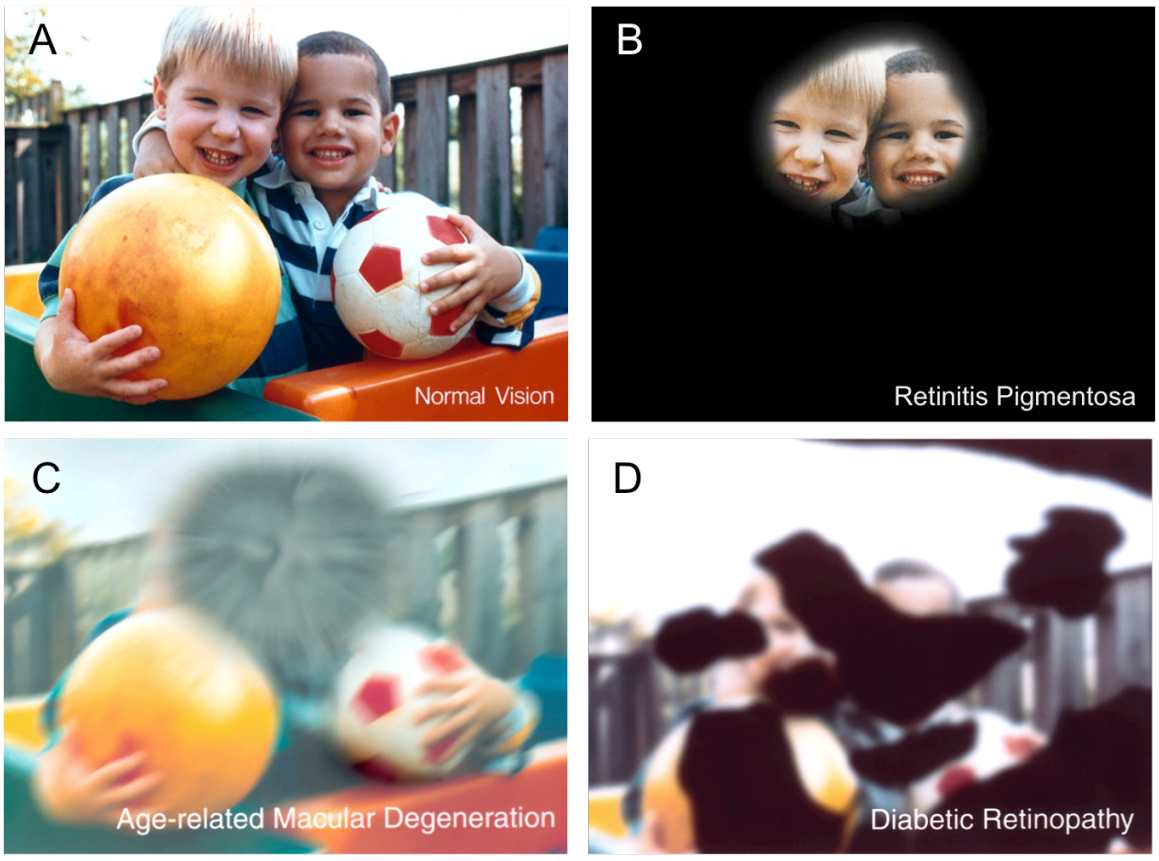

Figure 1.3: The effects of retinal degeneration.

(A) Normal vision of a particular scene is contrasted with what is seen from a patient suffering from (B) retinitis pigmentosa, (C) Age-related macular degeneration, and (D) diabetic retinopathy. Images courtesy of the National Eye Institute (http://www.nei.nih.gov/).

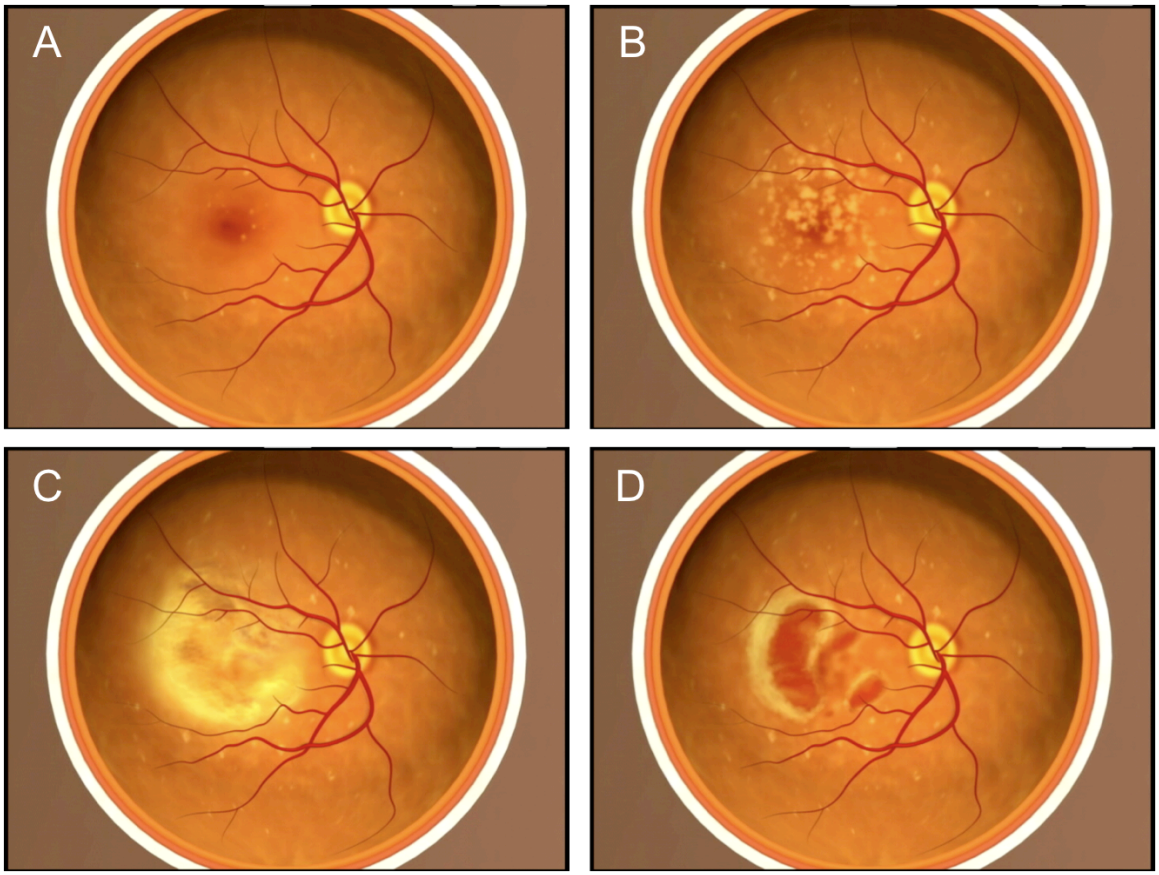

Figure 1.4: The forms of age-related macular degeneration.

Atrophic (dry) age-related macular degeneration progresses from an (A) early stage to an (B) intermediate stage and finally to an (C) advanced stage as shown by the amount of drusen accumulated on the macula. (D) Exudative (wet) AMD in contrast is characterized by the formation of fragile leaky blood vessels that form scars on the macula. Images courtesy of the National Eye Institute (http://www.nei.nih.gov/).

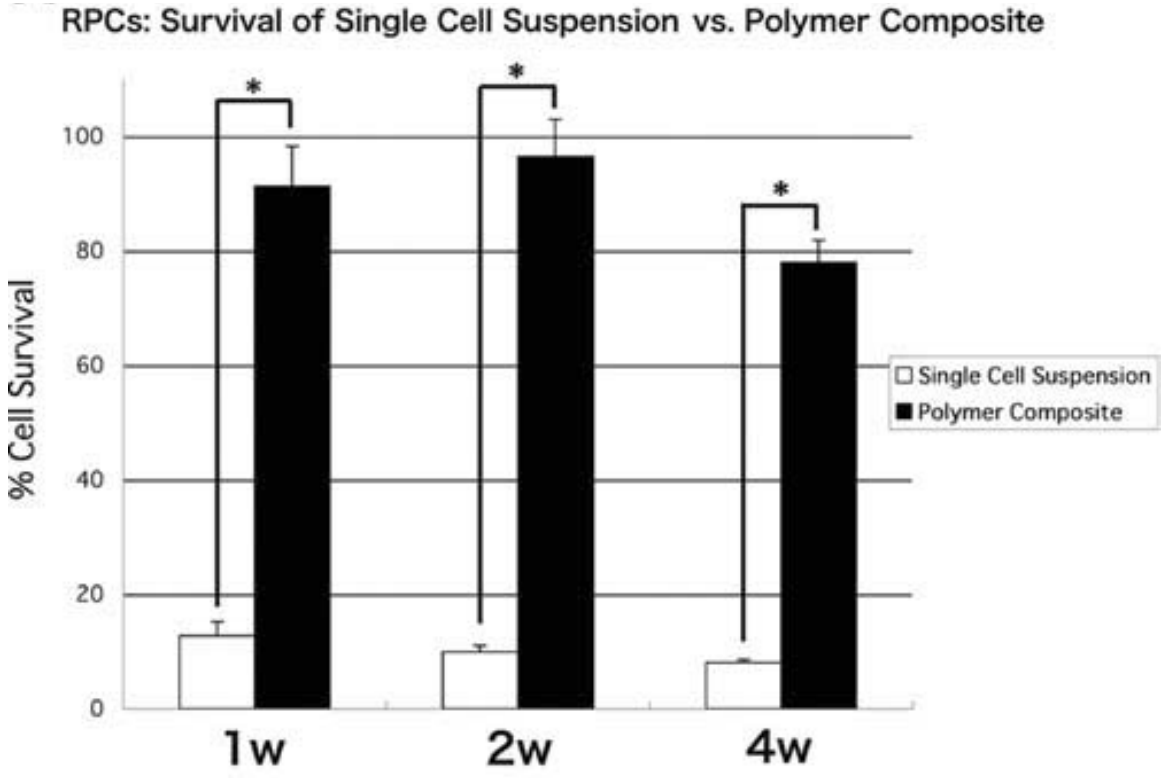

Figure 1.5: Retinal progenitor cell survival on polymer scaffolds.

Percent survival of implanted cells after 1, 2, and 4 weeks when implanted on a polymer composite versus a single cell suspension. Polymer scaffolds increase cell survival by approximately 10-fold. (Tomita et al., Stem Cells 2005).

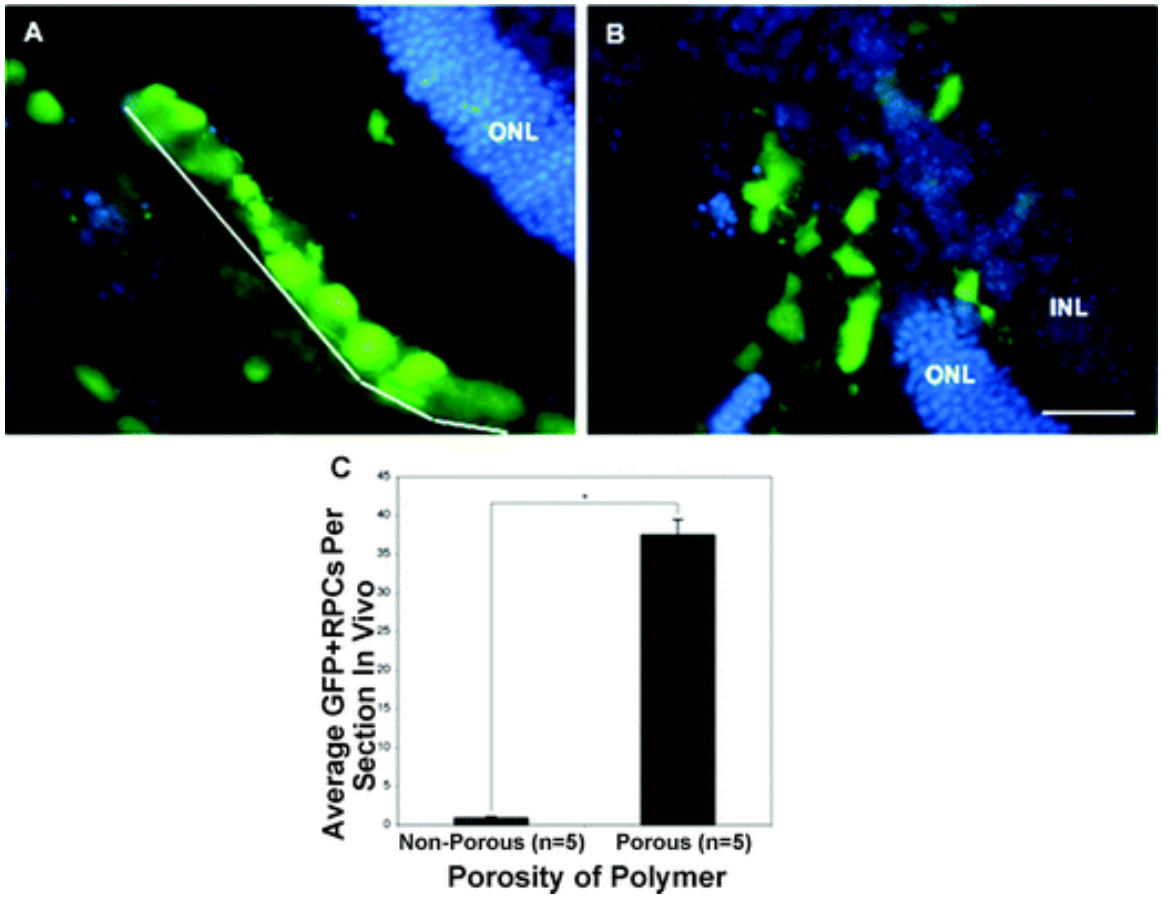

Figure 1.6: Implanted retinal progenitor cells using a PMMA scaffold.

(A) GFP+ progenitor cells implanted into the subretinal space of host mice. The white line represents the PMMA scaffold. (B) Progenitor cells migrating into the outer nuclear layer (ONL) and inner nuclear layer (INL) of the host retina. Scale bar (A,B) represents 50 µm. (C) Progenitor cell survival *in vivo* on porous and non-porous PMMA scaffolds four weeks after implantation. *$p<0.05$, Student's t-test. (Tao et al., Lab on a Chip 2007).

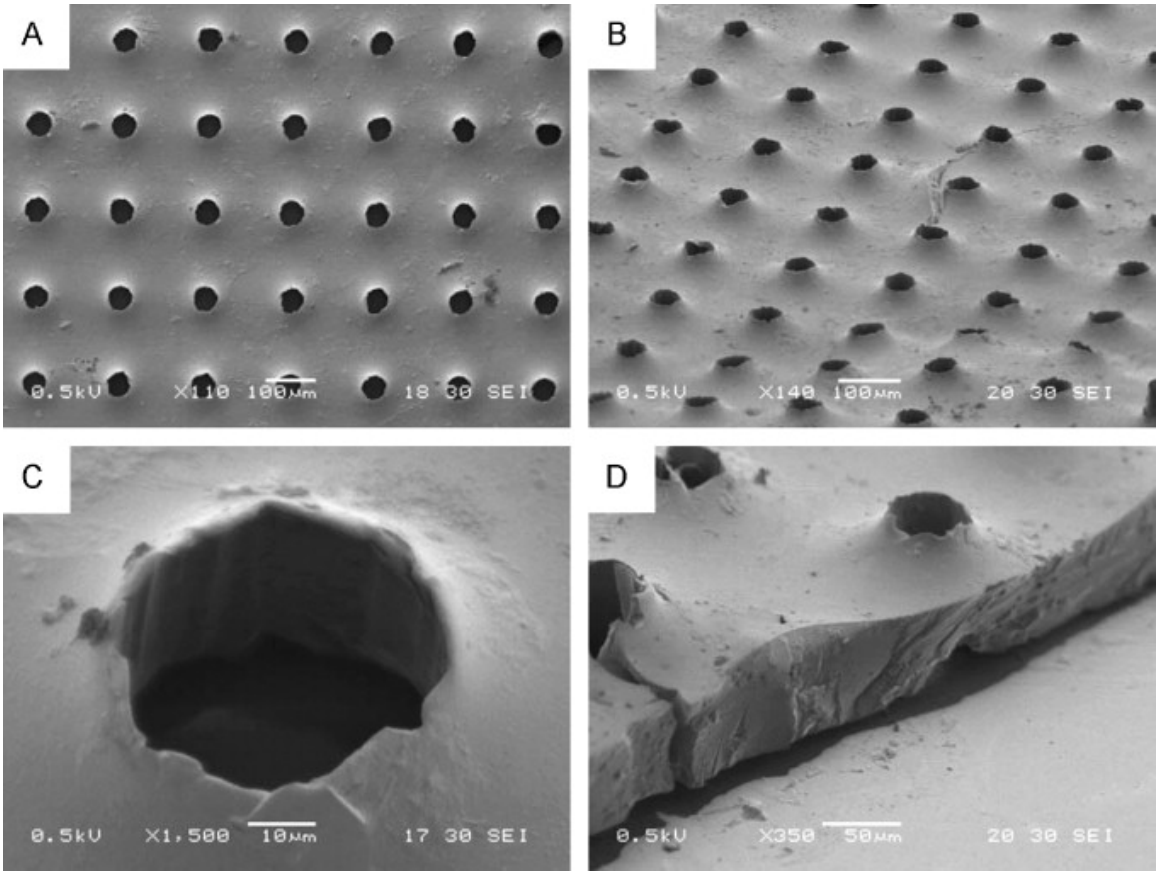

Figure 1.7: A PGS scaffold for retinal tissue engineering.

PGS scaffold containing 50 µm diameter microwells. (A) Top view. (B) View of scaffold at 60°. (C) Magnified view of microwell at 30°. (D) View of the edge of the scaffold at 60°.

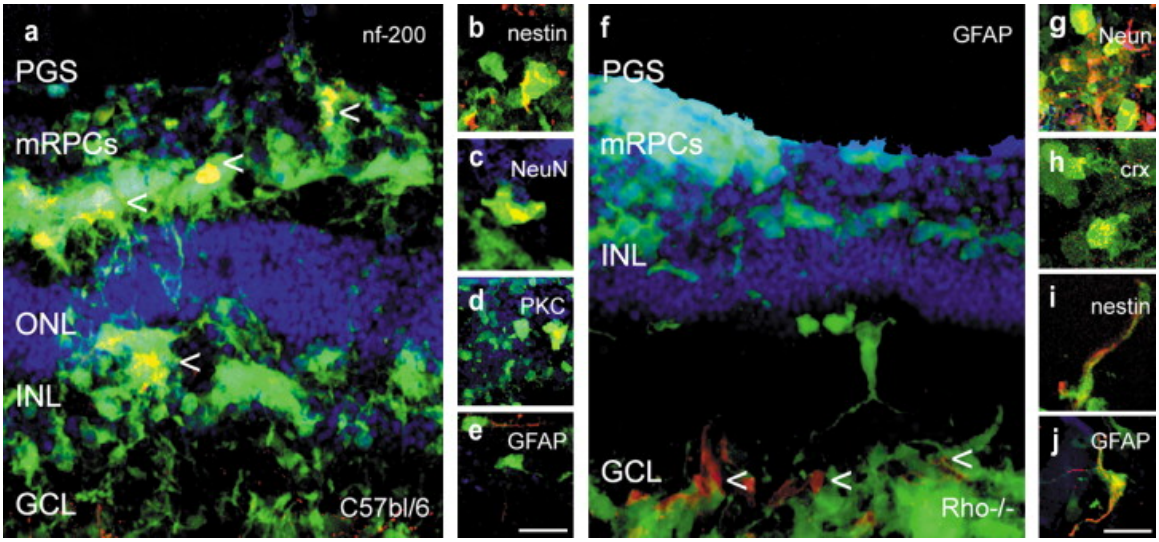

Figure 1.8: Retinal progenitor cells delivered to mouse retinal explants.

Delivery of mouse retinal progenitor cells (mRPCs) via a PGS scaffold to mouse retinal explants from wild type (C57bl/6) and a model for retinal degeneration (Rho-/-). (A) C57bl/6 explant. (B) Delivered progenitor cells expressed nestin in the outer nuclear layer (ONL), (C) NeuN (neuronal nuclei) in the ONL, (D) PKC in the inner nuclear layer (INL), (E) and GFAP in the ganglion cell layer (GCL). (F) Rho-/- explant. (G) Progenitor cells still attached to the PGS scaffold labeled for NeuN, (H) cells that migrated to the INL expressed crx, (I) nestin in the INL, and (J) GFAP in the GCL region. Scale bar represents 25 μm. (Redenti et al., Biomaterials 2009).

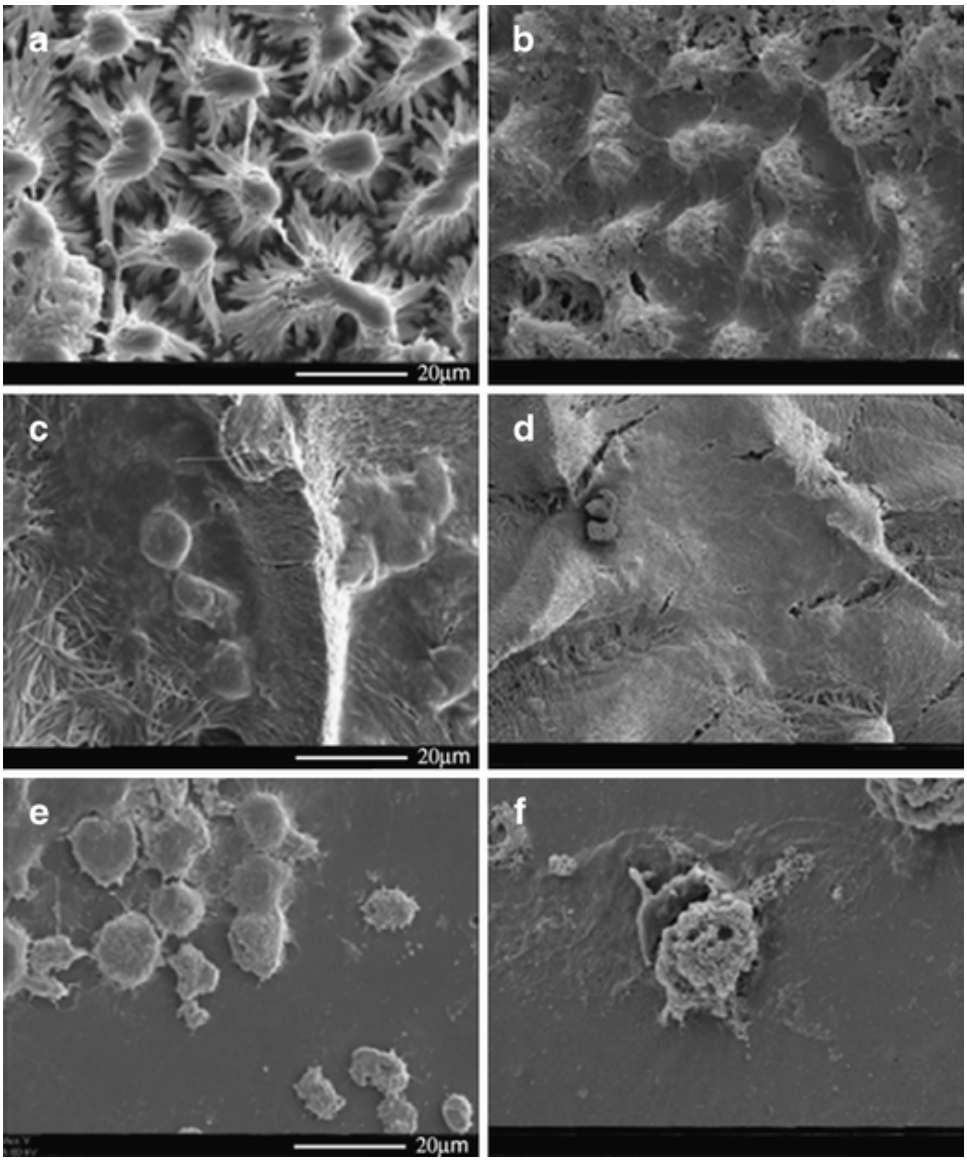

Figure 1.9: Mouse retinal progenitors grown on nanostructured PCL.

Scanning electron micrographs of progenitor cells grown on (A,B) SNW, (C,D) LNW, and (E,F) smooth PCL for 3 (A,C,E) and 7 days (B,D,F). (Redenti et al., J Ocul Biol Dis Inform, 2008).

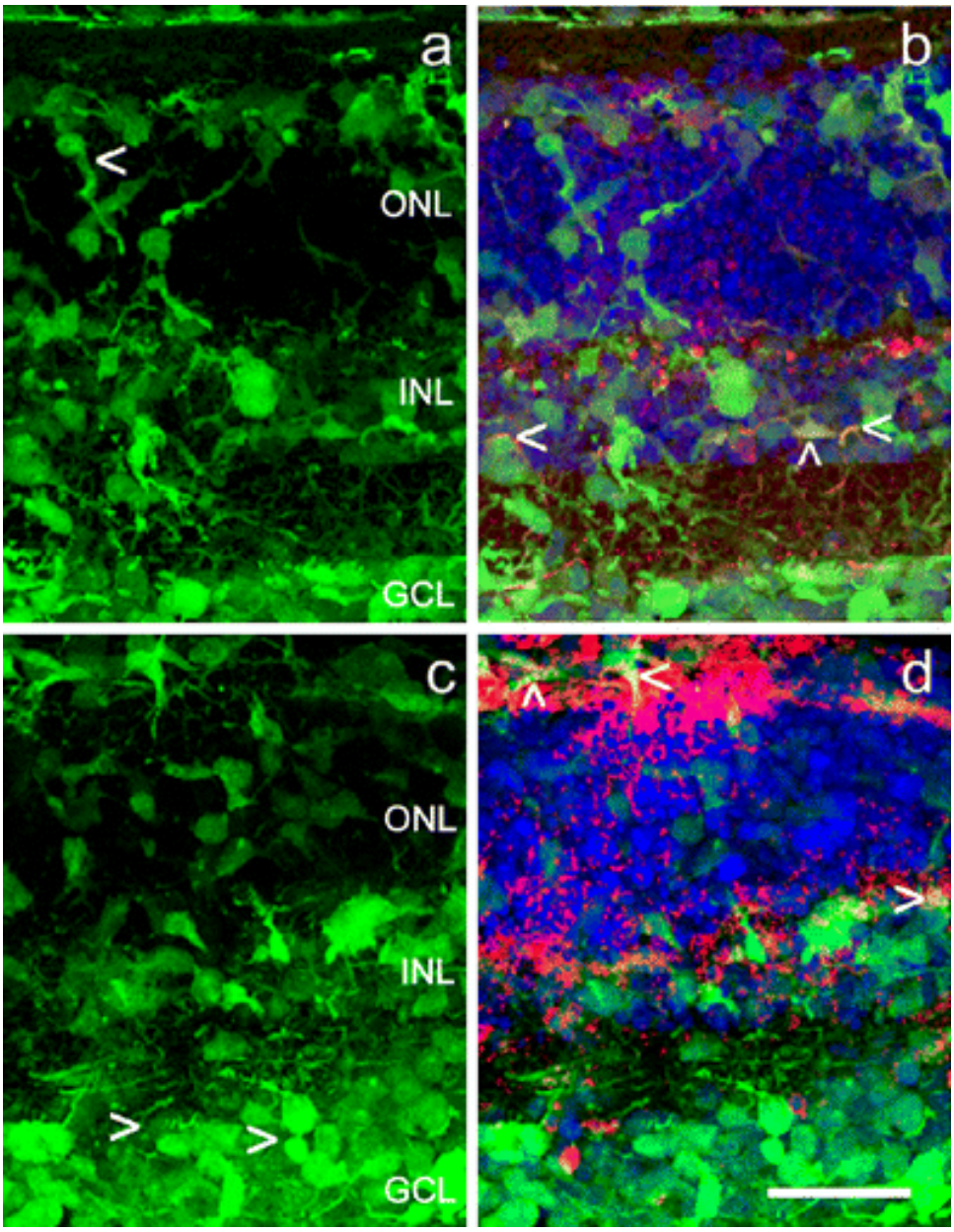

Figure 1.10: Delivery of progenitor cells to mouse retinal explants.

Progenitor cells delivered to C57bl/6 retinal explants via SNW (A,B) and LNW (C,D) PCL scaffolds. (B) PKC labeling and (D) recoverin labeling (red) demonstrated expression of mature retinal markers in implanted cells. (Redenti et al., J Ocul Biol Dis Inform, 2008).

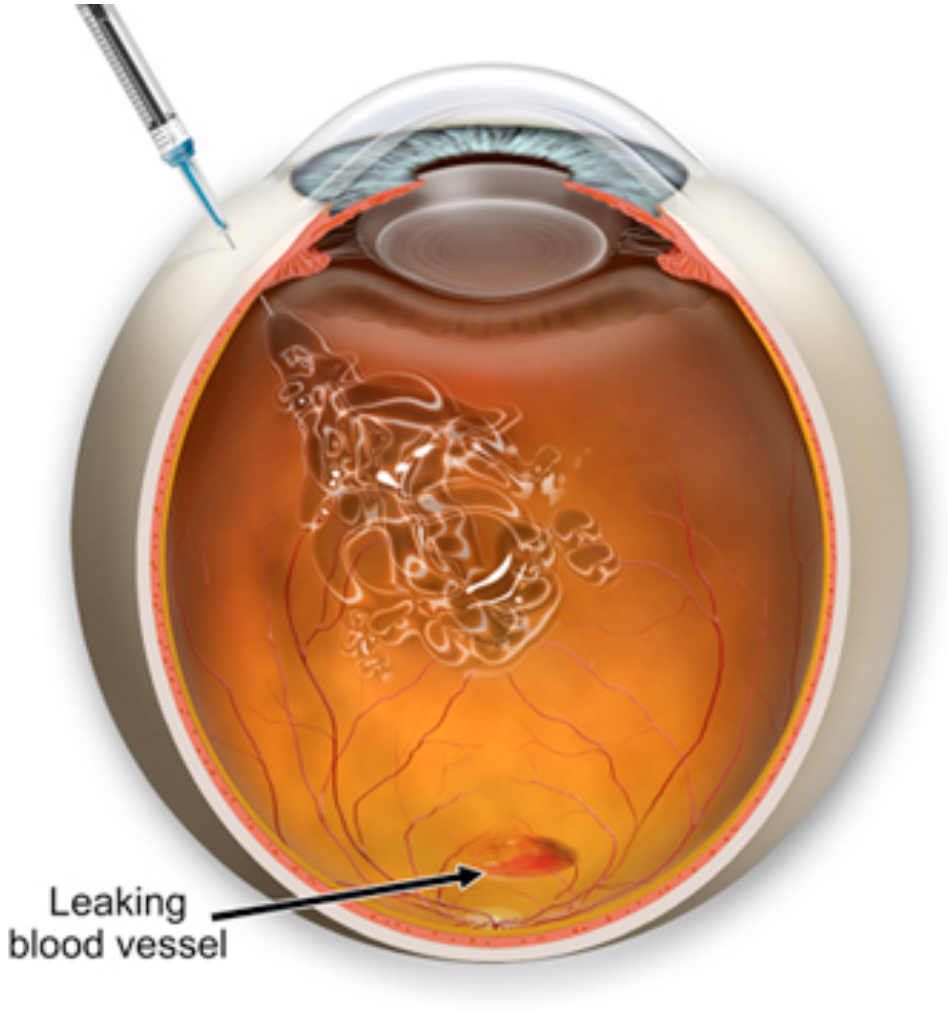

Figure 1.11: Intravitreal injections.

Itravitreal injections are a common yet invasive method for introducing anti-VEGF treatments into the eye. Image courtesy of the Medical Management Services Group (http://www.seewithlasik.com/docs/macular-degeneration-treatments.shtml).

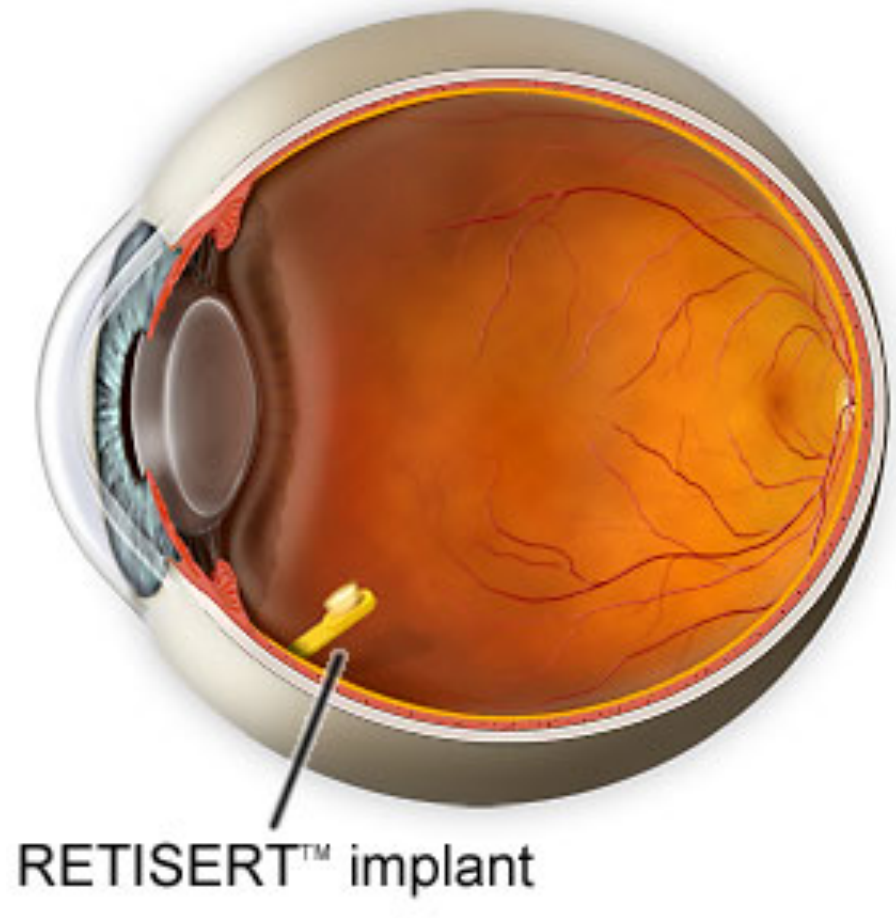

Figure 1.12: Retisert.

The Retisert implant manufactured by Bausch and Lomb is a nonbiodegradable implant surgically placed in the vitreous that is designed to release fluocinolone acetonide over a period of 3 years. Image courtesy of the Macula Center (http://www.maculacenter.com/Procedures/retisert.htm).

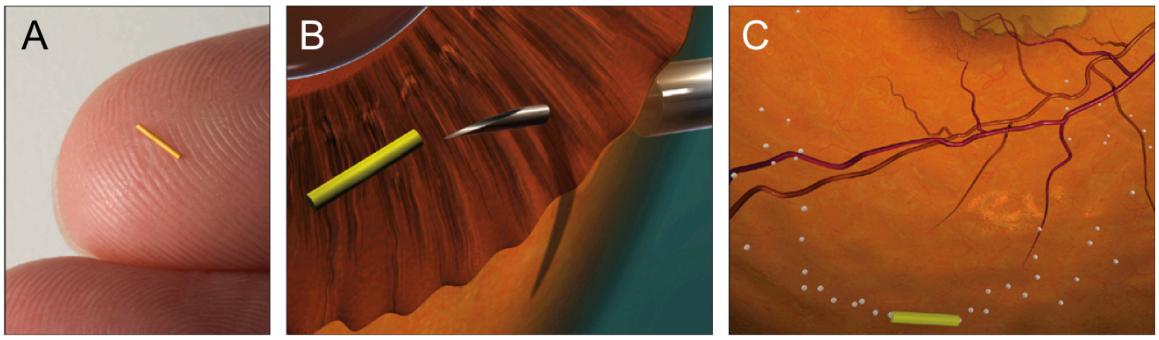

Figure 1.13: Iluvien.

Iluvien is a nonbiodegradable sustained-delivery device used to treat uveitis that delivers fluocinolone acetonide (FA) directly into the vitreous. (A) The insert is 3.5 mm long and 0.37 mm in diameter, shown next to a human finger for reference. (B) Iluvien is injected into the vitreous using a proprietary injector system and (C) releases FA into the vitreous cavity for up to three years. Images courtesy of Retinal Physician (http://www.retinalphysician.com/article.aspx?article=102296).

Chapter 2 – Methods

2.1 Scanning Electron Microscopy

A scanning electron microscope (SEM) generates high magnification images of a surface by bombarding it with high-energy electrons. SEMs can generate images of much higher magnification than other methods such as optical microscopy, as the image magnification is not directly related to the power of an objective lens but rather to the spot size generated by its electron source. Because of this, a SEM can generate images of a surface magnified 30,000X, corresponding to a spatial resolution of less than 100 nm[49].

An electron gun aims a focused beam of electrons at the sample surface and detects secondary electrons. In order to generate images, the beam raster-scans the area at a high frequency. The beam of electrons hitting the sample surface generates multiple signals, including secondary electrons, backscattered electrons, characteristic X-rays, visible light, and heat, although an SEM will rarely have detectors for all types of signals. Nearly all SEMs come equipped with a secondary electron detector, which is used to generate the high-resolution images SEMs are known for, and most will also have a second detector for one of the signals mentioned previously. A diagram of a typical SEM is shown in Figure 2.1, containing both a secondary electron detector and a backscattered electron detector. The diagram also contains two condenser lenses used to focus the electron beam on the surface and a pair of deflection coils used to deflect the beam in x and y directions to allow for raster scanning of the surface.

A conventional SEM will only image electrically conductive and grounded samples. Objects such as metal can normally be imaged easily, however non-conductive

materials will accumulate electrostatic charge, resulting in image artifacts and other problems. Consequently, non-conductive materials are often coated with a thin layer of conductive material, typically gold or a gold/palladium alloy, using a sputter coater to prevent the accumulation of electrical charge. In addition to making possible the imaging of non-conductive samples, sputter coating can improve the resolution and signal generated from a sample by increasing the amount of backscattering and secondary electron emission at the sample surface.

SEM also requires that samples be completely dry before imaging, as the sample is held under high vacuum during the imaging process. For biological samples this can be problematic as living cells and tissues require fixation before imaging can occur. Typical fixatives include buffered solutions of glutaraldehyde or combinations of glutaraldehyde and formaldehyde that act to preserve and stabilize sample structures before imaging[50]. After fixation, samples are dehydrated, often using ethanol or other organic solvents, before they are mounted on a specimen stub, sputter coated, and imaged.

2.2 Fluorescence Microscopy

Fluorescence occurs when a molecule absorbs light at a particular wavelength and later emits light at a different wavelength. Fluorescent molecules, or fluorophores, can exist at different energy states represented by a Jablonski diagram (Figure 2.2)[51] and are usually found in the ground state known as S_0. However, if a photon of sufficient energy is absorbed by the fluorophore, it enters an excited state known as S_1. Once in the excited S_1 state, a small amount of energy is lost through heat in a process known as

vibrational relaxation, after which the fluorophore returns to the ground state by emitting a photon (Figure 2.2a)[51].

Typically, the emitted photon has a longer and therefore lower energy wavelength due to the energy lost during vibrational relaxation. This difference in energy and wavelength between the absorbed and emitted photons is known as the Stokes shift. Larger Stokes shifts are often more desirable in fluorescence imaging as it is easier to separate the excitation light from the emitted light using filters (Figure 2.3)[51].

There exists a special case in which the emitted photon can be of a lower wavelength than the absorbed photon. In two-photon excitation, a fluorophore can simultaneously absorb two photons of the same wavelength, and the emitted photon can be of a shorter wavelength than the absorbed photons (Figure 2.2b)[51].

2.3 Microfabrication

The adaptation of technology from the microelectronics industry to study biology has transformed our understanding of how cells and tissues interact with their surrounding microenvironments. This use of technology, collectively known as microfabrication, has mostly utilized two compounds, SU-8 and poly(dimethylsiloxane) (PDMS), to fabricate three-dimensional patterns on the microscale. Typically these patterns are then used for two different experimental platforms: micro-contact printing or microfluidics, although several other platforms using other materials have been developed recently, including one which was used extensively in this work.

Microfabrication begins in a clean room with a photomask and a silicon wafer coated with SU-8, an epoxy-based negative photoresist (Figure 2.4). The photomask can

be either a piece of glass or transparent flexible plastic that contains opaque regions in a desired pattern. The photomask is placed directly above the SU-8-coated silicon wafer and exposed to ultraviolet light. The transparent regions of the photomask allow the ultraviolet light to pass through, crosslinking the exposed SU-8. The opaque regions on the photomask block the ultraviolet light, leaving the regions below unaffected. After the wafer is exposed to ultraviolet light it is submerged in a developer solution, which washes away the regions of SU-8 that were not photocrosslinked.

The resulting "master" wafer can be used for replica molding outside the clean room to make multiple copies of the desired three-dimensional pattern. Typically, these are constructed from PDMS, which is poured onto the master wafer in liquid form and cured until it forms a solid transparent rubber mold. The resulting PDMS molds can then be used as stamps for micro-contact printing[52, 53], stencils[54], microfluidics[55, 56], and other applications[57, 58]. For the research described in this dissertation the PDMS was instead used as another three-dimensional mold to fabricate polycaprolactone (PCL) thin films. As with the SU-8/PDMS molding, the microfabricated features from the PDMS transfer to the PCL thin films in a negative fashion. Thus, the features present in the PCL thin films mirror those found on the master wafer and are the opposite of those found on the PDMS mold.

The PCL thin films are spin cast using a solution of PCL dissolved in 2,2,2-trifluoroethanol. During spin casting, the liquid PCL forms a solid polymer thin film than can easily be peeled from the PDMS surface due to the flexibility of the PDMS. PCL can also be peeled from a flat silicon wafer surface but not from a patterned SU-8 surface as the PCL will stick to SU-8. Using the spin casting procedure, PCL thin films can be

fabricated fewer than ten micrometers thick. Varying the spin speed and PCL concentration can produce thin films anywhere from less than one micrometer thick to approximately one hundred micrometers thick. The majority of thin films used in the research presented in this dissertation were approximately six micrometers thick[59].

2.4 Profilometry

A profilometer is an instrument used to render a profile of the features or roughness of a surface. Although optical profilometers that do not rely on contact between a probe and the sample surface exist, typical profilometers use a diamond-tipped stylus in contact with a surface to generate a two dimensional representation of the surface characteristics. Once the stylus is lowered vertically into contact with the sample surface, it is dragged across the plane of the surface for a specified distance using a specified force. A typical profilometer can distinguish vertical features as large as a millimeter, with the most proficient measuring vertical steps as small as ten nanometers. For experiments described in this dissertation, profilometry was used to verify the size and uniformity of microfabricated SU-8 photoresist features on Silicon wafers.

2.5 Retinal Progenitor Cell Culture

Retinal Progenitor Cells were cultured in NeuroBasal Complete medium containing 2 mM L-Glutamine, 100 μg mL^{-1} penicillin-streptomycin, 20 ng mL^{-1} epidermal growth factor, 1X B27 neural supplement and 1X N-2 supplement. Full instructions for thawing frozen cells, feeding and passaging cells, and freezing cells are listed in the Appendix.

2.6 Reverse transcription quantitative real time polymerase chain reaction (qPCR)

Polymerase chain reaction (PCR) has revolutionized the study of biology since its development in the early 1980s. PCR is a method to amplify copies of DNA exponentially, generating millions of copies of a piece of DNA from a small number. The technique requires a thermal cycling process, in which the temperature of the system oscillates between a high temperature for DNA melting and a low temperature during which the DNA replicates.

The main components required for PCR to occur are primers and DNA polymerase (Figure 2.6)[60]. Primers are short sequences of DNA that bind to complementary regions on the single stranded melted DNA sequences. Once bound, the DNA polymerase catalyzes the polymerization of the single stranded DNA into double stranded DNA. Both of these components had been in use before the development of PCR for procedures such as DNA sequencing, but the discovery and use of a special DNA polymerase finally made PCR possible.

The high temperature required to denature double stranded DNA inactivated the DNA polymerase from E. coli that had been used for other procedures, rendering it useless. DNA polymerase known as Taq polymerase from Thermus aquaticus, a bacterium found in hot springs and hydrothermal vents, was found to be stable above the high melting temperature required for DNA melting. Its use in PCR made it unnecessary to add new DNA polymerase to the reaction with each cycle of replication, making PCR possible in a single tube.

After PCR became a commonly used laboratory technique the same principles were used to generate a technique in which the number of copies of the desired DNA sequences could be quantified. The ability to directly generate DNA from RNA, a process known as reverse transcription, also made it possible to quantify gene expression. Together, these processes make up reverse transcription quantitative real time polymerase chain reaction (qPCR).

While qPCR is used to generate and quantify large amounts of DNA, it is mainly used in gene expression analyses. Gene expression is regulated by messenger RNA (mRNA), with the number of copies of mRNA of a gene transcript corresponding to its expression rate. In order to use qPCR for gene expression analyses, mRNA is isolated and then reverse transcribed into complementary DNA (cDNA), which can then be amplified using PCR.

For all qPCR experiments used in the research described in this dissertation the fluorescent dye SYBR Green was used to quantify PCR products. SYBR Green preferentially binds to double-stranded DNA, resulting in increased fluorescence at the end of each PCR cycle as the amount of double-stranded DNA increases. Although this fluorescence can be quantified very accurately it cannot be directly associated with mRNA expression as it has no absolute units. Therefore, results are compared with known units via a standard curve and a control gene known as a housekeeping gene. The particular housekeeping gene used for the experiments described in this dissertation was glyceraldehyde 3-phosphate dehydrogenase (GAPDH), an enzyme that is involved in glycolysis that is highly expressed in most cells and tissues.

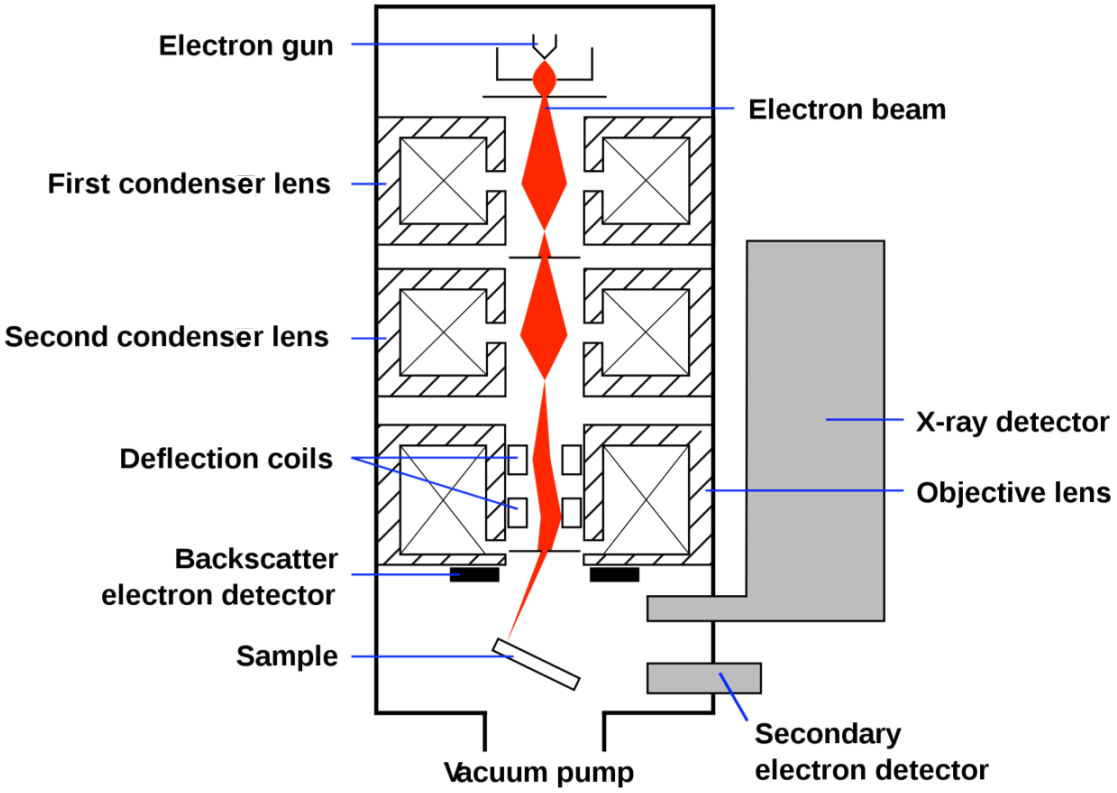

Figure 2.1: Scanning electron microscopy.

Diagram of a typical scanning electron microscope (SEM). An electron gun generates an intense beam of electrons that is directed through two condenser lenses and deflection coils and onto a sample surface. A backscatter electron detector and a secondary electron detector collect electrons from the sample surface and generate high-resolution images. Samples must be held under vacuum. Image courtesy of Wikipedia (http://en.wikipedia.org/wiki/Scanning_electron_microscope).

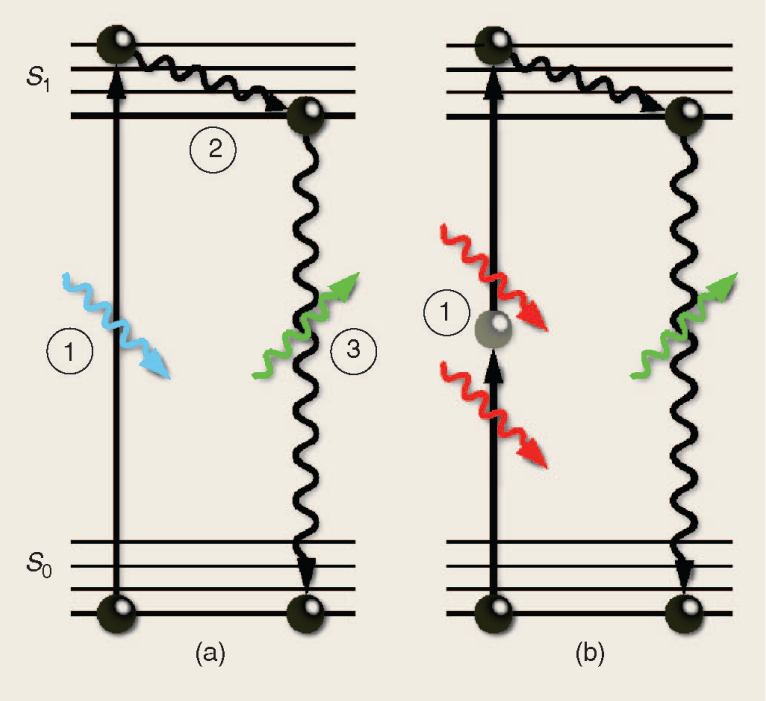

Figure 2.2: Jablonski diagrams.

Jablonski Diagrams represent the electronic states of a molecule and the transitions in between the different states[51]. (a) A molecule in the ground state S_0 absorbs a blue photon (1) and enters the S_1 excited state. The instability at this excited state results in vibrational relaxation (2) and a small amount of energy lost due to heat. The molecule returns to the ground state (3) by emitting a green photon. The emitted photon has less energy than the absorbed photon and therefore a longer wavelength. (b) During two-photon excitation, a molecule enters the excited state by simultaneously absorbing two photons of lower energy (1). The single emitted photon therefore has a shorter wavelength than the two absorbed photons.

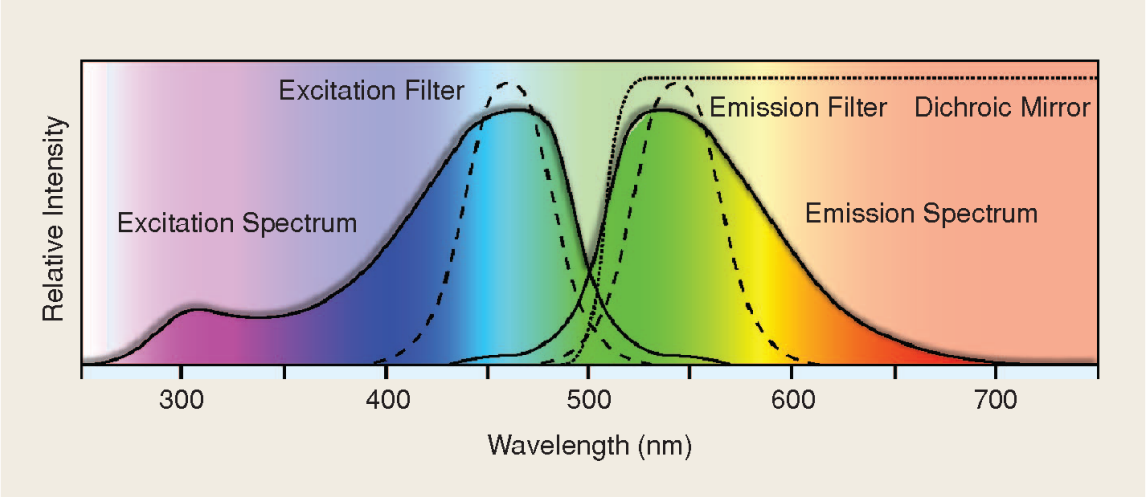

Figure 2.3: Fluorescence excitation and emission spectra.

A typical fluorescence excitation and emission spectra of a fluorophore[51]. An emission spectrum is generated by scanning the wavelengths of the emitted light while holding the excitation light at a constant wavelength. In contrast, an excitation spectrum is the opposite, so the emitted light is held at a constant wavelength while the excitation light is scanned through many different wavelengths. The Stokes shift is the difference between the maxima of the excitation and emission spectra. Larger Stokes shifts allow for easy separation of the excitation and emission by filters (larger dashed lines). Typical fluorescence microscopes also contain a dichroic mirror (smaller dashed line) that selectively reflects or passes light based on wavelength.

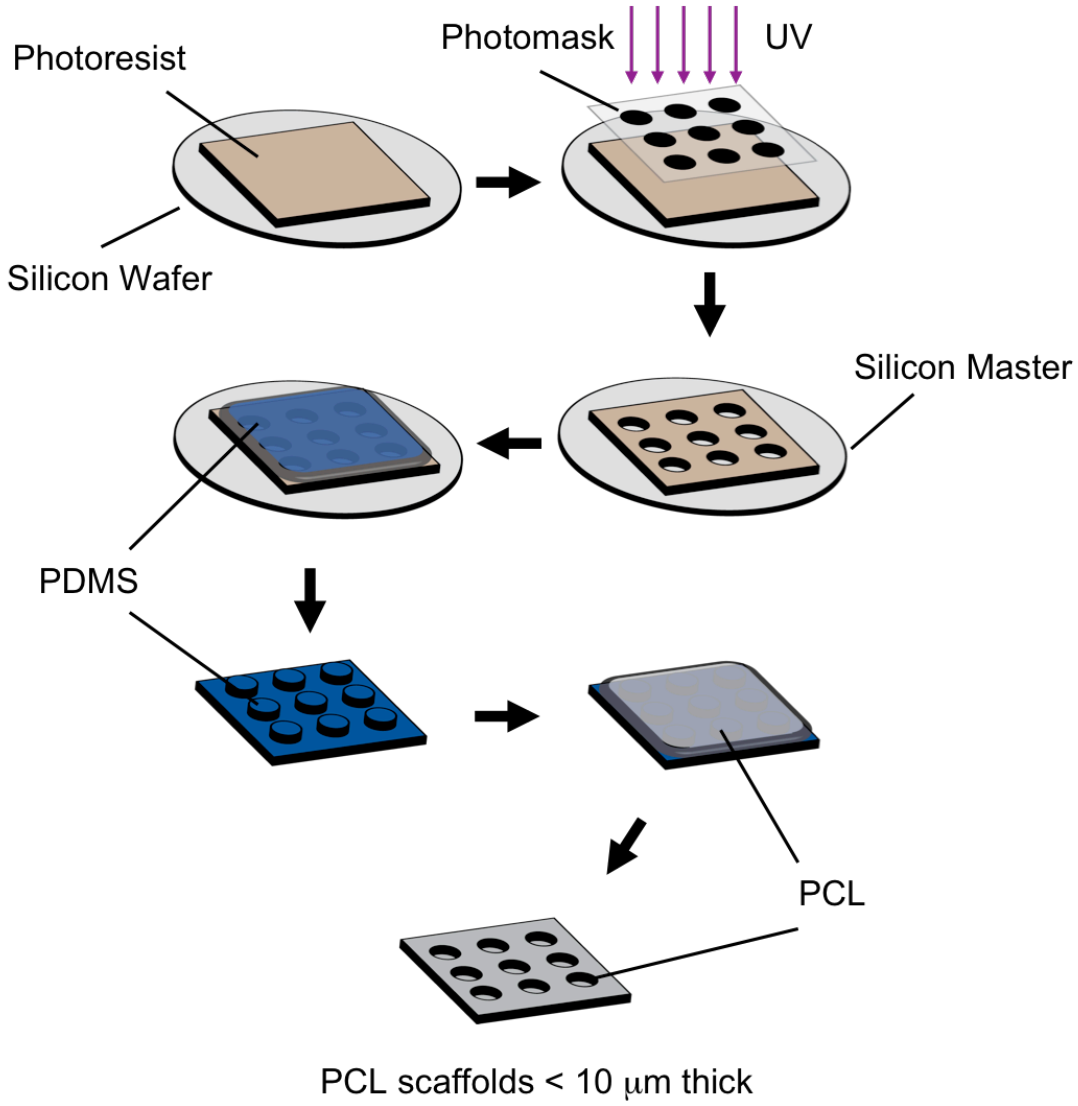

Figure 2.4: Polycaprolactone thin film microfabrication.

Photoresist is spin-cast onto a Silicon wafer and exposed to ultraviolet light through a photomask. Areas of the photoresist that are left unexposed due to the photomask are developed away, resulting in a Silicon master wafer that can be used for replica molding. Poly(dimethylsiloxane) (PDMS) is poured over the master and cured to form a negative mold of the master wafer. Polycaprolactone (PCL) is then poured onto the PDMS mold and spin cast to form a polymer thin film that can be peeled from the PDMS surface.

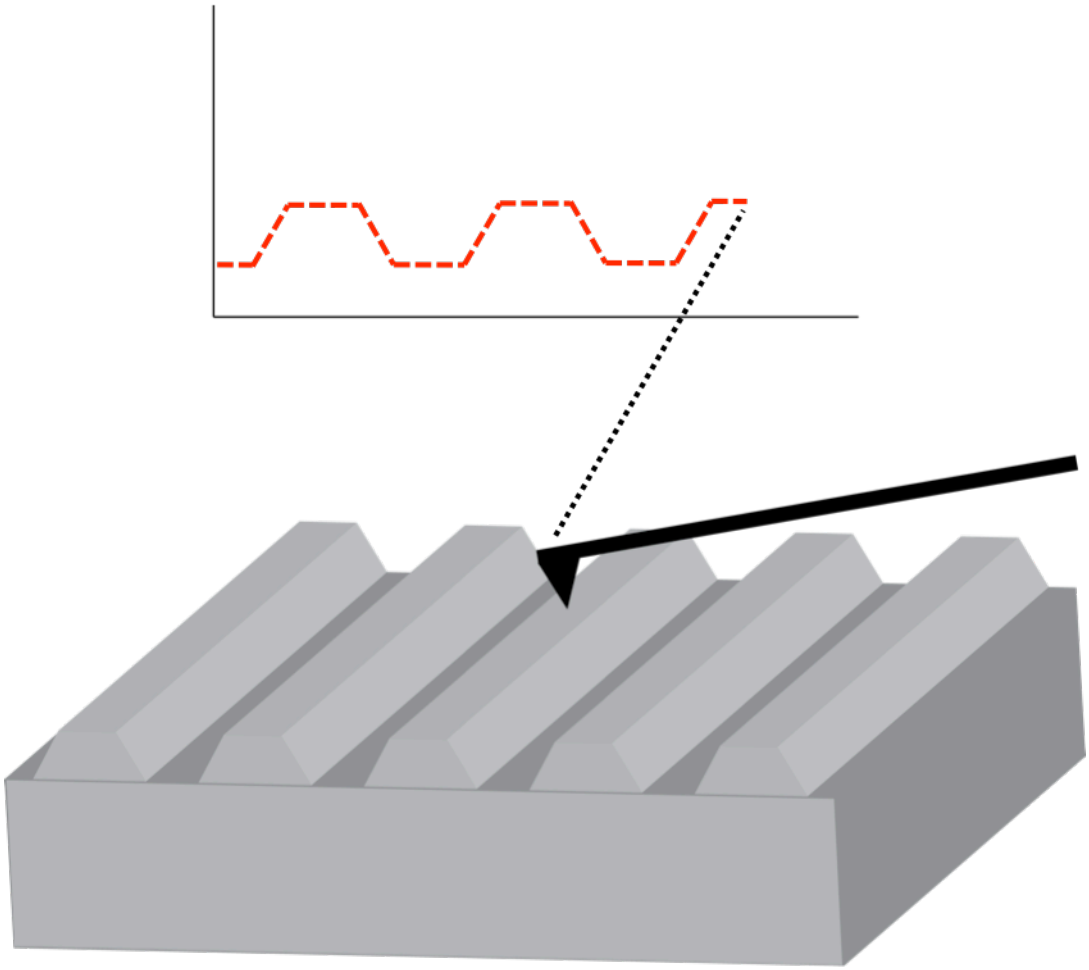

Figure 2.5: Profilometry.

Diagram of a profilometer. A diamond-tipped stylus is dragged across a surface at a known speed and force. The vertical movement of the stylus during this process is tracked, and a two-dimensional graphical representation of the surface roughness is plotted.

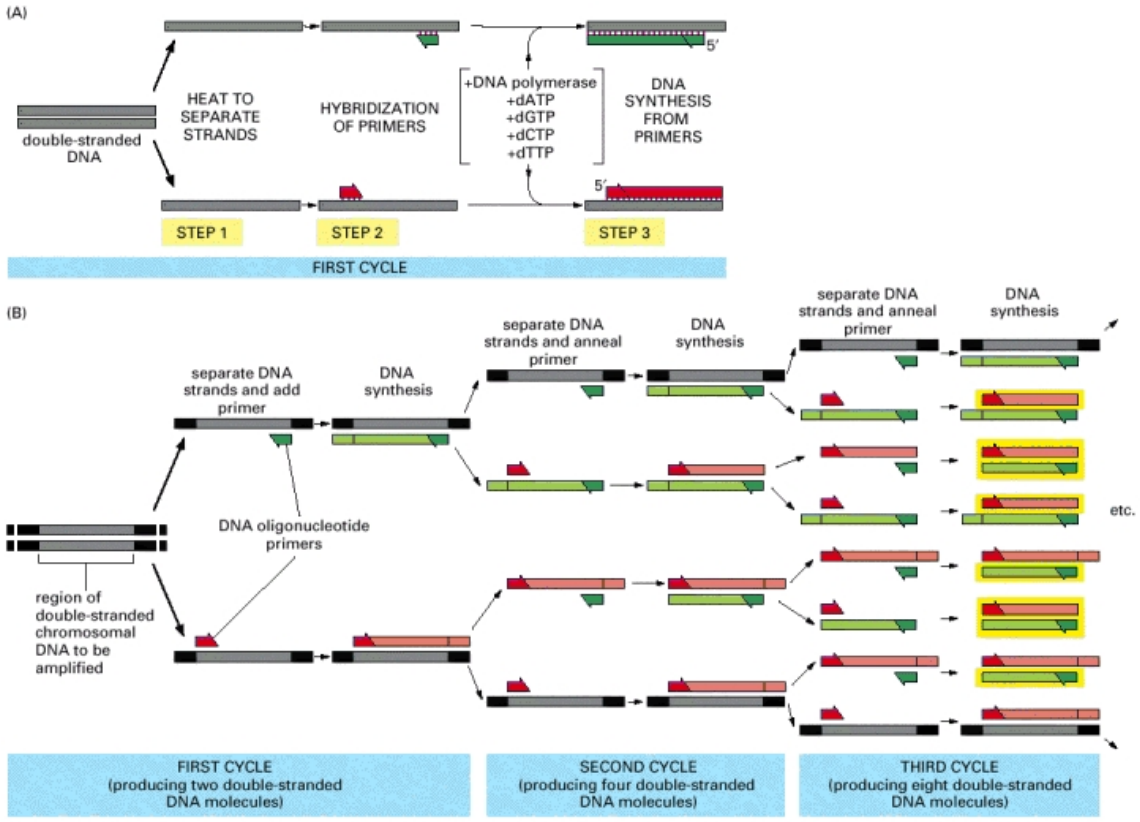

Figure 2.6: Quantitative polymerase chain reaction.

Polymerase chain reaction (PCR)[60] diagram. (a) In the first cycle of PCR double-stranded DNA is heated to separate the two strands into single-stranded DNA. After cooling, primers attach to complementary parts of the single-stranded DNA and DNA Polymerase synthesizes double-stranded DNA, creating two pieces of double-stranded DNA. This process is then repeated. (b) The number of strands of DNA doubles with each cycle, such that after three cycles there are sixteen strands of DNA, eight of which (in yellow) are exact copies of the desired sequence bracketed in the original sequence. In a typical experiment, between twenty and thirty cycles are repeated, resulting in millions of copies of the original DNA.

Chapter 3 - Enhanced Differentiation of Retinal Progenitor Cells Using Microfabricated Topographical Cues

3.1 Abstract

Due to the retina's inability to replace photoreceptors lost during retinal degeneration, significant interest has been placed in methods to implant replacement cells. Polymer scaffolds are increasingly being studied as vehicles for cellular delivery to degenerated retinas. Previously, we fabricated poly(methyl methacrylate) thin film scaffolds that increased survival and integration of implanted retinal progenitor cells (RPCs). Additionally, these scaffolds minimized the trauma and cellular response associated with implantation of foreign bodies into mouse eyes. Here, we demonstrate that biodegradable polycaprolactone (PCL) thin film scaffolds can be fabricated with integrated microtopography. Microfabricated topography in a PCL thin film enhanced the attachment and organization of RPCs compared to unstructured surfaces. Using real-time quantitative polymerase chain reaction we also observed that attachment to microtopography induced cellular differentiation. RPCs grown on PCL thin films exhibited an increase in gene expression for the photoreceptor markers recoverin and rhodopsin, an increase in the glial and Müller cell marker GFAP, and a decrease in SOX2 gene expression (a marker for undifferentiated progenitor cells) compared to cells grown on unmodified tissue culture polystyrene (TCPS).

3.2 Introduction

Degenerative diseases of the retina, including retinitis pigmentosa and age-related macular degeneration, are characterized by photoreceptor loss and eventually lead to irreversible visual disability [7-10]. Progress of retinal degeneration is typically slow, and many current clinical treatments focus primarily on delaying disease progression [11, 13, 61]. In the advanced stages of the diseases, photoreceptors are irreversibly lost due to the minimal innate ability of the eye to regenerate damaged tissue. To overcome this problem, a promising technique has emerged whereby an exogenous source of photoreceptors is introduced into the subretinal space [14].

During retinal degeneration, retinal circuitry initially remains intact, and implanted cells only need to make short synaptic connections to host tissue. Implanted multipotent retinal progenitor cells (RPCs) have been shown to migrate through a degenerating retina, extend processes as far as the optic nerve, and express markers of mature retinal neurons and glial cells [14-19]. Additionally, RPCs committed to a photoreceptor cell fate integrate, differentiate, form synaptic connections, and improve visual function upon implantation [20]. Despite these successes, bolus injections of cells to the subretinal space led to a high degree of cell death [21]. Minimizing cell death during implantation and increasing the number of viable cells implanted are subsequently areas for significant improvement of retinal tissue engineering.

Polymer scaffolds have been utilized in recent years to increase the number of viable cells delivered to a degenerated retina [21, 33, 36, 62, 63]. First generation polymer scaffolds were fabricated from poly(L-lactic acid)/poly(lactic-*co*-glycolic acid) (PLLA/PLGA) with a ten-fold increase in cell delivery [21]. However, significant

complications resulted from implantation including: inflammation, fibrosis, a significant foreign body response [64], and some cases led to retinal detachment due to scaffold thickness (~250 μm) [21, 33, 65]. Previously, we showed that a spin-cast poly(methyl methacrylate) (PMMA) thin film scaffold (6 μm) reduced the occurrence of trauma during implantation, and implanted RPCs were able to express at least three markers of mature retinal cells [63]. The limitation of a PMMA scaffold is that it is non-degradable and remains in the subretinal space permanently or until removed. A biodegradable scaffold made of poly(glycerol-sebacate) (PGS) of intermediate thickness (45 μm) has been shown to retain large amounts of RPCs through simulated implantations [36, 62].

Another potential scaffold material is polycaprolactone (PCL), which has been previously applied extensively for fabrication of medical implants [66-70] including subretinal steroid delivery [71]. It is biodegradable, biocompatible, and can be spin-cast into a thin film [72]. Previously, we showed that a structured PCL thin film scaffold (5 μm) increased expression of mature retinal markers [37]. Furthermore, PCL-delivered RPCs migrated into both normal and degenerated retina, demonstrating it may be an ideal material for retinal tissue regeneration.

In addition to delivering an appropriate number of healthy cells to the retina, a polymer scaffold might also promote differentiation of implanted cells prior to implantation to improve the yield of desired cellular phenotypes and decrease the probability of undesired mitotic activity post-implantation. PLLA/PLGA and PGS scaffolds have demonstrated the ability to promote differentiation of RPCs *in vitro* prior to implantation. This was established by associating cell attachment of the non-adherent RPCs to the polymer scaffolds with changes in gene expression [21, 33, 36, 62]. Other studies

have also shown that cell attachment to polymer membranes can induce differentiation, including human bone marrow-derived mesenchymal progenitor cells [73], human marrow stromal cells [74], and human chondrocytes [75]. However, this can be more difficult for cell types such as RPCs, which are grown in serum-free media supplemented with epidermal growth factor (EGF), and often form non-adherent neurospheres. Although RPCs proliferate rapidly under these conditions, they do not readily adhere to a growth substrate, such as tissue culture polystyrene (TCPS), unless it has been treated with an extracellular matrix protein, such as laminin [19], a component of serum. Furthermore, RPCs cultured with serum without supplemental EGF lose their ability to proliferate and attach to the TCPS surface [21, 76]. Some RPCs grown in these conditions differentiated and expressed mature retinal cell markers such as the Müller glial cell marker glial fibrillary acidic protein (GFAP), the rod bipolar cell marker protein kinase C alpha (PKC-α), and the rod photoreceptor markers recoverin and rhodopsin [21, 76]. Ideally a scaffold material would not require any surface modification to induce cell attachment. Previous scaffolds made from PGS [36, 62] and PMMA [63] required protein modification of the surface with either laminin or a combination of laminin and poly-L-lysine to achieve RPC attachment. Additionally, PLLA/PLGA scaffolds needed a concentrated cell solution to be added to the scaffolds drop-wise, which was then incubated overnight before more media was added [33].

Recently, the physical extracellular environment has increasingly been investigated to elucidate cell-substrate interactions. Several studies have shown that microscale and nanoscale topography induce reorientation and differentiation for multiple cell types, including astroglial cells [77], smooth muscle cells [78], mesenchymal stem cells [79],

neural progenitor cells [80], human corneal epithelial cells [81], and bovine aortic endothelial cells [82]. In particular, a number of studies have demonstrated the use of soft lithography to create topographical features with polydimethylsiloxane (PDMS), as this substrate is inexpensive, nontoxic, easily fabricated, and rapidly prototyped [83-85]. For tissue engineering applications, however, PDMS is an inadequate substrate, as it does not degrade. Therefore, a material that is biodegradable, biocompatible, can be spin cast into thin films, and patterned to create microtopographical features would be valuable for tissue engineering applications. Here, we have developed a method to fabricate 5 μm thick degradable PCL thin films that maintain an intended structural micro-architecture. Additionally, we demonstrate that specific microtopographical cues can enhance RPC attachment and differentiation *in vitro* using quantitative polymerase chain reaction.

3.3 Materials and Methods

3.3.1 Polycaprolactone thin film scaffold fabrication:

Polycaprolactone thin films were fabricated using a three-step process (Figure 3.1A). First, a micropatterned silicon master was fabricated using standard photolithography techniques [86]. A layer of SU-8 2010 negative photoresist (Microchem, Newton, MA) was spin cast at 1000 rpm for 30 seconds onto a 3" silicon wafer (Addison Engineering, San Jose, CA) using a PMW32 spin coater (Headway Research, Garland, TX) and pre-baked at 95°C for 3.5 minutes. An array of microwells was then patterned into the photoresist using a photomask and exposing the photoresist to UV light for 30 seconds at an intensity of 5 mW cm^{-2} using a Karl Suss MJB 3 mask aligner (SUSS MicroTec Inc., Waterbury

Center, VT). The SU-8 molds were then post-baked at 95°C for 4.5 minutes and developed with SU-8 Developer (Microchem, Newton, MA) for 2 minutes. Second, an inverse pattern of the silicon wafer was fabricated using polydimethylsiloxane (Sylgard 184, Dow Corning, Midland, MI). The base and curing agent were mixed at a 10:1 (v/v) ratio, degassed under vacuum, poured onto the SU-8 micropatterned wafer, and baked at 65°C for 2 hours. Once cured, the PDMS was peeled from the silicon master. Third, a polymeric thin film containing the inverse pattern of the PDMS was fabricated by spin casting a solution of polycaprolactone (MW 80,000, Sigma-Aldrich, St. Louis, MO) on top of the PDMS. Polycaprolactone was dissolved in 2,2,2-trifluoroethanol (Sigma-Aldrich, St. Louis, MO) at 65°C for 3 hours at a concentration of 0.1 g mL^{-1}. Polycaprolactone solution was poured onto the micropatterned PDMS and spin coated at 1500 RPM for 1 minute, after which the polycaprolactone thin film was detached and peeled from the PDMS using forceps. Prior to cell seeding, PCL thin films were sterilized via exposure to UV light for one hour.

3.3.2 Profilometry:

Characterization of PCL thickness was conducted with an Ambios Technology XP-2 Stylus Profiler (Santa Cruz, CA). The profilometry image was achieved using a scan speed of 0.03 mm/sec, a length of 0.5 mm and a stylus force of 0.5 mg.

3.3.3 Mouse Retinal Progenitor Cells:

Retinal progenitor cells were isolated and maintained as described previously [19, 87]. Briefly, cells were cultured in NeuroBasal medium (NB) (Invitrogen, Carlsbad, CA)

supplemented with 2 mM L-Glutamine (Sigma-Aldrich, St. Louis, MO), 100 μg mL^{-1} penicillin-streptomycin (Sigma-Aldrich, St. Louis, MO), 20 ng mL^{-1} epidermal growth factor (EGF; Promega, Madison, WI), and neural supplement (B27; Invitrogen, Carlsbad, CA) and plated into T-75 culture flasks as non-adherent neurospheres. On alternating days, half of the cell solution was removed from the culture flask and centrifuged at 1000 RPM for 3 minutes. The media was removed and the pellet of cells was re-suspended in fresh medium and returned to the flask. Cells were passaged 1:10 every 7 days. All cells used in this study were passaged fewer than 15 times. For all experiments, cells were seeded at an initial density of 5000 cells mm^{-2} and grown for two days.

3.3.4 Cell Attachment:

Thin films were immobilized in custom-made holders and fitted into a 12-well plate. After two days of growth cells were fixed in 4% formaldehyde for 2 hours, rinsed twice with PBS, and then permeabilized with 0.25% Triton X-100 for 1 hour. Nuclei were stained with DAPI and mounted between a glass slide and coverslip using SlowFade Gold with DAPI (Invitrogen, Carlsbad, CA). A 3.7 mm^2 area of the thin film was imaged using an Olympus BX60 Microscope (Center Valley, PA), and the number of cells on each surface was manually quantified. Figure 3.2 represents data from three individual experiments.

3.3.5 Scanning Electron Microscopy:

Cells were fixed in a solution of 3% glutaraldehyde (Sigma-Aldrich, St. Louis, MO), 0.1 M sucrose (Sigma-Aldrich, St. Louis, MO), and 0.1 M sodium cacodylate (Sigma-

Aldrich, St. Louis, MO) buffer for 72 hours at room temperature. Following fixation, samples were rinsed in buffer containing 0.1 M sucrose and 0.1 M sodium cacodylate for 5 minutes. Samples were then dehydrated by removing the sucrose-cacodylate buffer and adding a series of aqueous ethanol solutions for 10 minutes each in a graded series as follows: 35%, 50%, 70%, 95%, 100% (twice). The final 100% ethanol solution was replaced with hexamethyldisilazane (HMDS) (PolySciences, Inc., Warrington, PA) for 10 minutes and removed. Samples were allowed to air dry for 30 minutes before mounting and imaging. Samples were imaged using a NovelX *my*SEM (Lafayette, CA) scanning electron microscope with an accelerating voltage of 1 kV.

3.3.6 Real-time quantitative RT-PCR (qPCR):

Messenger RNA levels were quantified using a *Fast* SYBR® Green Cells-to-CT™ Kit (Applied Biosystems, Foster City, CA). Reverse transcription was performed on a Mastercycler ep gradient S (Eppendorf, Hamburg, Germany). Real-time quantitative PCR was performed using a StepOne Plus (Applied Biosystems, Foster City, CA) run for 40 cycles. The primers (Integrated DNA Technologies, San Diego, CA) used in this study are shown in Table 1. Each reaction was performed in triplicate and normalized to glyceraldehyde 3-phosphate dehydrogenase (GAPDH) as an endogenous control.

3.4 Results

3.4.1Thin film fabrication

Dissolved PCL was spin-cast onto a PDMS mold with an array of 25 μm diameter micropegs, resulting in a thin layer of polymer coating the PDMS surface. Flexibility of the PDMS mold allowed the PCL to be peeled from the surface, producing a thin film with 25 μm diameter microwells (an inverse of the PDMS pattern) (Figure 3.1A & 3.1B). PCL films were also fabricated from an unstructured PDMS mold and used as a control for potential material effects on cellular differentiation. Film thickness is dependent on the spin speed and viscosity of the dissolved polymer solution and was measured to be 5 μm thick (Figure 3.1C).

3.4.2 RPC attachment to thin film PCL scaffolds

RPCs were seeded on thin film scaffolds and TCPS at an initial density of 5000 cells mm^{-2}. A small number of cells (<30 cells mm^{-2}) attached to the two unstructured surfaces (Figure 3.2), either as small clusters (Figure 3.3A) or as individual cells (Figure 3.3B), although the vast majority of cells remained in solution as non-adherent neurospheres (Figure 3.3). In contrast, RPC attachment to PCL with 25 μm diameter wells resulted in a ten-fold increase in cell attachment relative to unstructured substrates (Figure 3.2). Cells adhered to the inside of microwells, usually either on the edges or the bottom of wells, with as many as three or four cells in each well (Figure 3.3C).

3.4.3 Cell morphology

Cells on each substrate maintained a similar circular morphology; however, RPCs grown on TCPS formed clusters, while cells grown on both PCL substrates attached as individual cells, even when found in close proximity to each other, such as in the event of

being confined inside a microwell (Figure 3.3C). It is possible that cell-cell communication is paramount to RPC proliferation, and therefore the failure of RPCs to re-cluster on PCL substrates induces differentiation. To investigate this, gene regulation of differentiation markers was determined using quantitative real-time polymerase chain reaction (qPCR).

3.4.4 Quantitative real-time polymerase chain reaction

Analogous to the attachment experiments, RPCs were grown under normal proliferative conditions on the same three substrates, and mRNA expression levels were quantified using qPCR. Four gene targets were investigated using the primers shown in Table 1. These included genes for recoverin, rhodopsin, glial fibrillary acidic protein (GFAP), and SOX2. Recoverin is a calcium-binding protein found in photoreceptors, rhodopsin is a G-protein coupled receptor also found in photoreceptors, and GFAP is an astrocyte marker, all three being markers for differentiation. SOX2 is also included as a marker for undifferentiated proliferating cells. Figure 3.4 shows the ratio of mRNA expression of each target gene to glyceraldehyde 3-phosphate dehydrogenase (GAPDH), a housekeeping gene commonly used to account for cell number variation. All three differentiation markers were up-regulated for both PCL surfaces, and SOX2 was down-regulated on the two PCL surfaces relative to TCPS. Additionally, up-regulation of recoverin and rhodopsin was significantly higher on films with microtopography compared to unstructured PCL, suggesting that topographical cues not only enhance attachment but also RPC differentiation.

3.5 Discussion

The ability to fabricate thin films is paramount to the success of retinal tissue engineering. Initial attempts at injecting RPCs into the subretinal space resulted in death for nearly ninety percent of the grafted cells [21]. To circumvent this problem, new vehicles for cell delivery were explored. Previously, polymer scaffolds were implanted into the subretinal space of animal models to avoid damaging the outer retina, although the use of thicker scaffolds still resulted in trauma to the host. Minimizing the thickness of an implant, especially in the subretinal space, limits the potential damage that can occur during and after implantation. The PCL thin film scaffolds used in this study (5 μm thickness) are fifty times thinner than the original PLLA/PLGA scaffolds [21, 33] used and nine times thinner than the more recent PGS scaffolds [36, 62].

Another critical aspect of retinal tissue engineering is cell attachment to the scaffold surface. To successfully implant RPCs into the subretinal space, cells must be firmly attached to the scaffold surface and be able to resist shear forces that occur during implantation of the film. Previous studies have indicated that scaffold topography can increase progenitor cell attachment, although protein modification of the surface has been used to induce cell attachment and differentiation [63, 80]. Here, to determine if either the polymer material or microtopography could potentially induce the same behavior of attachment, RPCs were seeded on PCL in the absence of chemical or protein modification. RPC attachment to the scaffold microtopography resulted in a highly organized pattern of cells (Figure 3.2D). The microwell topography also shielded attached cells from shear forces present in processes, such as staining and SEM preparation, and presumably would provide the same effect during implantation.

Cell attachment to unstructured and microstructured PCL resulted in the absence of clustering found in proliferating RPCs, although no further dramatic morphological changes occurred. It is clear the presence of microtopography influenced both cell attachment and gene expression. The up-regulation of fate-specific markers such as recoverin, rhodopsin, and GFAP indicates enhanced differentiation of the RPCs toward rod and glial cell fates, which is confirmed by the down-regulation of the proliferation marker SOX2. For the purpose of treating retinal degeneration, RPCs would ideally differentiate into rod photoreceptors. The cells used in this study have earlier been shown to primarily produce rod, bipolar, and glial cells,[37] and it is therefore possible microtopographical cues increase the rate of differentiation of individual RPCs into a predetermined differentiation pathway. Future studies that elucidate individual cell fates rather than global trends would therefore be valuable. It is also possible chemical cues in conjunction with microtopography may limit differentiation into a glial cell fate and promote rod specific differentiation.

In this study we demonstrate for the first time that microscale topographical cues influence cell attachment and differentiation of retinal progenitor cells independent of any biochemical cues. Interestingly, although RPC attachment to PCL microwells resulted in up-regulation of fate specific markers, such as recoverin, rhodopsin, and GFAP, no dramatic change in morphology was observed. This is in contrast to a previous study in which RPCs were grown on PCL thin films with a nanostructured surface [37]. As evidenced from this and other studies, it may be possible to generate fully differentiated photoreceptors from RPCs for implantation using a combination of physical and biochemical cues. Further studies involving prolonged growth of RPCs on

microstructured PCL and *in vivo* implantations of PCL thin films would be beneficial in determining the full extent to which microtopography influences progenitor cell fate determination.

3.6 Conclusions

In this study we have shown that microscale topography can strongly influence attachment and differentiation of retinal progenitor cells independent of any biochemical cues. Using comparative analysis of gene expression levels by qPCR, we have shown that RPCs grown on microfabricated topographical features express higher levels of photoreceptor and glial cell markers compared to RPCs grown on unstructured surfaces. Additionally, the thin film PCL scaffolds used in this study are on the order of the same thickness of other PMMA and PCL scaffolds that have been used with minimal trauma to the host. These results indicate that substrate topography influences RPC differentiation, and a biodegradable PCL thin film scaffold is a promising material for delivering RPCs to degenerated retinas.

3.7 Acknowledgements

All microfabrication work was performed in the UCSF Micro- and Nanofabrication Core. We thank Dr. Kristy M. Ainslie, Dr. Daniel A. Bernards, Dr. Rachel D. Lowe, Alana G. Lerner, and Lily Peng for their valuable insight and advice. This research was supported by a NSF NSEC grant to T.A.D., a grant from the California Institute for Quantitative Biosciences (QB3) to T.A.D., a grant from the Lincy Foundation to H.K., a Sandler Family Foundation Translational Research Fellowship to S.L.T., a Knights Templar Eye

Foundation Investigator Grant to S.L.T., and a grant from the Foundation Fighting Blindness to S.L.T.

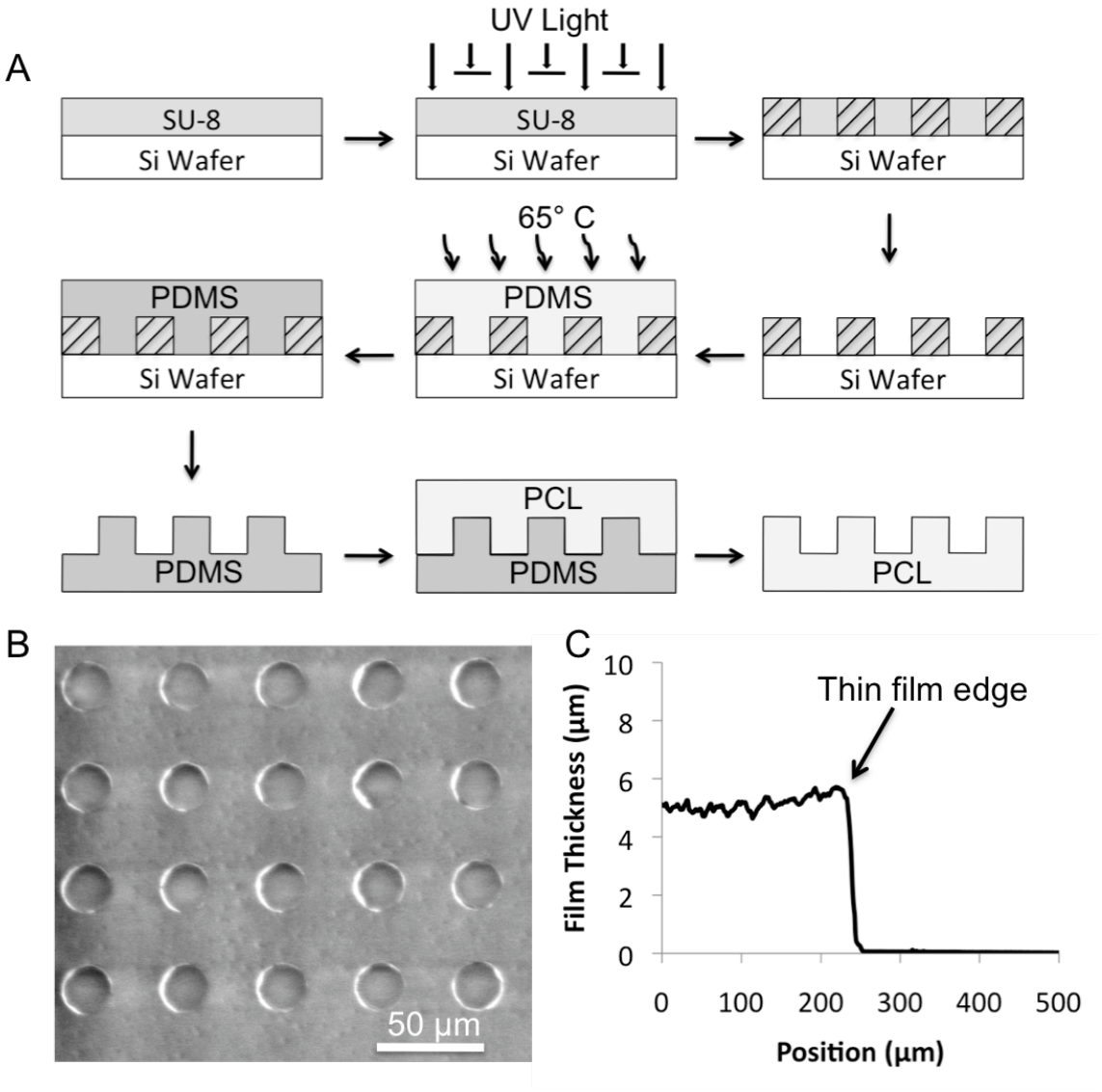

Figure 3.1: Polycaprolactone thin film fabrication.

(A) Schematic of PCL thin film scaffold fabrication. SU-8 photoresist is spin-cast onto a silicon wafer and exposed to UV light through a negative mask. Unexposed areas are not crosslinked and developed away, and PDMS is cured on the wafer. After peeling the PDMS mold from the wafer, PCL is spin-cast on the mold and peeled from the surface. (B) A scanning electron micrograph of a PCL thin film with 25 µm diameter wells. (C) Profile of PCL thin film.

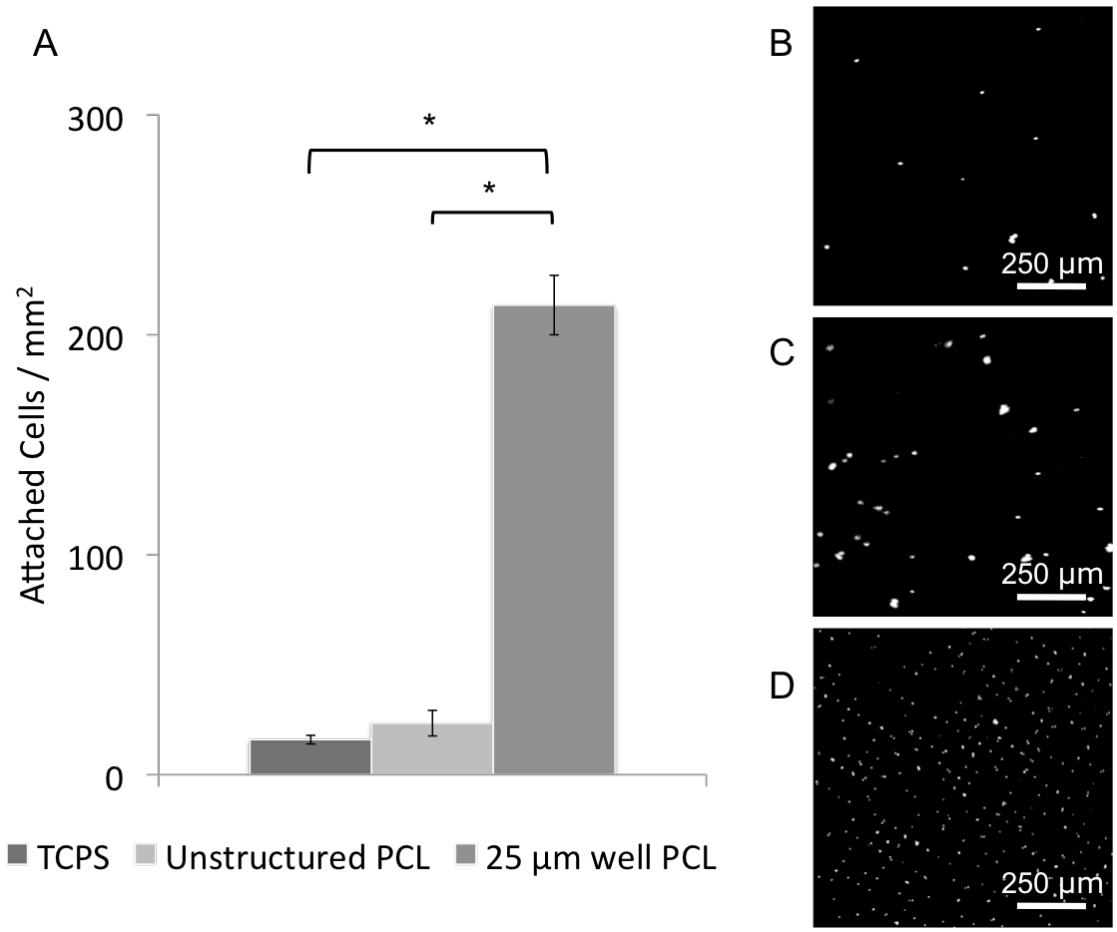

Figure 3.2: Retinal progenitor cell attachment to polycaprolactone.

(A) Attachment of RPCs to substrate surfaces after two days growth. Substrate microtopography of 25 µm well PCL leads to significantly more RPC attachment compared to unstructured PCL and TCPS surfaces. Fluorescence images of DAPI-stained RPC nuclei attached to (B) TCPS, (C) unstructured PCL, and (D) 25 µm well PCL. *$p < 0.05$, Student-Newman, Keuls test. Error bars indicate standard deviation over three independent experiments.

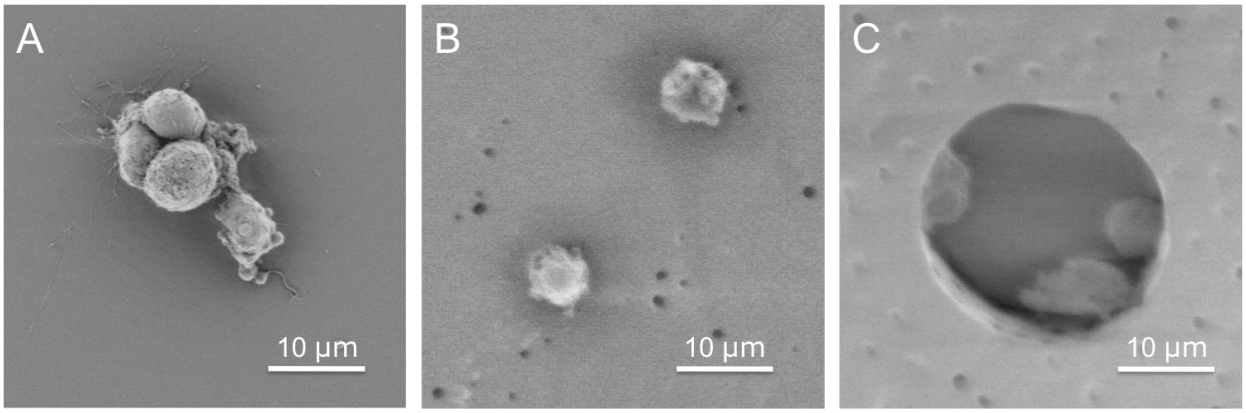

Figure 3.3: Scanning electron microscopy of retinal progenitor cells.

Scanning electron micrographs of RPCs grown on (A) TCPS, (B) unstructured PCL, and (C) PCL with 25 µm diameter wells. RPCs retain a circular morphology regardless of the substrate surface but do not form clusters on either PCL surface.

Table 3.1: qPCR Primers

Gene	Primer Sequence (5'-3')
Recoverin	F: TGTGAAACTCCTCCCAGATGATG R: TTCCAAAGAATGCCCAGATCTT
Rhodopsin	F: TTATGTGCCCTTCTCCAACGT R: TGGTTCCGCCAGGTAGTACGT
GFAP	F: CAGCCCTGAAGAATCCACAAC R: CCCTTAGCTTGGAGAGCAACA
SOX2	F: TTCCAAAAACTAATCACAACAATCG R: GAGACGGGCGAAGTGCAA
GAPDH	F: TGGCCTCCAAGGAGTAAGAAAC R: GGGATAGGGCCTCTCTTGCT

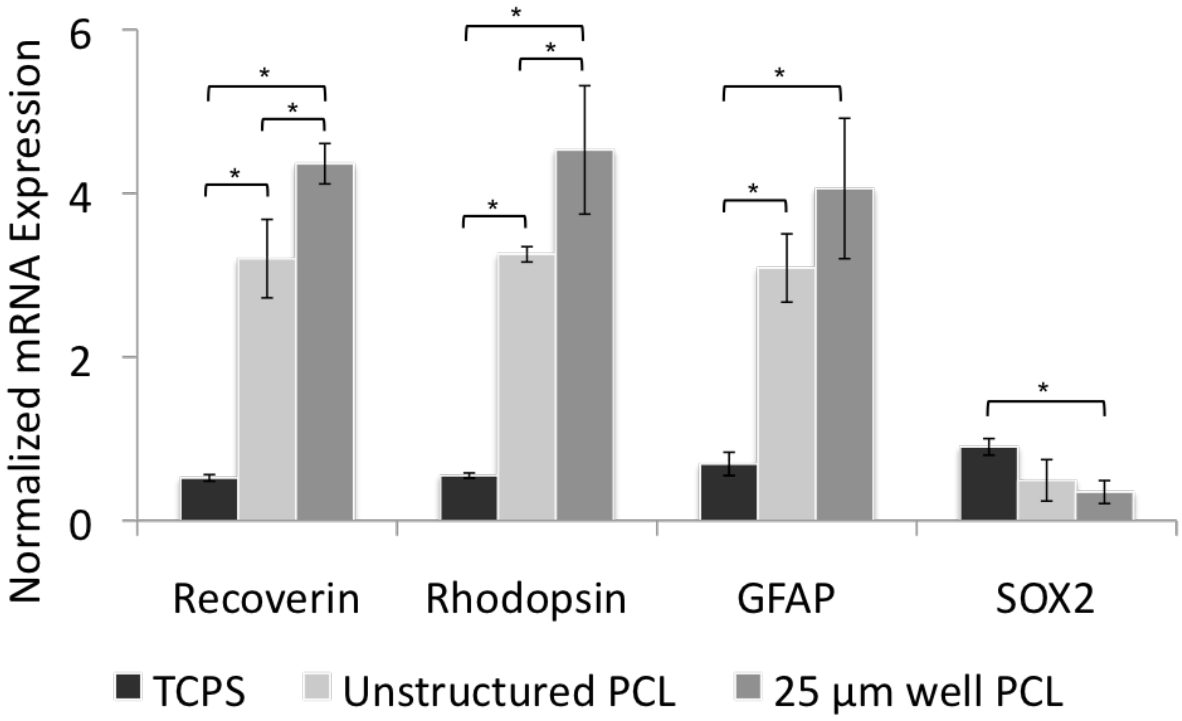

Figure 3.4: qPCR analysis of retinal progenitor cells grown on microstructured polycaprolactone.

mRNA expression normalized to GAPDH for RPCs grown in proliferative conditions. Expression of rod photoreceptor markers recoverin and rhodopsin and glial cell marker GFAP are increased on unstructured PCL and PCL with 25 µm diameter wells compared to TCPS. *$p < 0.05$, Student-Newman, Keuls test. Error bars indicate standard deviation over three independent experiments.

Chapter 4 – Growth and Differentiation of Retinal Progenitor Cells on Nanostructured Polycaprolactone Thin Films

4.1 Abstract

The retina is unable to regenerate itself after devastation by diseases such as age-related macular degeneration and retinitis pigmentosa. The photoreceptors, the retina's ever-important light sensing cells, are targeted by these diseases and must be replaced by an exogenous source if they are left dead or unable to perform their required functions. Retinal progenitor cells (RPCs) have shown promise as a potential cell source to replace nonfunctioning photoreceptors if they can be properly differentiated in vivo. Previously, we fabricated polycaprolactone (PCL) thin film scaffolds containing microtopographical features that served two functions. First, a PCL scaffold acted as a delivery vehicle to transport RPCs into an animal retina that protected the implanted cells from shear and other forces that led to cell death. Second, the incorporated microtopography enhanced RPC differentiation, resulting in the up-regulation of the differentiation markers recoverin and rhodopsin. Here, we incorporated nanotopography into PCL thin films to determine if structures on the nanoscale have the same effect on RPC differentiation as microscale topography. Using real-time quantitative reverse transcription polymerase chain reaction (qPCR) we confirmed our previous results that PCL initiates RPC differentiation but found that nanotopography does not significantly enhance this differentiation.

4.2 Introduction

Nanotopography has been shown to influence behaviors such as attachment, alignment, and differentiation in numerous cell types. In some cases, the influence of nanotopography may even trump the effects of microtopography on cells as it more accurately mimics the composition of basement membranes of various tissues[88].

An obvious example is the growth of corneal epithelial cells on grooves as small as 70 nm wide. These cells aligned and elongated along the patterns of grooves, and the degree to which this occurred increased with groove depth[89]. Other nanoscale topographies have also been shown to influence other cells types, including randomly distributed 11 nm high islands in polystyrene[90]. In this study, human fetal osteoblast adherence and differentiation was enhanced by the surface nanotopography compared to a planar control.

Based on our previous results that microtopography embedded in a polycaprolactone (PCL) thin film enhanced the differentiation of retinal progenitor cells (RPCs)[59] and our ability to fabricate nanostructured PCL[91], we hypothesized that nanotopography may also affect the growth and differentiation of RPCs compared to cell growth on a planar PCL thin film. RPCs had previously been grown on PCL nanowires, which resulted in cellular proliferation and down-regulation of early progenitor cell markers[37]. RPCs have the potential to replace degenerated photoreceptors and other retinal neurons in the eye if they can be properly delivered and kept alive[17, 19, 20, 92]. We hypothesized that a substrate surface containing an array of nanowells may increase RPC attachment and differentiation. However, using real-time quantitative reverse transcription polymerase chain reaction (qPCR) we determined that under proliferative

conditions nanotopography does not enhance RPC differentiation compared to an unstructured surface.

4.3 Materials and Methods

4.3.1 Nanostructured Polycaprolactone Thin Film Fabrication

Nanostructured PCL samples were fabricated by Dr. Daniel Bernards using a multistep process according to a previously published procedure[91]. Glass substrates were first cleaned using a piranha solution containing sulfuric acid and hydrogen peroxide at a 3:1 ratio for 30 minutes. Samples were then rinsed with deionized water and dried with nitrogen. Further cleaning was completed by exposure to oxygen plasma (200W, 0.5 mTorr) for 5 minutes. A zinc acetate (0.75M $ZnAc_2$) and ethanolamine (0.75M) in 2-methoxyethanol seed layer was spin-cast onto the cleaned glass surfaces at 1000 RPM for 60 seconds. Substrates were placed on a hot plate at 400 °C for 30 minutes to convert $ZnAc_2$ to ZnO and then placed in a solution of aqueous 5mM $ZnAc_2$ solution at 85-90 °C for 4 hours, replacing the growth bath once. PCL was dissolved in 2,2,2-trifluoroethanol at 60 °C while stirring and then spin-cast onto ZnO nanowire-coated glass substrates at 1000 RPM for 60 seconds. Substrates were then heated to 130 °C to remove any excess solvent and to sufficiently melt the PCL into the ZnO substrates. ZnO templates were then etched with 10 mM sulfuric acid for 30 minutes.

4.3.2 Scanning Electron Microscopy of Nanostructured PCL

Scanning electron microscopy was performed by Dr. Daniel Bernards using a FEI XL30 Sirion scanning electron microscope with field-emission gun source (FEI, Hillsboro, OR). Dimensions of zinc oxide nanowires and PCL nanowells were determined using *ImageJ* analysis software (National Institutes of Health, USA).

4.3.3 Growth and Differentiation of Retinal Progenitor Cells

Detailed methods can be found in other sections of this dissertation for culturing retinal progenitor cells (3.3.3), cell attachment to PCL thin films (3.3.4), scanning electron microscopy of RPC growth on PCL (3.3.5), and real-time quantitative reverse transcription polymerase chain reaction (3.3.6).

4.4 Results

4.4.1 Fabrication of Nanostructured Polycaprolactone Thin Films

Nanostructured PCL thin films were fabricated using the template/spin-casting procedure as shown (Figure 4.1A). Unstructured thin films were also produced by spin casting dissolved PCL onto a clean silicon wafer. Scanning electron micrographs of the template zinc oxide nanowires, PCL-coated nanowires, and nanostructured PCL are shown (Figure 4.1B-D).

4.4.2 RPC Morphology on Nanostructured Polycaprolactone Thin Films

RPCs were seeded on PCL thin film scaffolds and TCPS at an initial density of 5000 cells mm^{-2}. The vast majority of cells remained in solution as non-adherent

neurospheres, although some RCPs attached to each substrate. Cells attached to TPCS remained grouped together as neurospheres (Figure 4.2A), while cells attached to PCL retained a circular morphology but did not stay in clusters even when found in close proximity to other cells (Figure 4.2B-C). To determine if clustering influences differentiation of RPCs, we examined regulation of differentiation markers using qPCR as previously[59].

4.4.1 Quantitative Real-time Polymerase Chain Reaction

RPCs were grown under proliferative conditions in the same fashion as the morphology experiments, and mRNA expression levels of several differentiation markers were evaluated. These targets included two rod photoreceptor markers, recoverin and rhodopsin, the glial marker glial fibrillary acid protein (GFAP), and the proliferation marker SOX2. Figure 4.3 illustrates the ratio of mRNA expression of each differentiation marker to the housekeeping gene glyceraldehyde 3-phosphate dehydrogenase (GAPDH). Similar to RPCs grown on microfabricated PCL thin films[59], we found that RPCs grown on unstructured and nanostructured PCL thin films exhibited up-regulation of all three differentiation markers relative to TCPS. However, up-regulation of the three differentiation markers was not significantly higher on nanostructured PCL than on unstructured PCL, suggesting that nanotopography does not enhance differentiation of RPCs.

4.5 Discussion

Previously, we showed that microfabricated topographical cues embedded in PCL thin films enhanced the differentiation of RPCs compared to cells grown on TCPS[59]. Due to our ability to fabricate topography on a much smaller scale, we decided to determine if nanotopography would also influence the differentiation of RPCs in a similar fashion.

We grew RPCs in the same manner as previously described[59] but replaced the 25 μm diameter welled microfabricated PCL with nanostructured PCL. We examined the morphology of attached cells to each substrate surface by scanning electron microscopy and again found that RPCs grown on PCL maintained a circular morphology but failed to form the clusters found so prevalently when grown on TCPS. However, we did not notice any obvious differences between cells grown on nanostructured PCL compared to unstructured PCL, whereas previously RPCs preferentially attached to the inside walls of PCL microwells.

Similarly, the mRNA expression levels of recoverin, rhodopsin, and GFAP was found to increase in cells grown on both PCL substrates compared to TCPS, although we found no significant difference in expression levels between the unstructured and nanostructured PCL substrates.

4.6 Conclusions

In this study we have shown that surface nanotopography does not strongly influence the attachment and differentiation of retinal progenitor cells grown on polycaprolactone thin films under proliferative conditions. We did however confirm that PCL does enhance the differentiation of RPCs regardless of the surface characteristics

independent of any biochemical cues. These results indicate that although nanotopography does not influence RPC attachment or differentiation, a PCL thin film is still a promising material for delivering RPCs to degenerated retinas.

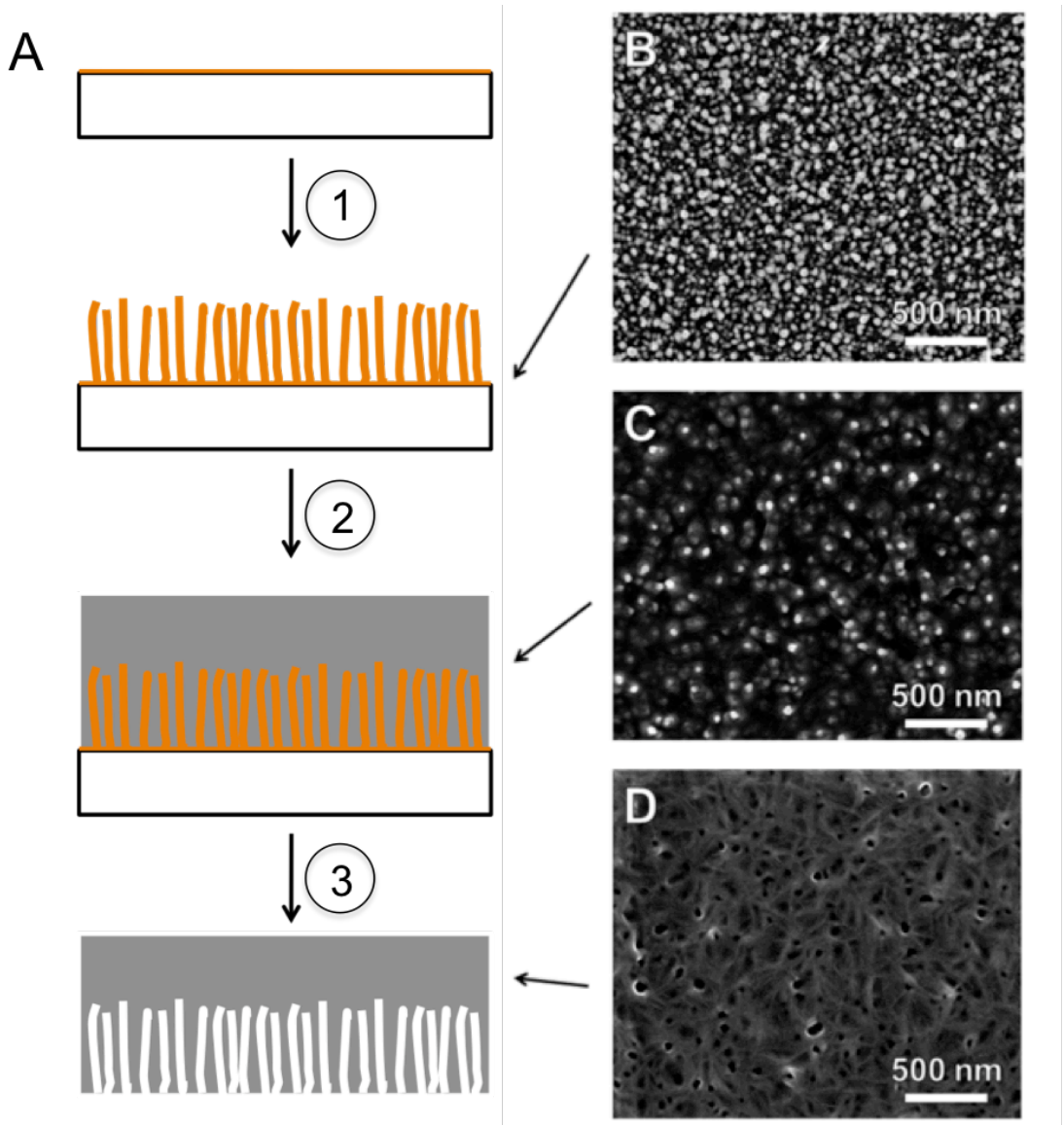

Figure 4.1: Fabrication of nanostructured polycaprolactone.

A) Process diagram showing (1) growth of zinc oxide nanowires, (2) spin-casting of polycaprolactone, and (3) etching of the zinc oxide nanowires to produce nanostructured polycaprolactone. Scanning electron micrographs of the fabrication stages are shown: (B) zinc oxide nanowires, (C) polycaprolactone-coated nanowires, and (D) nanostructured PCL. Figure modified from Bernards and Desai[91].

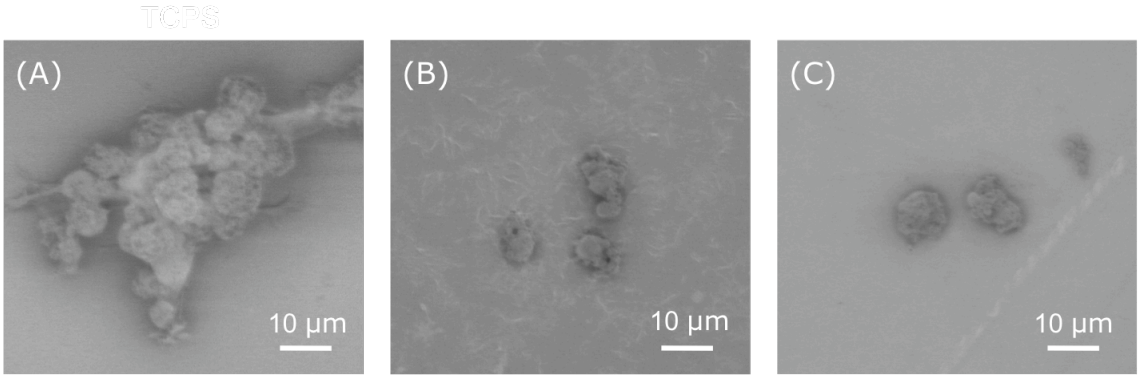

Figure 4.2: Scanning electron microscopy of retinal progenitor cells grown on nanostructured polycaprolactone.

Scanning electron micrographs of RPCs grown on (A) TCPS, (B) unstructured PCL, and (C) nanostructured PCL. RPCs retain a circular morphology regardless of the substrate but do not form clusters on either PCL surface.

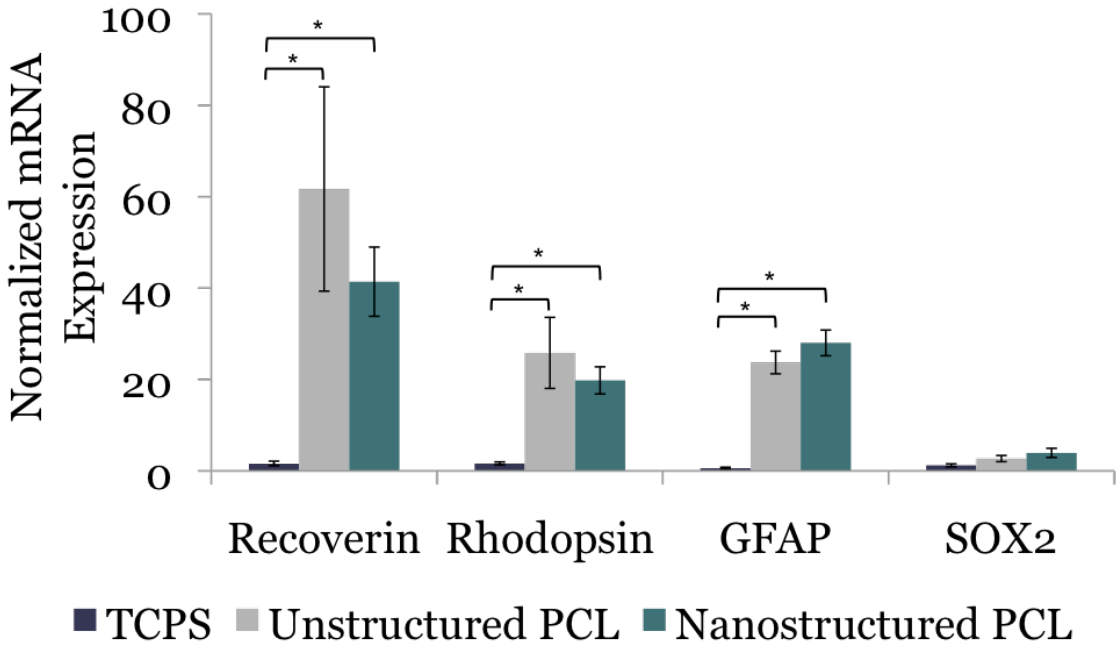

Figure 4.3: qPCR analysis of retinal progenitor cells grown on nanostructured polycaprolactone.

mRNA expression normalized to GAPDH for RPCs grown in proliferative conditions. Expression of rod photoreceptor markers recoverin and rhodopsin and glial cell marker GFAP are increased on unstructured PCL and nanostructured PCL compared to TCPS. The nanotopography however does not significantly increase or decrease expression of the specific markers. *p<0.05, Student-Newman, Keuls test. Error bars indicate standard deviation over three independent experiments.

Chapter 5 – Ocular Biocompatibility of a Structured Polycaprolactone Thin Film Implant

5.1 Abstract

This study assessed the ocular tolerance and durability of a microstructured biopolymer device implanted into the rabbit eye for a period of 1 to 6 months. Microgrooved polycaprolactone (PCL) thin films were implanted in New Zealand White rabbits via a small sclerotomy incision (1-2 mm) or needle injection (20 gauge) at 2 to 3 mm posterior to the limbus. PCL thin films were implanted into the anterior chamber of 3 eyes and into the peripheral anterior vitreous of 5 eyes. Throughout the course of each 1 to 6 month implantation period each eye was examined for ocular abnormalities and complications. Post-mortem histology was performed on enucleated eyes to evaluate device/tissue reactions and examine any potential morphologic abnormalities. Scanning electron microscopy was performed on retrieved devices to determine the durability and structural integrity of implanted devices. Ophthalmological examinations throughout the course of the study showed no adverse signs of ocular tolerance regarding inflammation or infection, cataract, or intraocular pressure. Post-mortem histological tissue examinations revealed no cellular inflammation or morphologic abnormalities at ocular sites including the trabecular meshwork, retina, and the specific sites of residence of the thin film devices following implantation. Scanning electron microscopy revealed no structural degradation and full integrity of the devices after implantation and 1 to 6 months of ocular residence. These results demonstrate that PCL thin films are well tolerated and structurally stable during residence in the rabbit eye. PCL is therefore a viable candidate as a material for further development of an implantable ocular drug delivery device.

5.2 Introduction

Effective methods of drug delivery in clinical ophthalmology have long been limited to topical eye drops and intraocular injections. Although these methods can generally be effective for treating some specific diseases, both methods have definitive drawbacks. For example, topical eye drops can be an effective treatment for glaucoma, however patient non-compliance is often a significant factor in the treatment of this disease[93, 94]. Additionally, topical eye drops are only effective at treating diseases that affect the front part of the eye. Due to the anatomy of the eye, drugs added topically to the cornea are rapidly flushed into the bloodstream and are unable to penetrate the back of the eye to treat affected areas such as the retina.

In order to effectively reach the retina a more direct and invasive method is required. Intraocular injections achieve this by directly injecting a solution of drug into the eye, often into the vitreous. Currently intraocular injection is the only approved method of delivery for anti-VEGF therapies such as Lucentis that have revolutionized the treatment of wet age-related macular degeneration. Although effective, intraocular injections can lead to numerous complications including ocular inflammation, elevated intraocular pressure, cataract, vitreous hemorrhage, endophthalmitis, and retinal tears and detachment[95]. Furthermore, drug half-life in the eye can be very short. Lucentis has a half-life in the eye of only 2.88 days, while its full anti-VEGF counterpart Avastin has a half-life of a slightly longer period of only 4.32 days[96, 97]. Delivery of these drugs therefore requires monthly intraocular injections to maintain therapeutic concentrations in the eye. It is possible that these treatments may be even more effective if the intraocular concentration of the drug could be maintained at a constant level. The ability to prolong

the half-life of an anti-VEGF treatment in the eye by developing an injectable sustained-delivery device would therefore minimize the number of intraocular injections required for treatment and also maintain a constant concentration of drug in the eye.

To achieve sustained delivery of a therapeutic in the eye, a drug delivery device must be able to shield its highly concentrated drug reservoir from the rest of the vitreous. Without this ability drug will rapidly diffuse into the eye and not only create an unwanted spike in concentration but will also rapidly be removed from the eye. We envision a drug delivery device that utilizes micro- and nano-electromechanical systems (MEMS and NEMS) to create a constant release of drug into the eye. While this type of technology has traditionally been used for applications such as microfluidics[98, 99], microelectronics[100], and cell mechanobiology[101-103], it has recently garnered attention for its use in drug delivery systems[91, 104-106]. We have developed a method to fabricate thin films from polycaprolactone (PCL) that can micro- or nanostructured through a templating process. Here, we show that microstructured PCL devices implanted in the rabbit eye are well tolerated after a period of 1-6 months, and retain their structural integrity throughout the course of these experiments. We believe PCL to be a viable biomaterial for use in the eye.

5.3 Materials and Methods

5.3.1 Microgrooved Thin Film Fabrication

Polycaprolactone thin films were fabricated using a three-step process (Figure 5.1). First, a micropatterned silicon master was fabricated using standard photolithography

techniques. A layer of SU-8 2010 negative photoresist (Microchem, Newton, MA, USA) was spin cast at 1000 RPM for 30 seconds onto a 3" silicon wafer (Addison Engineering, San Jose, CA, USA) with a PMW32 spin coater (Headway Research, Garland, TX), which was then pre-baked at 95°C for 3.5 minutes. Next, the photoresist was exposed to UV light through a photomask for 30 seconds at an intensity of 5 mW cm^{-2} using a Karl Suss MJB 3 mask aligner (Hoffmann Instruments, Los Osos, CA), which resulted in an array of micro-grooves. Photopatterned SU-8 was then post-baked at 95°C for 4.5 minutes and subsequently developed with SU-8 Developer (Microchem, Newton, MA) for 2 minutes to produce complete SU-8 molds. Polydimethylsiloxane (Sylgard 184, Dow Corning, Midland, MI) was cast on SU-8 molds to generate inverted patterns. Base and curing agent were mixed at a 10:1 (v/v) ratio, degassed under vacuum, poured onto SU-8 molds, and baked at 65°C for 2 hours. After curing solid PDMS films were peeled from the SU-8 molds and used to fabricate structured PCL. For this polycaprolactone (MW 80,000; Sigma-Aldrich, St. Louis, MO) was dissolved in 2,2,2-trifluoroethanol (Sigma-Aldrich, St. Louis, MO) at 65°C for 2 hours at a concentration of 0.1 g mL^{-1}. PCL solutions were spin cast onto micropatterned PDMS at 1500 RPM for 1 minute, and the resulting PCL thin films were then peeled from the PDMS using forceps. Prior to implantation, thin films were sterilized by UV exposure for 1 hour.

5.3.2 Animal Surgery

New Zealand White female rabbits (2.5-3.5 kg) from the Western Oregon Rabbit Company (Philomath, OR) were anesthetized by inhalation of 2-4% Isoflurane. Pupils were dilated by administering 1 % tropicamide, 2.5% phenylephrine hydrochloride, and

0.5% proparacaine drops to each eye. A surgical microscope (Carl Zeiss Surgical GmbH, Germany) was used with a silicone flat lens (Dutch Ophthalmics, Kingston, NH) to visualize the retina. After disinfection with 5% povidone iodine, the thin film devices were implanted into the anterior chamber in 3 eyes and into the vitreous cavity in 5 eyes via 20-gauge needle injection (Figure 5.2). Incisions were closed with vicryl sutures (Ethicon Inc., West Somerville, NJ). Subconjunctival antibiotics (Cefazolin, 150uL) were given after the procedure.

5.3.3 Ocular Tolerance

Ocular tolerance was evaluated with serial ophthalmic exams over 1 to 6 months using pneumotonometry (Mentor Inc., Norwell, MA), slit lamp microscopy (Kowa Company, Japan) and indirect ophthalmoscopy (Keeler, United Kingdom). Eyes were evaluated for evidence of ocular inflammation, cataract, vitreous hemorrhage, endophthalmitis, and retinal tears and detachment.

5.3.4 Histology

At intervals of 1, 2, 3, 4, 5, and 6 months after surgery, rabbits were humanely killed under deep anesthesia by intravenous overdose of pentobarbital sodium. The eyes were enucleated and the implants were retrieved prior to preservation in 2.5% glutaraldehyde and 1.5 % paraformaldehyde in 0.1M sodium cacodylate buffer solution for 24 hours at 4°C. The ocular tissue was embedded in paraffin, then sectioned at 5 μm and mounted on glass slides. Standard staining with hemotoxylin and eosin was used to delineate ocular structures.

5.4.5 Scanning Electron Microscopy

Retrieved devices were evaluated by scanning electron microscopy (SEM) to determine durability of the microstructural architecture. Devices were fixed in a 3% glutaraldehyde (Sigma-Aldrich, St. Louis, MO) in 0.1 M sucrose-cacodylate (Sigma-Aldrich, St. Louis, MO) buffer for 72 hr at room temperature. Following fixation, samples were rinsed three times in 0.1 M sucrose-cacodylate buffer for 5 min. Samples were then dehydrated by removing the sucrose-cacodylate buffer and adding and replacing a series of ethanol solutions in a graded series as follows: 35%, 50%, 70%, 95%, 100% (twice). Each ethanol solution was applied for 10 min. The final 100% ethanol solution was replaced with hexamethyldisilazane (HMDS) (PolySciences, Inc., Warrington, PA) for 10 min and removed promptly. Samples were allowed to air dry for 30 min and then mounted and imaged using a Novelx *my*SEM scanning electron microscope.

5.4 Results

5.4.1 Microgrooved Polycaprolactone Thin Films

Smooth polycaprolactone thin films and microgrooved thin films containing 50 μm-wide channels were implanted in 8 rabbit eyes for a period of 1 to 6 months. The thin films used in this study were previously measured to be approximately 5 μm thick[59].

5.4.2 Ocular Findings in Device-Injected Rabbit Eyes

Ocular tolerance was studied in 11 eyes (3 control, 3 anterior chamber implants, 5 vitreous implants) for a period of 1 to 6 months (Table 5.1). None of the 8 device-implanted eyes developed chronic inflammation from the PCL implant. In 7 of the 8 injected eyes, transient conjunctival injection occurred, although this resolved within 1 week in 4 of the eyes. In 2 of the 8 eyes iritis occurred, although these acute inflammatory responses are not uncommon after needle injection using a 20-gauge needle. In 3 eyes posterior capsular traumatic cataracts resulted from the needle injection, although these remained stable throughout the duration of the experiments and follow-up examinations (Table 5.3). No eyes developed endophthalmitis, retinal detachment, vitreous hemorrhage, or retinal degeneration (Tables 5.2 and 5.3). Full details of the complications are shown in Table 5.2 for the 3 eyes in which the PCL devices were injected into the anterior chamber and Table 5.3 for the 5 eyes in which the PCL devices were injected directly into the vitreous cavity. Furthermore, all 8 devices remained relatively stationary, with no device migration exceeding 1 clock hour or posterior dislocation observed during the 1 to 6 month experimental period.

5.4.3 Histology

Histological exams of all 8 device-implanted eyes showed no inflammation or morphologic abnormalities at specific areas such as the trabecular meshwork, lens, or retina. Figure 5.4 demonstrates the ocular tolerance of the PCL device with representative histological images from a rabbit eye containing a PCL implant 4 months post-op. Further analysis revealed no evidence of retinal degeneration or device rejection such as fibrotic encapsulation in any of the study eyes over 1 to 6 months.

5.4.4 Scanning Electron Microscopy Evaluation of Retrieved PCL Thin Films

Thin film devices retrieved from all 8 eyes were imaged using scanning electron microscopy to evaluate device integrity and degradation. All devices maintained structural integrity over 1 to 6 months as represented by Figure 5.5. No cellular debris, inflammatory cells, or fibrosis was found on the smooth or microgrooved device surfaces. Devices containing a microgrooved surface also showed no structural damage or degradation due to implantation (Figure 5.5B and C).

5.5 Discussion

Effective drug delivery methods in clinical ophthalmology have long been limited to topical eye drops and intraocular injections. In the past decade, sustained-release drug delivery devices such as the Dexamethasone Posterior Segment Drug Delivery System (DEX-PS DDS)[39] and Retisert[43] have proven that long term delivery of therapeutics can be beneficial to eye disease treatment. However, these types of devices are only capable of delivering small molecule therapeutics such as corticosteroids. There is therefore an urgent need for an injectable device capable of delivering protein therapeutics for an extended period. Ideally, such a device would be constructed of a biodegradable material able to decompose and not require surgical removal from the eye after fully distributing its therapeutic load. We have evaluated polycaprolactone thin films in the rabbit eye as a potential material from which such a device could be constructed.

In order for a drug delivery device to properly function in the eye it must not cause extensive inflammation or lead to an immune response in the eye.

Polycaprolactone thin films were implanted in 8 rabbit eyes for a period of 1-6 months, during which the ocular tolerance of the device was evaluated. Importantly, none of the 8 eyes developed chronic inflammation, suggesting that polycaprolactone is a viable material candidate for a sustained-release drug delivery device. It is also important to note that none of the 8 eyes developed endophthalmitis, retinal detachment, vitreous hemorrhage, or retinal degeneration. The few complications that did occur were minor or remained stable throughout the course of the experiment and are commonly associated with intraocular injections.

Implanted thin films also did not invoke an immune response from the host rabbits. Thin films removed from the rabbit eye after 1-6 months showed no signs of fibrotic encapsulation or cellular debris. This was true for both microstructured and unstructured PCL thin films, suggesting that the surface structures are benign in terms of ocular tolerance. These results prove that PCL is well tolerated in the eye in the form of a thin film, and a drug delivery device made from PCL should be explored further.

5.6 Conclusions

Polycaprolactone thin films are well tolerated in the rabbit eye for at least 6 months, showing no signs of chronic inflammation during this period. After 6 months implanted thin films are also structurally intact, suggesting that a drug delivery device made of this material would not lose integrity or biodegrade during the time it is required to administer therapeutics. These results suggest polycaprolactone is a viable candidate material for long-term drug delivery to the eye.

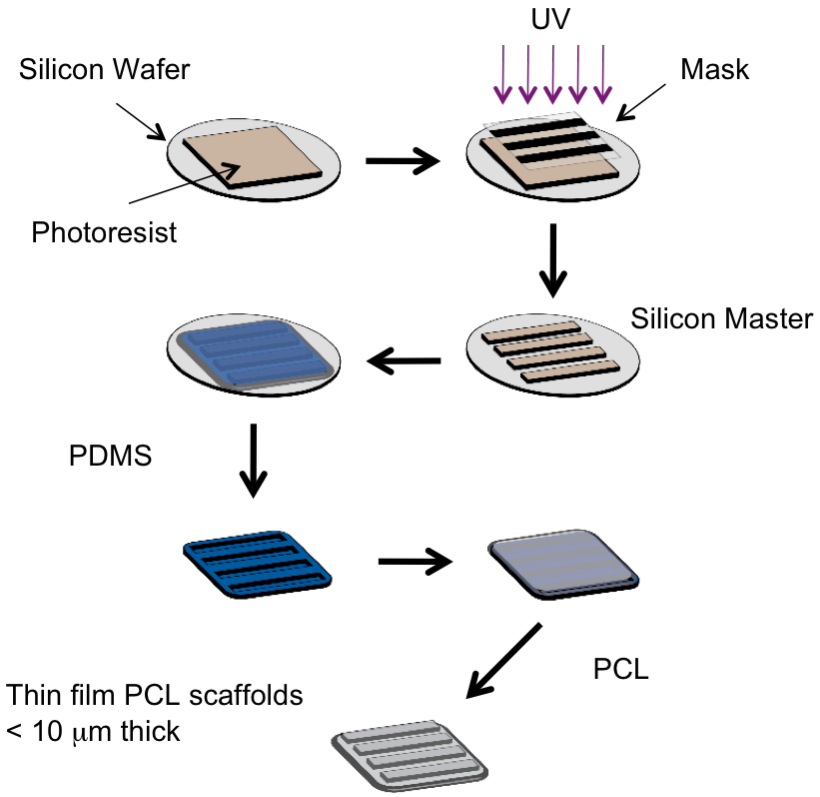

Figure 5.1: Microgrooved PCL Thin Film Fabrication.

Polycaprolactone thin films were fabricated using a three-step process. First, a micropatterned silicon master was fabricated using standard photolithography techniques. A layer of negative photoresist was spin cast onto a silicon wafer, and an array of micro-grooves was patterned using a photomask and UV light. Areas of the wafer that were not photo-crosslinked were removed by washing the wafer in developer. Second, an inverse pattern of the silicon wafer was fabricated using poly(dimethylsiloxane). The base and curing agent were mixed, degassed under vacuum, poured onto the micropatterned wafer and baked. Once cured, the PDMS was peeled from the silicon master. Third, a polymeric thin film containing the inverse pattern of the PDMS was fabricated by spin coating a solution of polycaprolactone on top of the PDMS. A copious amount of polycaprolactone solution was poured onto the micropatterned PDMS and spin cast.

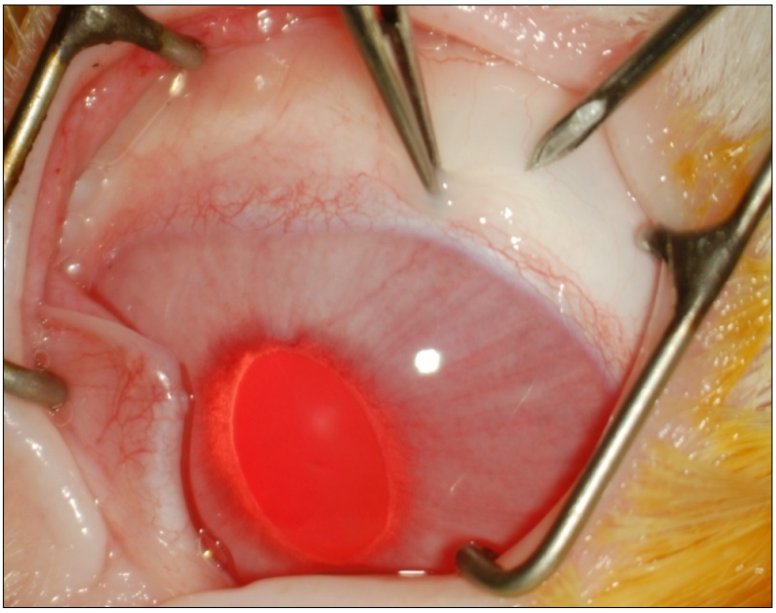

Figure 5.2: Polycaprolactone Thin Film Device Implantation.

Devices were implanted in New Zealand rabbit eyes (8 eyes in 6 rabbits) into the anterior chamber (3 eyes) and vitreous cavity (5 eyes) using a 20-gauge needle injection.

Table 5.1: Summary of clinical follow-up examinations.

Ocular finding	
Ocular inflammation* Transient conjunctival injection Iritis	 7 of 8 eyes 2 of 8 eyes
Cataract **	3 of 8 eyes
Intraocular pressure	18 mmHg (mean) Range (7.5 to 35 mmHg)
Endophthalmitis	None
Vitreous hemorrhage	None
Retinal detachment	None
Retinal degeneration	None
Device migration/dislocation	None

* Conjunctival injection resolved in 4 eyes within 1 week
Iritis resolved in both eyes after one week

** Traumatic cataract from needle injection which remained stable for duration of follow-up

Table 5.2: Full results from 3 anterior chamber implants.

	Post-op Day	IOP	Conj. Injection	Corneal Edema	Wound Leakage	A/C cell	A/C fibrin	Hyphema	Cataract	Vitreous Hemorrhage	Vitreous cell	Retinal tear	Retinal tear	Retinal Detachment	Endophthalmitis	Presence of Device	Site of Device
Rabbit A, OD	1	7.5	2	N	N	0	N	N	N	N	N	N	N	N	N	Y	11
	7	24	0	N	N	0	N	N	N	N	N	N	N	N	N	Y	11
	14	24	0	N	N	0	N	N	N	N	N	N	N	N	N	Y	10
	30	20	0	N	N	0	N	N	N	N	N	N	N	N	N	Y	10
	60	23.5	1	N	N	0	N	N	N	N	N	N	N	N	N	Y	10
	90	23	0	N	N	0	N	N	N	N	N	N	N	N	N	Y	10
	120	12.5	1	N	N	0	N	N	N	N	N	N	N	N	N	Y	10
Rabbit B, OD	1	17.5	2	N	N	0	N	N	N	N	N	N	N	N	N	Y	6
	7	16	3	N	N	0	N	N	N	N	N	N	N	N	N	Y	5
	14	13	0	N	N	0	N	N	N	N	N	N	N	N	N	Y	5
	30	18.5	0	N	N	0	N	N	N	N	N	N	N	N	N	Y	6
Rabbit C, OD	1	10.5	2	N	N	0	N	N	N	N	N	N	N	N	N	Y	10
	7	14	0	N	N	0	N	N	N	N	N	N	N	N	N	Y	10
	14	10	0	N	N	0	N	N	N	N	N	N	N	N	N	Y	10
	30	27	0	N	N	0	N	N	N	N	N	N	N	N	N	Y	10

Table 5.3: Full results from 5 vitreous cavity implants.

	Post-op Day	IOP	Conj. Injection	Corneal Edema	Wound Leakage	A/C cell	A/C fibrin	Hyphema	Cataract	Vitreous Hemorrhage	Vitreous cell	Retinal tear	Retinal Detachment	Endophthalmitis	Presence of Device	Site of Device
Rabbit C, OS	1	12.5	2	N	N	0	N	N	N	N	N	N	N	N	Y	6
	7	10	0	N	N	0	N	N	N	N	N	N	N	N	Y	6
	14	15	0	N	N	0	N	N	N	N	N	N	N	N	Y	6
	30	7.5	0	N	N	0	N	N	N	N	N	N	N	N	Y	6
Rabbit D, OD	1	10.5	0	N	N	0	N	N	Y	N	N	N	N	N	Y	11
	7	15	0	N	N	0	N	N	Y	N	N	N	N	N	Y	11
	14	15	0	N	N	0	N	N	Y	N	N	N	N	N	Y	11
	30	30	0	N	N	0	N	N	Y	N	N	N	N	N	Y	11
	60	28	0	N	N	0	N	N	Y	N	N	N	N	N	Y	11
Rabbit E, OS	1	24	2	Y	N	0	N	N	N	N	N	N	N	N	Y	2
	7	35	1	N	N	0	N	N	N	N	N	N	N	N	Y	2
	14	13.5	2	N	N	0	N	N	N	N	N	N	N	N	Y	3
	30	27	1	N	N	0	N	N	N	N	N	N	N	N	Y	2
	60	25.5	0	N	N	0	N	N	N	N	N	N	N	N	Y	2
	90	20	0	N	N	0	N	N	Y	N	N	N	N	N	Y	2
	120	20	0	N	N	0	N	N	Y	N	N	N	N	N	Y	2
	150	23.5	0	N	N	0	N	N	Y	N	N	N	N	N	Y	2.5
	180	25	0	N	N	0	N	N	Y	N	N	N	N	N	Y	3
Rabbit F, OS	1	17	1	N	N	0	N	N	N	N	N	N	N	N	Y	7
	7	14.5	1	N	N	0	N	N	N	N	N	N	N	N	Y	7
	14	13.5	0	N	N	0	N	N	N	N	N	N	N	N	Y	7
	30	15.5	0	N	N	0	N	N	N	N	N	N	N	N	Y	7
	60	16	0	N	N	0	N	N	N	N	N	N	N	N	Y	7
	90	16.5	0	N	N	0	N	N	N	N	N	N	N	N	Y	6
	120	23	0	N	N	0	N	N	N	N	N	N	N	N	Y	6
	150	19.5	0	N	N	0	N	N	N	N	N	N	N	N	Y	6.5
	180	25	0	N	N	0	N	N	N	N	N	N	N	N	Y	6
Rabbit F, OD	1	14	1	N	N	0	N	N	Y	N	N	N	N	N	Y	10
	7	17.5	0	N	N	0	N	N	Y	N	N	N	N	N	Y	10
	14	23.5	1	N	N	0	N	N	Y	N	N	N	N	N	Y	10
	30	15.5	0	N	N	0	N	N	Y	N	N	N	N	N	Y	10
	60	23.5	1	N	N	0	N	N	Y	N	N	N	N	N	Y	10
	90	15	0	N	N	0	N	N	Y	N	N	N	N	N	Y	10
	120	28	0	N	N	0	N	N	Y	N	N	N	N	N	Y	11
	150	27	0	N	N	0	N	N	Y	N	N	N	N	N	Y	11
	180	24	0	N	N	0	N	N	Y	N	N	N	N	N	Y	11

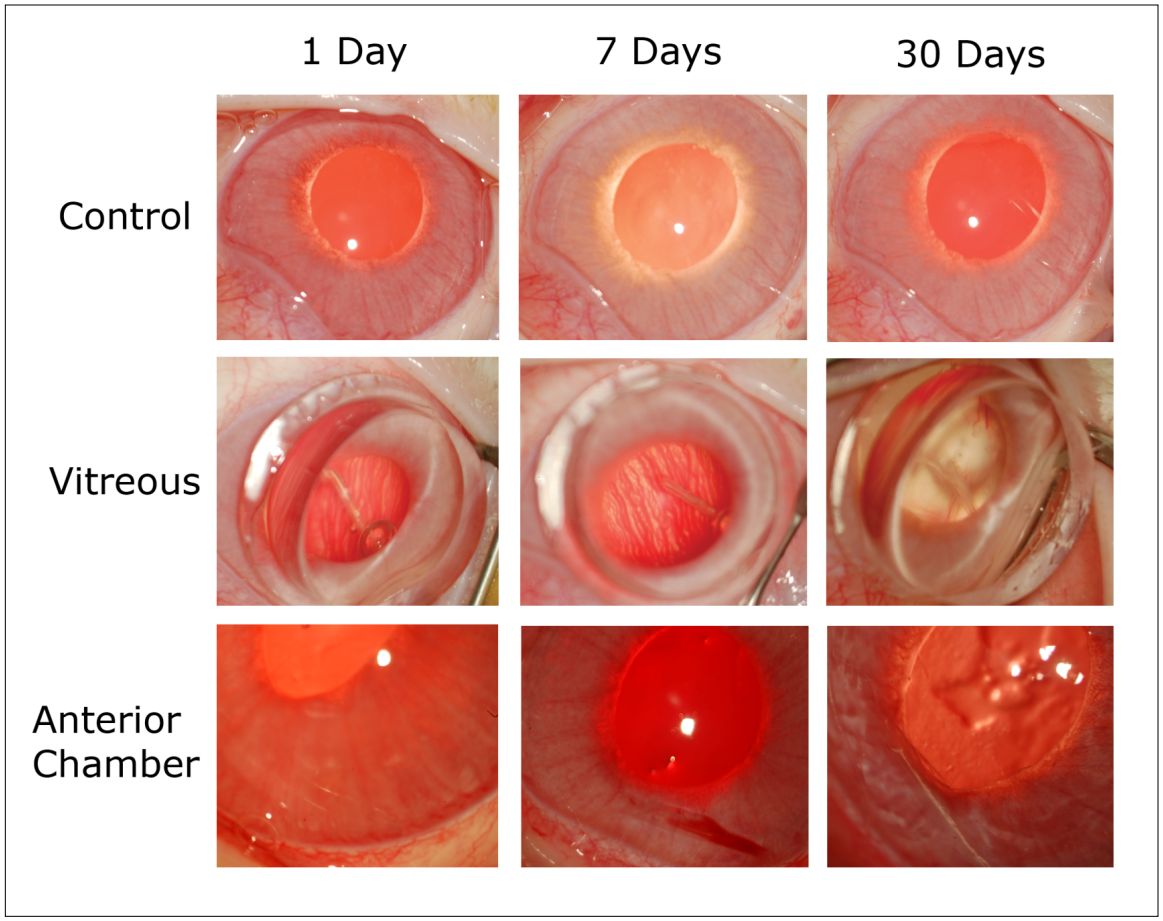

Figure 5.3: Clinical follow-up examinations of polycaprolactone implantations.

Representative images of clinical follow-up examinations at 1, 7 and 30 days post-op. The control images show the anterior segment demonstrating no inflammation. A posterior segment exam of a vitreous implant shows no posterior segment complications. An exam of the anterior segment shows no inflammation.

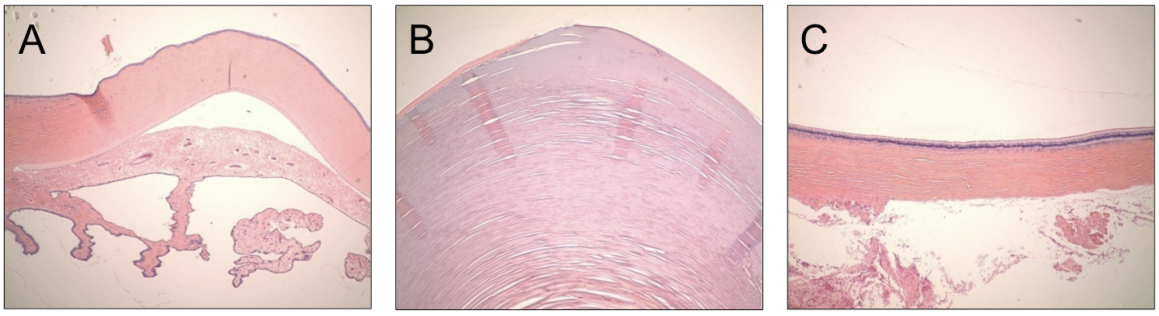

Figure 5.4: Rabbit histology.

Representative histology photographs from post-op month 4 eye containing PCL implant. (A) The anterior segment cross section shows no corneal edema, loss of endothelial cells, anterior chamber inflammation, or angle, iris, or ciliary body inflammation. (B) The lens cross section shows no lens epithelial changes or cataractous changes. (C) The retina cross section shows no retinal or choroidal inflammation, or retinal degeneration. All images magnified 5X.

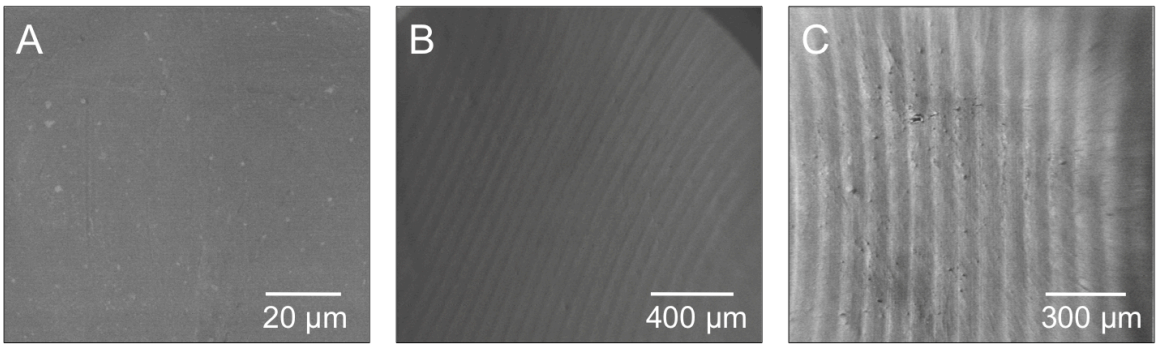

Figure 5.5: Scanning electron micrographs of implanted polycaprolactone thin films.

Representative scanning electron micrographs of a PCL device retrieved from the vitreous cavity at 4 months post-op. Results demonstrated no cellular debris, inflammatory cells, or fibrosis was found on the device surfaces. (A) Smooth and (B and C) microgrooved PCL thin films showed no structural damage or device degradation after implantation and 4 months of ocular residency.

Chapter 6 – A Multilayered Flexible Thin Film Polymer Drug Delivery Platform for the Long-Term Release of Protein Therapeutics

6.1 Abstract

We present a novel biodegradable drug delivery platform based on polycaprolactone (PCL) thin film technology with the ability to release active protein therapeutics for up to 8 weeks with zero-order release kinetics. Drug delivery devices capable of long-term controlled release of protein therapeutics would be beneficial in treating multiple diseases. Furthermore, constructing these devices from biodegradable materials eliminates the need for eventual device removal. Previously, drug delivery devices such as microparticles and nanoparticles made from biodegradable polymers such as poly(lactic-co-glycolic acid) (PLGA) and PCL have been developed with the capacity to deliver small molecule drugs for days to weeks. We have developed a thin film drug delivery device that extends this delivery window into multiple months, and we demonstrate that it is capable of delivering bovine serum albumin or active immunoglobulin G throughout the course of this time frame.

6.2 Introduction

Chronic diseases often require long-term treatment strategies that rely on conventional drug delivery methods such as injections and other procedures that necessitate regular hospital visits. Controlled long-term drug delivery has many advantages over these traditional methods. Maintaining drug concentration within a clinically relevant therapeutic window minimizes overdosing and drug waste and leads to fewer side effects and an increase in patient compliance and drug efficacy. Several technologies have been developed that utilize these principles of long-term drug delivery, including implantable infusion pumps for the delivery of chemotherapeutics[107-109], insulin pumps for the treatment of diabetes mellitus[110], and spinal drug administration systems for the treatment of lower back pain[111, 112]. Although these drug delivery systems can be effective for periods of up to several years, they rely on mechanically complex pumps that either require surgical implantation or for the device to reside outside the body. Significant disadvantages of these technologies include risks associated with surgical implantation such as infection and device rejection, device refilling or removal once the drug reservoir has emptied, and cumbersome external devices that must be constantly monitored.

Recent developments in long-term drug delivery systems have focused on miniaturization to target specific organs and overcome the aforementioned obstacles. The eye is particularly well suited for long-term controlled drug delivery due to its small size and the chronic nature of many of the diseases that affect it including uveitis, diabetic macular edema, glaucoma, and age-related macular degeneration[113]. Two long-term controlled release drug delivery devices, Retisert and Iluvien, are intravitreal inserts

that have been developed specifically for the eye and have been shown to deliver fluocinolone acetonide for up to 3 years[39, 43-47]. This corticosteroid is used to treat uveitis and diabetic macular edema and is most effective if delivered directly into the vitreous. Although effective, these devices are non-degradable and are limited to the delivery of a small molecule drug.

A third corticosteroid-based long-term controlled release intravitreal insert, Ozurdex, was recently approved to treat macular edema by releasing dexamethasone for 6 months[39-42, 114, 115]. While this device is biodegradable and does not require extraction once its drug reservoir has emptied, it is limited to the delivery of a small molecule. Other controlled release drug delivery devices made from biodegradable polymers have been studied but not yet brought to market. Delivery platforms such as microparticles[116, 117] and nanoparticles[118, 119] have been used to encapsulate drugs in polymers such as poly(lactic acid) (PLA)[120, 121], poly(lactic-co-glycolic acid) (PLGA)[122-124], and polycaprolactone (PCL)[125, 126]. Controlled release of small molecule drugs such as haloperidol[127], honokiol[128], dexamethasone[129], and budesonide[130] from these devices can be regulated for periods of days[131] to weeks[127]. However, the long-term delivery of protein therapeutics has not been achieved.

Protein therapeutics are often the most effective and sometimes the only available treatments for many diseases. Neovascular age-related macular degeneration is most effectively treated with anti-vascular endothelial growth factor formulations such as Lucentis and Avastin[30, 96, 132, 133]. These treatments must be injected directly into the vitreous on a monthly basis, an invasive procedure whose side effects can include endophthalmitis, intraocular pressure elevation, cataract, and retinal detachment[39]. A

long-term controlled release drug delivery device capable of delivering protein therapeutics to the eye would minimize the number of intraocular injections required for treatment while maintaining a therapeutic concentration of drug within the eye.

In this study, we present a novel drug delivery platform for long-term controlled release of protein therapeutics based on a porous PCL/gelatin thin film technology. Previously, we used PCL thin films for a retinal tissue engineering application[59]. As a long-term drug delivery device must be well tolerated throughout the duration of its implantation and degradation, PCL was chosen due to its biocompatibility and biodegradability in vivo[68, 71, 134]. PCL capsules of similar molecular weight to that used in this study were previously implanted subcutaneously in rats. Over the course of two years these capsules maintained their structure and were then metabolized and excreted without accumulating in any organs[134].

Dissolved PCL and gelatin were combined and spin cast to form polymer thin films. Upon exposure to water, the hydrophobic PCL portion of the film maintained its structure whereas the gelatin rapidly dissolved, leaving microporous architecture. These thin films were then used as the top layer of a two-layer thin film device with lyophilized protein contained between the microporous layer and nonporous PCL base layer.

We demonstrate the elution of two proteins, bovine serum albumin (BSA) and immunoglobulin G (IgG) from these thin films with zero-order release kinetics for 8 weeks. This type of drug delivery platform could be used to treat multiple eye diseases and could also be effective in many other parts of the body. The polymer thin films used to fabricate the device presented in this study are scrollable and can be inserted into the tip of a small needle and injected into the eye using the same procedure currently used for

clinical intraocular injections. A biodegradable and injectable thin film device capable of delivering protein therapeutics for multiple months could eliminate the need for repeated intraocular injections while maintaining a constant level of therapeutic in the eye throughout the lifetime of the device.

6.3 Materials and Methods

6.3.1 Microporous Thin Film Fabrication

Thin films were spin-cast onto a flat circular poly(dimethylsiloxane) (PDMS) (Sylgard 184, Dow Corning, Midland, MI) mold due to its flexibility and the delicacy of the PCL/gelatin thin films. To fabricate the PDMS mold, the base and curing agent were mixed at a 10:1 ratio, degassed under vacuum, poured onto a 3" Silicon wafer, and baked at 65°C for 2 hours. Once cured, the PDMS was peeled from the silicon master and cut into a 35 mm diameter circle. Separate solutions of polycaprolactone (PCL) (MW 80,000, Sigma-Aldrich, St. Louis, MO) and gelatin (from porcine skin, Sigma-Aldrich) were constantly stirred in 0.1 g mL^{-1} 2,2,2-trifluoroethanol (TFE) (Sigma-Aldrich) on a hot plate at 80°C until dissolved. PCL and gelatin solutions were then combined into centrifuge tubes in the following volumetric ratios: 7:3, 8:2, 9:1, and 10:0 (PCL:Gelatin). To mix the PCL and gelatin together, solutions were vortexed for 30 seconds and inverted twice. This process was repeated for at least 5 minutes per solution immediately prior to casting. PCL/gelatin solutions were spin cast using a P6700 Series Spincoater (Specialty Coating Systems, Indianapolis, IN) at 1500 RPM for 1 minute as previously

described[59]. Thin films were carefully peeled from the PDMS mold after spin casting using forceps.

6.3.2 Thin Film Degradation Analysis

Thin films were stored in PBS under constant agitation for 5 days. Prior to imaging, samples were rinsed with deionized water and dehydrated in a vacuum oven. Samples were imaged using a *my*SEM scanning electron microscope (NovelX, Lafayette, CA) with an accelerating voltage of 1 kV. For pore area and porosity calculations, 3 thin films of each PCL:Gelatin ratio were imaged. For each thin film, 10 random areas per thin film were imaged and compiled. Pore areas were calculated using ImageJ (National Institutes of Health, Bethesda, MD).

6.3.3 Multilayered Thin Film Device Fabrication

Devices were fabricated from two thin films, a nonporous PCL base layer and a microporous 9:1 PCL/gelatin top layer as illustrated in Figure 6.3. PCL base layers were fabricated using a concentrated solution of PCL (0.2 g mL^{-1} in TFE), which were spin cast at 1500 RPM for 2 minutes onto a silicon wafer. Lyophilized protein (1-4 mg) was placed in between the two device layers and secured on a silicon wafer. An annulus-shaped piece of PDMS was heated to 80°C then placed on top of the two thin films. A flat stainless steel weight (170 g) was used to press down on the PDMS annulus for 30 seconds, melting and sealing the two films together. Elution of BSA and IgG from thin film devices was monitored for 10 weeks and compared to elution from nonporous PCL-only devices. Three devices of each type were fabricated and analyzed per experiment.

6.3.4 Profilometry

Device thickness was characterized with an Ambios Technology XP-2 Stylus Profiler (Santa Cruz, CA). Profilometry was conducted with a scan speed of 0.01 mm sec^{-1}, a length of 1.5 mm and a stylus force of 0.2 mg.

6.3.5 Micro Bicinchoninic Acid Assay

A micro bicinchoninic acid assay (Thermo Scientific Pierce, Rockford, IL) was performed to quantify protein elution from PCL thin film devices. Multilayered thin films loaded with lyophilized BSA (Sigma-Aldrich) or IgG (isolated from bovine serum, Sigma-Aldrich) were placed in 5 mL of PBS in centrifuge tubes and shaken continuously at room temperature for 10 weeks. 1 mL of solution was removed during sampling and replaced with fresh PBS. Samples were read at 562 nm on a SpectraMax 190 microplate reader (Molecular Devices, Sunnyvale, CA). Data and linear regression analysis were performed in Excel (Microsoft, Redmond, WA).

6.3.6 Bovine IgG Enzyme Linked Immunosorbent Assay (ELISA)

A bovine IgG enzyme linked immunosorbent assay (ELISA) (Bethyl Laboratories, Inc., Montgomery, TX) was performed to verify the activity of eluted IgG from PCL/gelatin devices. Total protein sample concentrations were first determined with a micro bicinchoninic acid assay, and then diluted 1/100 to fall within the dynamic range of the ELISA assay. These samples were then assayed, and the resulting concentration values were compared to the previous bicichoninic acid assay results. A

ratio of the two concentration values was calculated over four time points between 1 and 70 days after device construction.

6.4 Results and Discussion

6.4.1 Microporous Thin Film Fabrication and Degradation

Solutions of PCL and gelatin were combined, respectively, in the following volumetric ratios: 7:3, 8:2, 9:1 and 10:0. After vigorous mixing, the combined solutions were spin cast into flexible polymer thin films**.** Initially nonporous, thin films were exposed to PBS for 5 days to eliminate the readily soluble gelatin components of the thin films. After 5 days of degradation in PBS, thin films were imaged using scanning electron microscopy (Figure 6.1). Micropores were found in all thin films containing gelatin, while PCL-only thin films showed no signs of degradation or porous architecture. Individual pore areas were quantified and are displayed in Figure 6.1.

Thin films fabricated with the highest concentration of gelatin (7:3) contained a broad range of pore sizes, the smallest less than 2 μm in diameter and the largest over 30 μm in diameter (Figure 6.1a and 6.1b). Thin films with a medium gelatin concentration (8:2) also contained a wide range of pore sizes, although the largest pores found in these films were smaller than in the 7:3 gelatin thin films and only reached a maximum of 28 μm in diameter (Figure 6.1c and 6.1d). Thin films with the lowest gelatin concentration (9:1) contained much smaller pores, 95% of which were smaller than 10 μm in diameter (Figure 6.1e and 6.1f). Thin films fabricated without gelatin (10:0) were nonporous throughout the entire spin cast thin film surface (not shown).

The percent porosity, or the pore area divided by the total area of each thin film was quantified and is shown in Figure 6.2a. As the gelatin rapidly dissolves in PBS, increasing the amount of gelatin in the thin films led to more porosity after degradation. The 7:3 films were the most porous, followed by the 8:2 films, and then by the 9:1 films. Since the 10:0 films contained no gelatin, no degradation and therefore no porosity was observed.

The porosity found in the thin films is due to the incomplete mixing of PCL and gelatin. Although both species dissolve in TFE, combining the two solutions results in a heterogeneous emulsion that must be constantly mixed or the two solutions will separate into two immiscible liquids. Due to the high viscosity of the dissolved solutions it was empirically determined that maintenance of a consistent mixture necessitated near-constant vortexing prior to spin casting. Adding increasing amounts of gelatin resulted in aggregation of the gelatin in the PCL/gelatin mixture that was not found in the 9:1 thin films.

Degradation was also quantified using the amount of mass lost after 5 days in PBS. Initial mass was determined prior to PBS immersion, while post-degradation mass was determined after 5 days in PBS and subsequent dehydration of the thin films in a vacuum oven. Results were consistent with pore area and percent porosity; the 7:3 thin films lost the most mass, approximately 25% of their initial mass, while 8:2 films lost just less than 10% on average. 9:1 thin films lost less than 5%, and films containing no gelatin gained a very small amount of mass due to the immersion in PBS (Figure 6.2b). This most likely occurred due to water and salt absorption, causing the PCL areas to swell during immersion in PBS.

6.4.2 Multilayered Thin Film Device Fabrication and Drug Elution

PCL thin film devices were constructed from a PCL base layer and a microporous 9:1 PCL/gelatin top layer as diagramed in Figure 6.3. To restrict protein elution by minimizing the porosity of the device, only 9:1 PCL/gelatin thin films were used to make the microporous top layer for all protein-loaded experimental devices. Lyophilized protein was deposited between the two thin film layers, which were then melted together using a PDMS annulus. Devices were immersed in PBS, and elutions of BSA and IgG from the PCL/gelatin thin film devices were quantified over a 10-week period. Nonporous devices made from two PCL-only thin films were also constructed and used as controls.

BSA elution from porous PCL/gelatin thin film devices and nonporous PCL-only thin film devices is presented in Figure 6.4a. BSA eluted from the PCL/gelatin devices with zero-order kinetics for the first seven weeks, corresponding to slightly more than 60% of the ~3 mg BSA loaded into each device. Similarly, IgG elution is presented in Figure 6.4b. Zero-order elution from the 9:1 PCL/gelatin devices was also achieved with IgG for the first seven weeks.

Protein elution from one BSA-loaded and one IgG-loaded PCL/gelatin thin film device is directly compared in Figure 6.5. Elution for 7 weeks are displayed, corresponding to zero-order release kinetics with R^2 values of 0.99 and 0.94 for BSA and IgG, respectively. BSA eluted at a rate of 36 μg/day, while IgG eluted at a slower rate of 20 μg/day. IgG's slower elution rate is most likely due to its larger molecular weight (150 kDa versus 66 kDa for BSA).

IgG concentration was quantified using two different assays to verify protein activity throughout the course of the experiment. Figure 6.6 shows a comparison of the IgG concentration calculated by BCA and ELISA assays. The ratio of these two concentrations is plotted for four time points from 1 to 70 days of elution. The BCA assay quantifies total protein concentration, while the ELISA is much more specific and only quantifies bound IgG. A ratio of 1 represents an equal concentration of IgG between both assays, demonstrating that the IgG released from PCL/gelatin thin film devices is active after 70 days of elution. As the differences between the four data points are not significant and the standard deviations all fall within a ratio of 1 these results show that the IgG did not degrade over the course of the experiment.

6.5 Conclusions

Long-term zero-order elution kinetics from drug delivery devices is a highly desirable characteristic. It is well established that drug concentration within a therapeutic window can be directly correlated to drug efficiency, as underdosing can result in drug ineffectiveness and drug overdosing can result in adverse side effects. Implantable drug delivery devices offer the potential to improve drug efficacy by maintaining the most effective drug concentrations at the affected site and eliminating repetitive drug delivery procedures. For example, Lucentis, a 48 kDa antibody fragment used to treat age-related macular degeneration, must be injected into the vitreous of the eye monthly to remain effective. A drug delivery device that maintains a therapeutically effective concentration of Lucentis in the eye could be even more effective at minimizing vision loss. The PCL/gelatin drug delivery device described in this study is capable of holding over 3 mg

of lyophilized protein, a 6-fold increase over the 0.5 mg monthly dose of Lucentis. The current design elutes its payload in approximately 8-10 weeks, however it may be possible to decrease the pore size further, potentially down to the nanoscale, thereby substantially extending the lifetime of the device.

This study demonstrates that long-term controlled release of protein therapeutics from a biodegradable and biocompatible polycaprolactone thin film drug delivery device can be achieved with zero-order release kinetics for 8 weeks. Previously, biodegradable drug delivery platforms have succeeded in demonstrating long-term delivery of small molecules but have not had the same success with large molecules. For example, microparticles and nanoparticles can be effective at releasing therapeutics at a desirable rate for days to weeks but cannot contain a large enough drug reservoir to effectively deliver therapeutics for multiple months. A thin film drug delivery device containing a large drug reservoir, however, could be used to treat diseases that require constant release of therapeutic. We demonstrate that a microporous polycaprolactone/gelatin thin film device can successfully deliver large molecule protein therapeutics for multiple weeks with zero-order kinetics.

6.6 Acknowledgements

We thank Dr. Daniel A. Bernards, Dr. Miquella G. Chavez, Dr. Rachel D. Lowe, Dr. Robert M. Tucker, and Dr. Robert B. Bhisitkul for valuable insight and advice throughout the course of this study. This research was supported by the National Institutes of Health (NIH-NEI EY002161), an Allergan Horizon Grant, and the California Institute for Quantitative Biosciences (QB3).

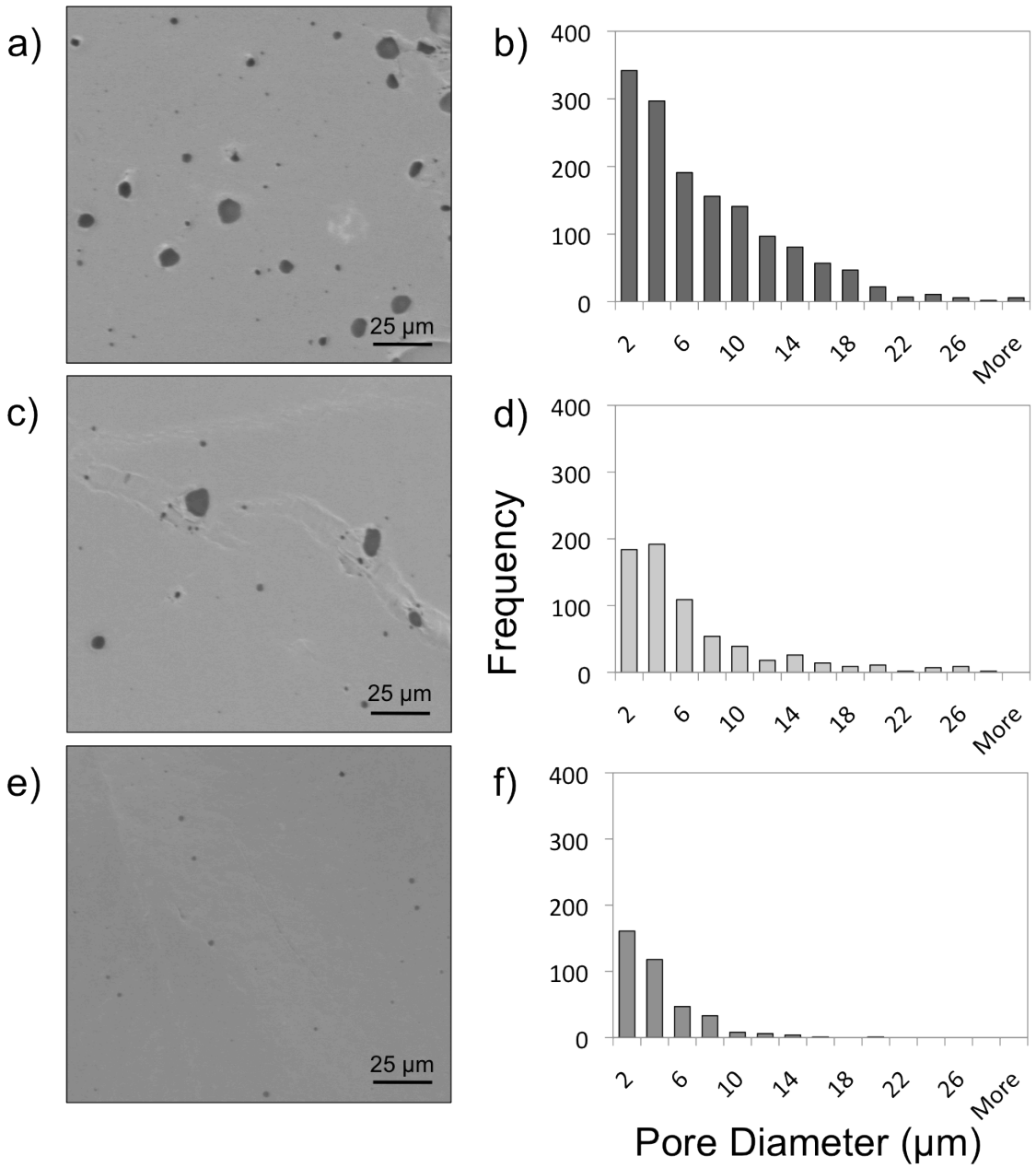

Figure 6.1: Scanning electron micrographs of PCL/gelatin thin films.

Scanning electron micrographs and corresponding pore size histograms of PCL/gelatin thin films after five days of degradation in PBS. Thin films were made from mixtures of PCL and gelatin at ratios of 7:3 (a and b), 8:2 (c and d), and 9:1 (e and f). Thin films made from PCL only did not contain any pores (not shown).

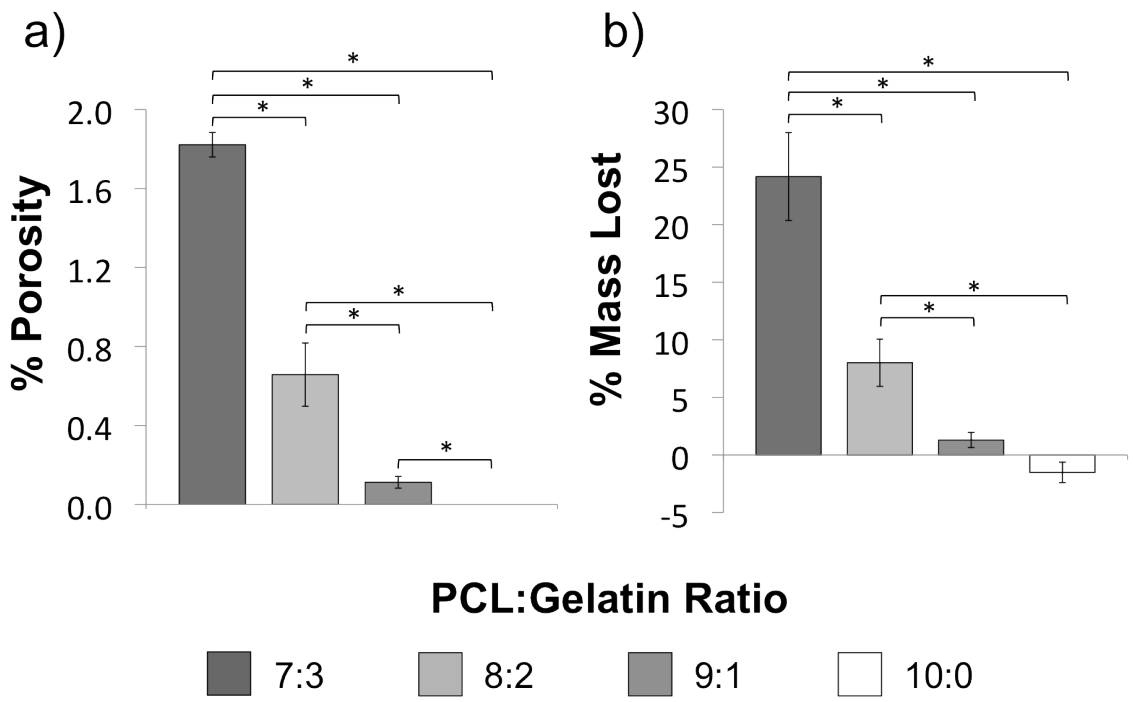

Figure 6.2: Degradation of PCL/gelatin thin films.

a) Percent porosity of PCL/gelatin thin films of varying gelatin concentrations after 5 days of degradation in PBS. Overall porosity increases with gelatin concentration. b) Porosity resulting from gelatin dissolution lead to a decrease in mass. PCL swelling and salt absorption leads to a small overall increase in mass for thin films containing no gelatin. *p<0.05, Student-Newman, Keuls test. Error bars indicate standard deviation over three independent experiments.

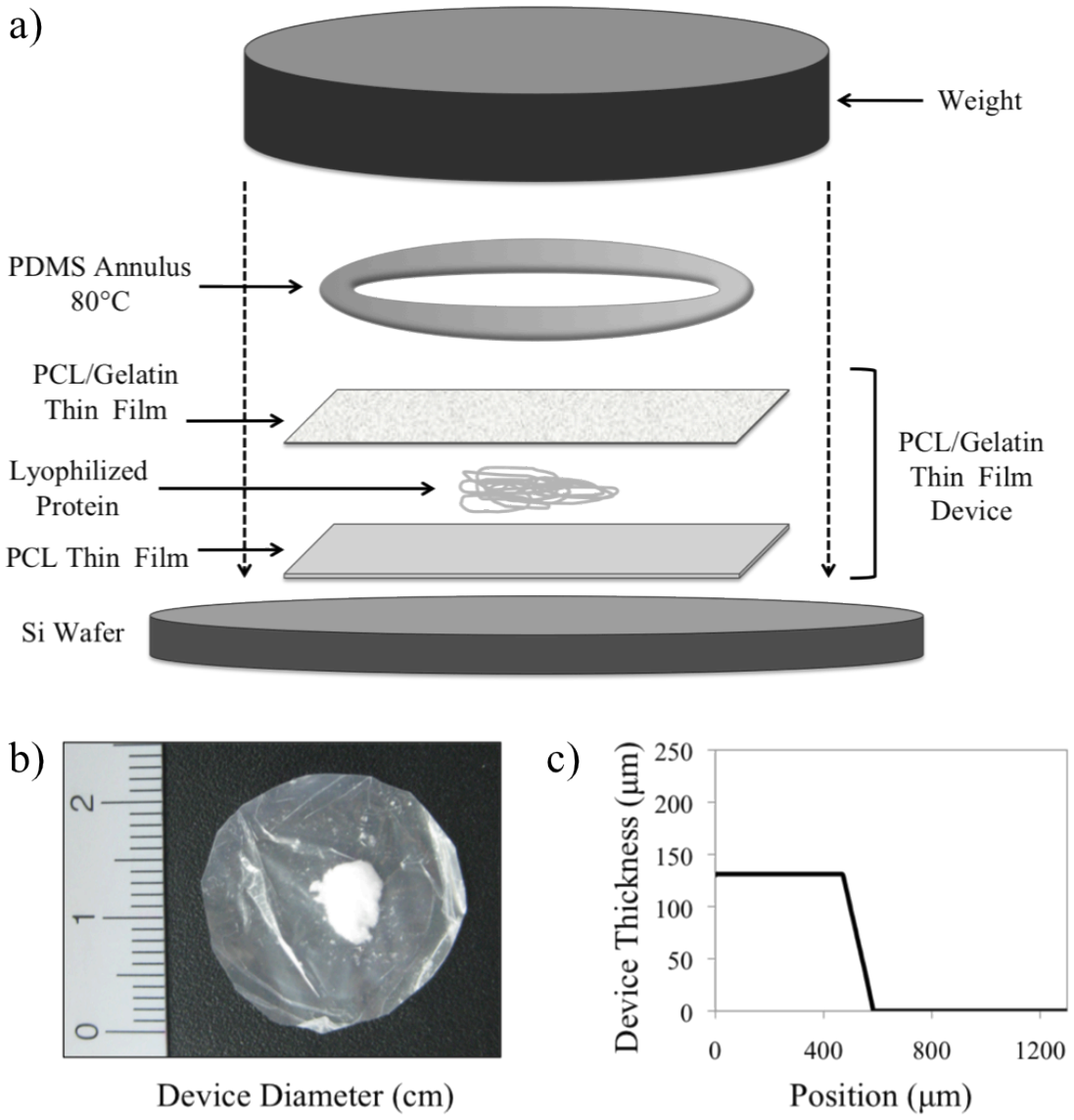

Figure 6.3: Multilayered Polymer Thin Film Device Fabrication.

a) Lyophilized protein was contained between a nonporous PCL thin film base layer and a microporous PCL/gelatin thin film. The thin films were placed on a silicon wafer and then pressed with a PDMS annulus heated to 80°C. The heated annulus melted the PCL and sealed the two thin films together. A small flat weight was used to ensure uniform sealing. b) A finished device ~2mm in diameter. c) Profile of PCL/Gelatin Device edge.

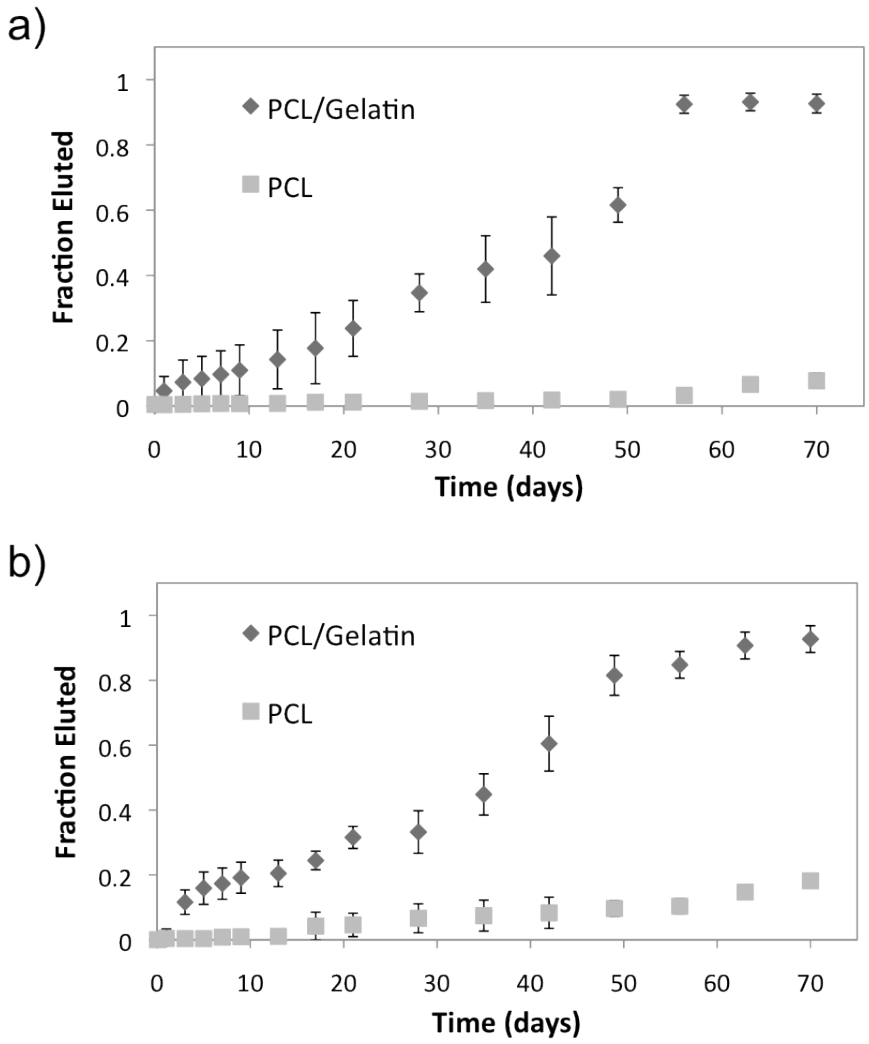

Figure 6.4: Protein elution from PCL/gelatin thin film device.

a) Fractional elution of BSA from 9:1 PCL/gelatin and PCL-only thin film devices. Zero-order elution was observed for the first 7 weeks in PCL/gelatin devices, after which device failure led to a burst release phase. PCL-only devices began to leak after 8 weeks. b) Fractional elution of IgG from 9:1 PCL/gelatin thin film devices. Zero-order elution of IgG from PCL/gelatin devices was observed for nearly all 10 weeks. Device failure occurred earlier and to a larger extent than BSA devices. Error bars indicate standard deviation over three independent experiments.

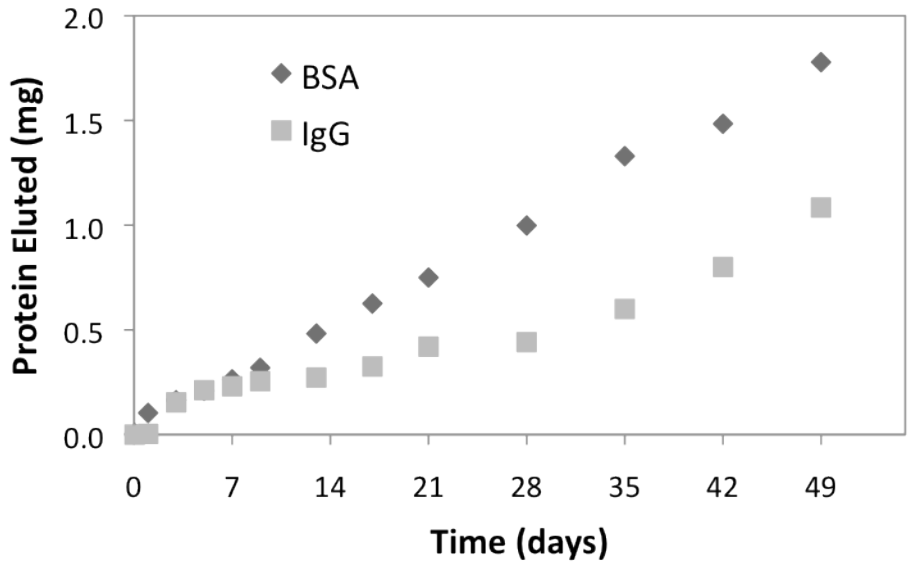

Figure 6.5: Rate of elution of BSA and IgG from PCL/gelatin thin film devices.

Comparison of BSA and IgG elution from 9:1 PCL/gelatin thin film devices. Larger molecular weight IgG (150 kDa) eluted at a slower rate than BSA (66 kDa). Linear regression analysis resulted in elution rates of 0.36 μg/day for BSA ($R^2 = 0.99$) and 0.20 μg/day for IgG ($R^2 = 0.94$).

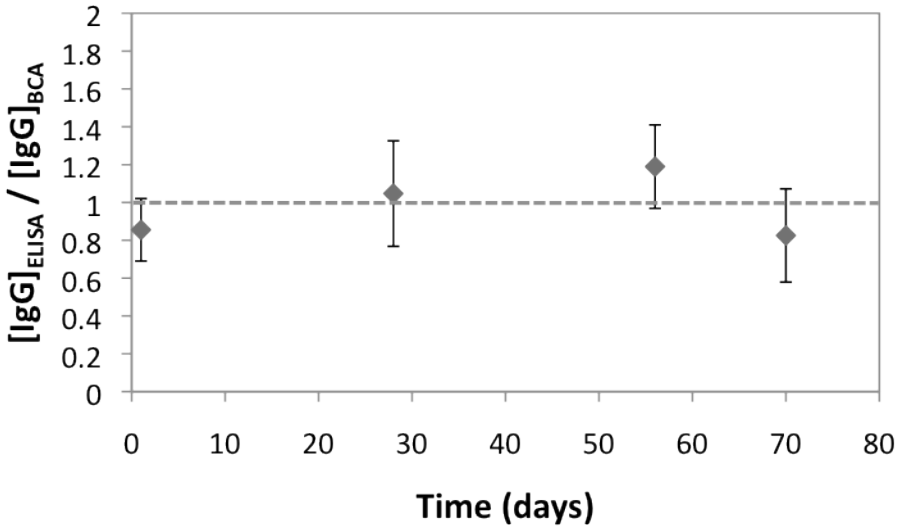

Figure 6.6: Ratio of eluted IgG concentrations determined by ELISA and BCA assays.

Concentrations compared at 1, 28, 56, and 70 days of elution. Error bars indicated standard deviation over three independent experiments.

Chapter 7 – Summary and Conclusions

Tissue engineering and drug delivery are two intertwined fields that will rely heavily on the further development of biomaterials in the coming years. The research presented in this dissertation focused on the development of polycaprolactone thin films for tissue engineering and drug delivery applications. The many experiments detailed here combined these thin films with other technologies such as micro and nanofabrication and led to a valuable collaboration between our home department, Bioengineering, and the Department of Ophthalmology.

We targeted age-related macular degeneration due to the inherent need to create a cure for this devastating disease and due to the complex requirements associated with implanting a device or material into the back of the eye. Previous work showed that thin films were an attractive cellular delivery vehicle for implanting retinal progenitors and other cells into a degenerated retina. These preliminary devices, although promising, were unable to cure macular degeneration, and therefore much more work was required. Experiments were needed to determine information such as how progenitor cells respond to three-dimensional topographical cues, the timescale by which polycaprolactone degrades in the eye, and many other factors.

After answering several of these questions we decided to transform our polycaprolactone thin films into more than just a vehicle for cellular delivery to the eye. Since current treatments for macular degeneration require monthly intraocular drug injections, we decided to use our thin film technology to create a drug delivery device for the eye capable of long-term delivery of protein therapeutics. We collaborated with Professor Robert Bhisitkul in the Department of Ophthalmology and initially investigated ocular tolerance of polycaprolactone in the rabbit eye. After finding that

polycaprolactone thin films are well tolerated for several months with no apparent side effects we decided to experiment with how to transform our thin films into drug-eluting devices.

Our first attempt at developing a drug-eluting device is presented in this dissertation in addition to the previously mentioned ocular tolerance data. We believe that with further development this thin film technology could be extremely beneficial to the treatment of macular degeneration and many other diseases.

References

1. D. Vaughan, T. Asbury and Lange Medical Books/McGraw-Hill., Lange Medical Books/McGraw-Hill, New York, 2004, p. v.
2. J. E. Dowling, *The retina : an approachable part of the brain*, Belknap Press of Harvard University Press, Cambridge, Mass., 1987.
3. C. A. Curcio, K. R. Sloan, R. E. Kalina and A. E. Hendrickson, *Journal of Comparative Neurology*, 1990, **292**, 497-523.
4. R. H. Masland, *Nat Neurosci*, 2001, **4**, 877-886.
5. I. Provencio, I. R. Rodriguez, G. S. Jiang, W. P. Hayes, E. F. Moreira and M. D. Rollag, *Journal of Neuroscience*, 2000, **20**, 600-605.
6. J. Hannibal, P. Hindersson, S. M. Knudsen, B. Georg and J. Fahrenkrug, *Journal of Neuroscience*, 2002, **22**, -.
7. D. T. Hartong, E. L. Berson and T. P. Dryja, *Lancet*, 2006, **368**, 1795-1809.
8. C. Rivolta, D. Sharon, M. M. DeAngelis and T. P. Dryja, *Human Molecular Genetics*, 2002, **11**, 1219-1227.
9. A. Abdelsalam, L. Del Priore and M. A. Zarbin, *Survey of Ophthalmology*, 1999, **44**, 1-29.
10. A. D. Kulkarni and B. D. Kuppermann, *Advanced Drug Delivery Reviews*, 2005, **57**, 1994-2009.
11. M. N. Delyfer, T. Leveillard, S. Mohand-Said, D. Hicks, S. Picaud and J. Sahel, *Biology of the Cell*, 2004, **96**, 261-269.
12. Z. F. Bashshur, A. Bazarbachi, A. Schakal, Z. A. Haddad, C. P. El Haibi and B. N. Noureddin, *American Journal of Ophthalmology*, 2006, **142**, 1-9.

13. R. B. Bhisitkul, *Brit J Ophthalmol*, 2006, **90**, 1542-1547.

14. J. S. Meyer, M. L. Katz, J. A. Maruniak and M. D. Kirk, *Stem Cells*, 2006, **24**, 274-283.

15. M. Takahashi, T. D. Palmer, J. Takahashi and F. H. Gage, *Molecular and Cellular Neuroscience*, 1998, **12**, 340-348.

16. K. Canola, B. Angenieux, M. Tekaya, A. Quiambao, M. I. Naash, F. L. Munier, D. F. Schorderet and Y. Arsenijevic, *Invest Ophth Vis Sci*, 2007, **48**, 446-454.

17. H. Klassen, J. F. Kiilgaard, T. Zahir, B. Ziaeian, I. Kirov, E. Scherfig, K. Warfvinge and M. J. Young, *Stem Cells*, 2007, **25**, 1222-1230.

18. M. J. Young, J. Ray, S. J. O. Whiteley, H. Klassen and F. H. Gage, *Molecular and Cellular Neuroscience*, 2000, **16**, 197-205.

19. H. J. Klassen, T. F. Ng, Y. Kurimoto, I. Kirov, M. Shatos, P. Coffey and M. J. Young, *Invest Ophthalmol Vis Sci*, 2004, **45**, 4167-4173.

20. R. E. MacLaren, R. A. Pearson, A. MacNeil, R. H. Douglas, T. E. Salt, M. Akimoto, A. Swaroop, J. C. Sowden and R. R. Ali, *Nature*, 2006, **444**, 203-207.

21. M. Tomita, E. Lavik, H. Klassen, T. Zahir, R. Langer and M. J. Young, *Stem Cells*, 2005, **23**, 1579-1588.

22. J. Z. Nowak, *Pharmacol Rep*, 2006, **58**, 353-363.

23. R. N. Frank, *N Engl J Med*, 2004, **350**, 48-58.

24. R. Klein, B. E. Klein, S. E. Moss, M. D. Davis and D. L. DeMets, *Arch Ophthalmol*, 1984, **102**, 520-526.

25. R. Klein, B. E. Klein, S. E. Moss, M. D. Davis and D. L. DeMets, *Arch Ophthalmol*, 1984, **102**, 527-532.

26. C. J. Chiu, R. Klein, R. C. Milton, G. Gensler and A. Taylor, *Br J Ophthalmol*, 2009, **93**, 1241-1246.

27. A. J. Augustin, S. Scholl and J. Kirchhof, *Clin Ophthalmol*, 2009, **3**, 175-182.

28. M. V. Emerson and A. K. Lauer, *Clin Ophthalmol*, 2008, **2**, 377-388.

29. P. P. Yip, C. F. Woo, H. H. Tang and C. K. Ho, *Br J Ophthalmol*, 2009, **93**, 754-758.

30. D. J. Pieramici and M. D. Rabena, *Eye*, 2008, **22**, 1330-1336.

31. R. L. Avery, D. J. Pieramici, M. D. Rabena, A. A. Castellarin, M. A. Nasir and M. J. Giust, *Ophthalmology*, 2006, **113**, 363-372.

32. A. M. Joussen and N. Bornfeld, *Dtsch Arztebl Int*, 2009, **106**, 312-317.

33. E. B. Lavik, H. Klassen, K. Warfvinge, R. Langer and M. J. Young, *Biomaterials*, 2005, **26**, 3187-3196.

34. B. A. Tucker, S. M. Redenti, C. H. Jiang, J. S. Swift, H. J. Klassen, M. E. Smith, G. E. Wnek and M. J. Young, *Biomaterials*, 2010, **31**, 9-19.

35. S. L. Tao, C. Young, S. Redenti, Y. Zhang, H. Klassen, T. A. Desai and M. J. Young, *Lab on a Chip*, 2007, **7**, 695-701.

36. W. L. Neeley, S. Redenti, H. Klassen, S. Tao, T. Desai, M. J. Young and R. Langer, *Biomaterials*, 2008, **29**, 418-426.

37. S. Redenti, S. Tao, J. Yang, P. Gu, H. Klassen, S. Saigal, T. Desai and M. J. Young, *Journal of Ocular Biology, Diseases, and Informatics*, 2008, **1**, 19-29.

38. S. A. Vinores, *Histol Histopathol*, 1995, **10**, 141-154.

39. S. S. Lee, P. M. Hughes and M. R. Robinson, *Current Opinion in Ophthalmology*, 2009, **20**, 511-519.

40. H. W. Kwak and D. J. Damico, *Arch Ophthalmol-Chic*, 1992, **110**, 259-266.

41. B. D. Kuppermann, M. S. Blumenkranz, J. A. Haller, G. A. Williams, D. V. Weinberg, C. Chou, S. M. Whitcup and D. D. P. I. S. G, *Arch Ophthalmol-Chic*, 2007, **125**, 309-317.

42. G. A. Williams, J. A. Haller, B. D. Kuppermann, M. S. Blumenkranz, D. V. Weinberg, C. Chou, S. M. Whitcup and D. D. P. I. S. G, *American Journal of Ophthalmology*, 2009, **147**, 1048-1054.

43. D. A. Mohammad, B. V. Sweet and S. G. Elner, *Annals of Pharmacotherapy*, 2007, **41**, 449-455.

44. D. G. Callanan, G. J. Jaffe, D. F. Martin, A. Pearson and T. L. Comstock, *Arch Ophthalmol-Chic*, 2008, **126**, 1191-1201.

45. M. Taban, C. Y. Lowder and P. K. Kaiser, *Retina-the Journal of Retinal and Vitreous Diseases*, 2008, **28**, 1280-1288.

46. K. E. Bollinger and S. D. Smith, *Current Opinion in Ophthalmology*, 2009, **20**, 99-103.

47. P. A. Campochiaro, G. Hafiz, S. M. Shah, S. Bloom, D. M. Brown, M. Busquets, T. Ciulla, L. Feiner, N. Sabates, K. Billman, B. Kapik, K. Green, F. Kane and F. S. Grp, *Ophthalmology*, 2010, **117**, 1393-U1157.

48. S. R. Kedhar and D. A. Jabs, *Herpes*, 2007, **14**, 66-71.

49. S. Swapp, Scanning Electron Microscopy (SEM), http://serc.carleton.edu/research_education/geochemsheets/techniques/SEM.html, Accessed June 14, 2010.

50. Karnovsk.Mj, *Journal of Cell Biology*, 1965, **27**, A137-&.

51. C. Vonesch, F. Aguet, J. L. Vonesch and M. Unser, *Ieee Signal Processing Magazine*, 2006, **23**, 20-31.

52. R. Singhvi, A. Kumar, G. P. Lopez, G. N. Stephanopoulos, D. I. C. Wang, G. M. Whitesides and D. E. Ingber, *Science*, 1994, **264**, 696-698.

53. C. S. Chen, M. Mrksich, S. Huang, G. M. Whitesides and D. E. Ingber, *Science*, 1997, **276**, 1425-1428.

54. A. Folch, B. H. Jo, O. Hurtado, D. J. Beebe and M. Toner, *Journal of Biomedical Materials Research*, 2000, **52**, 346-353.

55. P. J. A. Kenis, R. F. Ismagilov and G. M. Whitesides, *Science*, 1999, **285**, 83-85.

56. E. Delamarche, A. Bernard, H. Schmid, A. Bietsch, B. Michel and H. Biebuyck, *Journal of the American Chemical Society*, 1998, **120**, 500-508.

57. J. L. Tan, J. Tien, D. M. Pirone, D. S. Gray, K. Bhadriraju and C. S. Chen, *Proceedings of the National Academy of Sciences of the United States of America*, 2003, **100**, 1484-1489.

58. W. R. Legant, A. Pathak, M. T. Yang, V. S. Deshpande, R. M. McMeeking and C. S. Chen, *Proceedings of the National Academy of Sciences of the United States of America*, 2009, **106**, 10097-10102.

59. M. R. Steedman, S. L. Tao, H. Klassen and T. A. Desai, *Biomedical Microdevices*, 2010, **12**, 363-369.

60. B. Alberts, Johnson, A., Lewis, J., Raff, M., Roberts, K., and Walter, P., *Molecular Biology of the Cell*, Garland Science, New York, 2002.

61. Z. F. Bashshur, A. Schakal, R. N. Hamam, C. P. El Haibi, R. F. Jaafar and B. N. Noureddin, *Arch Ophthalmol-Chic*, 2007, **125**, 1357-1361.

62. S. Redenti, W. L. Neeley, S. Rompani, S. Saigal, J. Yang, H. Klassen, R. Langer and M. J. Young, *Biomaterials*, 2009, **30**, 3405-3414.

63. S. Tao, C. Young, S. Redenti, Y. Q. Zhang, H. Klassen, T. Desai and M. J. Young, *Lab on a Chip*, 2007, **7**, 695-701.

64. C. A. Sundback, J. Y. Shyu, Y. D. Wang, W. C. Faquin, R. S. Langer, J. P. Vacanti and T. A. Hadlock, *Biomaterials*, 2005, **26**, 5454-5464.

65. K. Warfvinge, J. F. Kiilgaard, E. B. Lavik, E. Scherfig, R. Langer, H. J. Klassen and M. J. Young, *Arch Ophthalmol-Chic*, 2005, **123**, 1385-1393.

66. K. J. Lowry, K. R. Hamson, L. Bear, Y. B. Peng, R. Calaluce, M. L. Evans, J. O. Anglen and W. C. Allen, *Journal of Biomedical Materials Research*, 1997, **36**, 536-541.

67. Q. Huang, D. W. Hutmacher and E. H. Lee, *Tissue Engineering*, 2002, **8**, 469-482.

68. G. Giavaresi, M. Tschon, V. Borsari, J. H. Daly, J. J. Liggat, M. Fini, V. Bonazzi, A. Nicolini, A. Carpi, M. Morra, C. Cassinelli and R. Giardino, *Biomedicine & Pharmacotherapy*, 2004, **58**, 411-417.

69. J. Holmbom, A. Sodergard, E. Ekholm, M. Martson, A. Kuusilehto, P. Saukko and R. Penttinen, *Journal of Biomedical Materials Research Part A*, 2005, **75A**, 308-315.

70. C. Chiari, U. Koller, R. Dorotka, C. Eder, R. Plasenzotti, S. Lang, L. Ambrosio, E. Tognana, E. Kon, D. Salter and S. Nehrer, *Osteoarthritis and Cartilage*, 2006, **14**, 1056-1065.

71. N. R. Beeley, J. V. Rossi, P. A. Mello-Filho, M. I. Mahmoud, G. Y. Fujii, E. de Juan, Jr. and S. E. Varner, *J Biomed Mater Res A*, 2005, **73**, 437-444.

72. Z. G. Tang, N. P. Rhodes and J. A. Hunt, *Chemical Engineering Research & Design*, 2007, **85**, 1044-1050.

73. M. Endres, D. W. Hutmacher, A. J. Salgado, C. Kaps, J. Ringe, R. L. Reis, M. Sittinger, A. Brandwood and J. T. Schantz, *Tissue Engineering*, 2003, **9**, 689-702.

74. G. Marletta, G. Ciapetti, C. Satriano, F. Perut, M. Salerno and N. Baldini, *Biomaterials*, 2007, **28**, 1132-1140.

75. N. Garcia-Giralt, R. Izquierdo, X. Nogues, M. Perez-Olmedilla, P. Benito, J. L. Gomez-Ribelles, M. A. Checa, J. Suay, E. Caceres and J. C. Monllau, *Journal of Biomedical Materials Research Part A*, 2008, **85A**, 1082-1089.

76. H. Klassen, D. S. Sakaguchi and M. J. Young, *Progress in Retinal and Eye Research*, 2004, **23**, 149-181.

77. J. B. Recknor, J. C. Recknor, D. S. Sakaguchi and S. K. Mallapragada, *Biomaterials*, 2004, **25**, 2753-2767.

78. E. K. F. Yim, R. M. Reano, S. W. Pang, A. F. Yee, C. S. Chen and K. W. Leong, *Biomaterials*, 2005, **26**, 5405-5413.

79. E. K. F. Yim, S. W. Pang and K. W. Leong, *Experimental Cell Research*, 2007, **313**, 1820-1829.

80. J. B. Recknor, D. S. Sakaguchi and S. K. Mallapragada, *Biomaterials*, 2006, **27**, 4098-4108.

81. N. W. Karuri, P. F. Nealey, C. J. Murphy and R. M. Albrecht, *Scanning*, 2008, **30**, 405-413.

82. H. Wang, S. F. Chen, B. D. Ratner, E. H. Sage and S. Y. Jiang, *Journal of Physical Chemistry C*, 2007, **111**, 14602-14606.

83. G. M. Whitesides, E. Ostuni, S. Takayama, X. Jiang and D. E. Ingber, *Annu Rev Biomed Eng*, 2001, **3**, 335-373.

84. D. Motlagh, S. E. Senyo, T. A. Desai and B. Russell, *Biomaterials*, 2003, **24**, 2463-2476.

85. R. G. Thakar, M. G. Chown, A. Patel, L. Peng, S. Kumar and T. A. Desai, *Small*, 2008, **4**, 1416-1424.

86. D. C. Duffy, J. C. McDonald, O. J. A. Schueller and G. M. Whitesides, *Analytical Chemistry*, 1998, **70**, 4974-4984.

87. M. Okabe, M. Ikawa, K. Kominami, T. Nakanishi and Y. Nishimune, *Febs Letters*, 1997, **407**, 313-319.

88. J. Y. Lim and H. J. Donahue, *Tissue Engineering*, 2007, **13**, 1879-1891.

89. A. I. Teixeira, G. A. Abrams, P. J. Bertics, C. J. Murphy and P. F. Nealey, *Journal of Cell Science*, 2003, **116**, 1881-1892.

90. J. Y. Lim, J. C. Hansen, C. A. Siedlecki, J. Runt and H. J. Donahue, *J R Soc Interface*, 2005, **2**, 97-108.

91. D. A. Bernards and T. A. Desai, *Advanced Materials*, 2010, **22**, 2358-2362.

92. U. Aftab, C. H. Jiang, B. Tucker, J. Y. Kim, H. Klassen, E. Miljan, J. Sinden and M. Young, *Experimental Eye Research*, 2009, **89**, 301-310.

93. A. J. Winfield, D. Jessiman, A. Williams and L. Esakowitz, *Brit J Ophthalmol*, 1990, **74**, 477-480.

94. B. Sleath, A. L. Robin, D. Covert, J. E. Byrd, G. Tudor and B. Svarstad, *Ophthalmology*, 2006, **113**, 431-436.

95. K. M. Sampat and S. J. Garg, *Curr Opin Ophthalmol*, **21**, 178-183.

96. S. J. Bakri, M. R. Snyder, J. M. Reid, J. S. Pulido, M. K. Ezzat and R. J. Singh, *Ophthalmology*, 2007, **114**, 2179-2182.

97. S. J. Bakri, M. R. Snyder, J. M. Reid, J. S. Pulido and R. J. Singh, *Ophthalmology*, 2007, **114**, 855-859.

98. J. C. McDonald, D. C. Duffy, J. R. Anderson, D. T. Chiu, H. Wu, O. J. Schueller and G. M. Whitesides, *Electrophoresis*, 2000, **21**, 27-40.

99. S. K. Sia and G. M. Whitesides, *Electrophoresis*, 2003, **24**, 3563-3576.

100. J. V. Barth, G. Costantini and K. Kern, *Nature*, 2005, **437**, 671-679.

101. Y. N. Xia and G. M. Whitesides, *Annual Review of Materials Science*, 1998, **28**, 153-184.

102. G. M. Whitesides, E. Ostuni, S. Takayama, X. Y. Jiang and D. E. Ingber, *Annual Review of Biomedical Engineering*, 2001, **3**, 335-373.

103. D. H. Kim, P. K. Wong, J. Park, A. Levchenko and Y. Sun, *Annu Rev Biomed Eng*, 2009, **11**, 203-233.

104. D. A. Bernards and T. A. Desai, *Soft Matter*, 2010, **6**, 1621-1631.

105. M. R. Prausnitz, *Advanced Drug Delivery Reviews*, 2004, **56**, 581-587.

106. J. Panyam and V. Labhasetwar, *Advanced Drug Delivery Reviews*, 2003, **55**, 329-347.

107. H. Buchwald, T. B. Grage, P. P. Vassilopoulos, T. D. Rohde, R. L. Varco and P. J. Blackshear, *Cancer*, 1980, **45**, 866-869.

108. G. R. Weiss, M. B. Garnick, R. T. Osteen, G. D. Steele, R. E. Wilson, D. Schade, W. D. Kaplan, L. M. Boxt, K. Kandarpa, R. J. Mayer and E. T. Frei, *Journal of Clinical Oncology*, 1983, **1**, 337-344.

109. N. E. Kemeny, D. Niedzwiecki, D. R. Hollis, H. J. Lenz, R. S. Warren, M. J. Naughton, J. C. Weeks, E. R. Sigurdson, J. E. Herndon, C. F. Zhang and R. J. Mayer, *Journal of Clinical Oncology*, 2006, **24**, 1395-1403.

110. F. M. Alsaleh, F. J. Smith, S. Keady and K. M. G. Taylor, *Journal of Clinical Pharmacy and Therapeutics*, 2010, **35**, 127-138.

111. M. Winkelmuller and W. Winkelmuller, *Journal of Neurosurgery*, 1996, **85**, 458-467.

112. J. H. Raphael, J. L. Southall, T. V. Gnanadurai, G. J. Treharne and G. D. Kitas, *Bmc Musculoskeletal Disorders*, 2002, **3**, -.

113. R. Gaudana, J. Jwala, S. H. Boddu and A. K. Mitra, *Pharm Res*, 2009, **26**, 1197-1216.

114. S. R. J. Taylor, H. Isa, L. Joshi and S. Lightman, *Ophthalmologica*, 2010, **224**, 46-53.

115. G. R. da Silva, A. D. Cunha, E. Ayres and R. L. Orefice, *Journal of Materials Science-Materials in Medicine*, 2009, **20**, 481-487.

116. R. A. Jain, *Biomaterials*, 2000, **21**, 2475-2490.

117. H. Kawaguchi, *Progress in Polymer Science*, 2000, **25**, 1171-1210.

118. K. S. Soppimath, T. M. Aminabhavi, A. R. Kulkarni and W. E. Rudzinski, *Journal of Controlled Release*, 2001, **70**, 1-20.

119. M. N. V. R. Kumar, *Journal of Pharmacy and Pharmaceutical Sciences*, 2000, **3**, 234-258.

120. V. Lassalle and M. L. Ferreira, *Macromolecular Bioscience*, 2007, **7**, 767-783.

121. B. Conti, F. Pavanetto and I. Genta, *Journal of Microencapsulation*, 1992, **9**, 153-166.

122. C. Wischke and S. P. Schwendeman, *International Journal of Pharmaceutics*, 2008, **364**, 298-327.

123. S. D. Allison, *Expert Opinion on Drug Delivery*, 2008, **5**, 615-628.

124. A. Giteau, M. C. Venier-Julienne, A. Aubert-Pouessel and J. P. Benoit, *International Journal of Pharmaceutics*, 2008, **350**, 14-26.

125. A. Luciani, V. Coccoli, S. Orsi, L. Ambrosio and P. A. Netti, *Biomaterials*, 2008, **29**, 4800-4807.

126. S. Aishwarya, S. Mahalakshmi and P. K. Sehgal, *Journal of Microencapsulation*, 2008, **25**, 298-306.

127. A. Budhian, S. J. Siegel and K. I. Winey, *International Journal of Pharmaceutics*, 2008, **346**, 151-159.

128. X. W. Wei, C. Y. Gong, S. A. Shi, S. Z. Fu, K. Men, S. Zeng, X. L. Zheng, M. L. Gou, L. J. Chen, L. Y. Qiu and Z. Y. Qian, *International Journal of Pharmaceutics*, 2009, **369**, 170-175.

129. T. Loftsson, D. Hreinsdottir and E. Stefansson, *Journal of Pharmacy and Pharmacology*, 2007, **59**, 629-635.

130. U. B. Kompella, N. Bandi and S. P. Ayalasomayajula, *Invest Ophth Vis Sci*, 2003, **44**, 1192-1201.

131. X. W. Wei, C. Y. Gong, M. Y. Gou, S. Z. Fu, Q. F. Guo, S. Shi, F. Luo, G. Guo, L. Y. Qiu and Z. Y. Qian, *International Journal of Pharmaceutics*, 2009, **381**, 1-18.

132. K. C. S. Fong, N. Kirkpatrick, Q. Mohamed and R. L. Johnston, *Clinical and Experimental Ophthalmology*, 2008, **36**, 748-755.

133. G. Landa, W. Amde, V. Doshi, A. Ali, L. McGevna, R. C. Gentile, T. O. Muldoon, J. B. Walsh and R. B. Rosen, *Ophthalmologica*, 2009, **223**, 370-375.

134. H. Sun, L. Mei, C. Song, X. Cui and P. Wang, *Biomaterials*, 2006, **27**, 1735-1740.

Appendix: RPC Culture Protocol

Ingredient	Quantity
NeuroBasal Medium	500 ml
B-27 Supplement	10 ml
L-glutamine	5 ml
Penicillin/Streptomycin	5 ml
N-2 Supplement	5 ml
rhEGF (10 μg/ml in NB)	1 ml
Nystatin	1 ml

Thawing Frozen Cells:

1. Incubate 9 ml of NB Complete media in a T-75 flask for 30 minutes in an incubator with 5% CO_2 for 30 minutes prior to thawing cells.
2. Incubate Phosphate Buffered Saline and NB Complete Media in a water bath at 37° C for 30 minutes prior to thawing cells.
3. Remove cells from liquid nitrogen and quickly thaw in the 37° C water bath.
4. Spray vial with 70% ethanol and transfer contents to a sterile 15 ml centrifuge tube.
5. Rinse vial with warm PBS 3-4 times and transfer contents to 15 ml tube each time.
6. Centrifuge the 15 ml tube at 1000 RPM for 3 minutes.
7. Remove the supernatant using a pipette.
8. Re-suspend cells in 1 ml NB Complete media.
9. Transfer contents of tube into the flask containing 9 ml of NB Complete medium.

10. Place the T-75 flask back in the incubator.

Feeding Cells:

1. Incubate NB Complete medium in a 37° C water bath for 30 minutes prior to feeding cells.
2. Remove the T-75 flask of cells from the incubator and place in a tissue culture hood. Remove 5 ml of the cell solution from the T-75 flask and place in a 15 ml centrifuge tube.
3. Spin down the cell solution in the 15 ml tube at 1000 RPM for 3 minutes.
4. Remove the supernatant and discard. Replace with 5 ml fresh NB Complete media and gently break up the pellet of cells at the bottom of the tube by pipetting up and down several times.
5. Return 5 ml cell solution to T-75 flask and place back in incubator.
6. Feed cells on alternating days until confluent.

Passaging Cells:

1. Feed cells 3-4 hours prior to passaging using previous instructions.
2. Incubate NB Complete medium and Hank's Buffered Salt Solution medium in a 37° C water bath for 30 minutes prior to passaging cells.
3. Transfer contents of T-75 flask to 15 ml centrifuge tube.
4. Add 10 ml of HBSS to empty T-75 flask and remove, placing in a second 10 ml centrifuge tube.
5. Centrifuge both tubes at 1000 RPM for 3 minutes.
6. Place 9 ml fresh NB Complete media in a new T-75 flask.

7. Remove media and HBSS supernatant from centrifuge tubes. Re-suspend cells in the first centrifuge tube in 10 ml NB Complete media. Transfer this cell solution to the second centrifuge tube and mix thoroughly.
8. Add 1 ml of re-suspended cells to the new T-75 flask and place flask in incubator. Discard the rest of the cell solution or place in additional T-75 flasks.

Freezing Cells:

1. Feed cells 3-4 hours prior to freezing using previous feeding instructions.
2. Transfer cells from T-75 flask to a sterile 15 ml centrifuge tube.
3. Pipette up and down several times to break up cell pellets.
4. Count and calculate the cell concentration.
5. Cells will need to be frozen in high concentration, typically 3.0 x 10^7 cells/ml in 1 ml aliquots.
6. Spin down the cells at 1000 RPM for 3 minutes.
7. Re-suspend the cells with ½ volume NB Complete medium.
8. Add ½ volume 2X Freezing Media (60% MEM, 20% FBS, 20% DMSO) to tube.
9. Aliquot the cells into freezing vials and place in freezing container filled with isopropyl alcohol.
10. Place freezing container in -80° C freezer overnight, and then place individual vials in liquid nitrogen for long-term storage.

Publishing Agreement

It is the policy of the University to encourage the distribution of all theses, dissertations, and manuscripts. Copies of all UCSF theses, dissertations, and manuscripts will be routed to the library via the Graduate Division. The library will make all theses, dissertations, and manuscripts accessible to the public and will preserve these to the best of their abilities, in perpetuity.

Please sign the following statement:
I hereby grant permission to the Graduate Division of the University of California, San Francisco to release copies of my thesis, dissertation, or manuscript to the Campus Library to provide access and preservation, in whole or in part, in perpetuity.

12/6/2010

Author Signature Date